8-2023

Investigation of Cyclic Gaseous Solvent Injection for Enhanced Oil Recovery in Unconventional Formations

Samuel Asante Afari

[How does access to this work benefit you? Let us know!](#)

Follow this and additional works at: https://commons.und.edu/theses

Part of the Petroleum Engineering Commons

INVESTIGATION OF CYCLIC GASEOUS SOLVENT INJECTION FOR ENHANCED OIL
RECOVERY IN UNCONVENTIONAL FORMATIONS

by

Samuel Asante Afari

Bachelor of Science, Kwame Nkrumah University of Science and Technology, Ghana, 2010

Master of Science, Heriot Watt University, Scotland, UK, 2012

Master of Science, University of Wyoming, Laramie, USA, 2019

A dissertation

Submitted to the Graduate Faculty

of the

University of North Dakota

in partial fulfillment of the requirements

for the degree of

Doctor of Philosophy

Grand Forks, North Dakota

August 2023

Name: Samuel Asante Afari
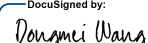
Degree: Doctor of Philosophy

     This document, submitted in partial fulfillment of the requirements for the degree from the University of North Dakota, has been read by the Faculty Advisory Committee under whom the work has been done and is hereby approved.

Kegang Ling
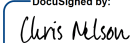
Hui Pu

Dongmei Wang

Lu Jin

_____

_____

     This document is being submitted by the appointed advisory committee as having met all the requirements of the School of Graduate Studies at the University of North Dakota and is hereby approved.

Chris Nelson
Dean of the School of Graduate Studies

7/20/2023
_____
Date

iii

PERMISSIONS

Title: Investigation of Cyclic Gaseous Solvent Injection for Enhanced Oil Recovery in Unconventional Formations

Department: Petroleum Engineering

Degree: Doctor of Philosophy

In presenting this thesis in partial fulfillment of the requirements for a graduate degree from the University of North Dakota, I agree that the library of this University shall make it freely available for inspection. I further agree that permission for extensive copying for scholarly purposes may be granted by the professor who supervised my thesis work or, in his absence, by the Chairperson of the department or the dean of the School of Graduate Studies. It is understood that any copying or publication or other use of this thesis or part thereof for financial gain shall not be allowed without my written permission. It is also understood that due recognition shall be given to me and to the University of North Dakota in any scholarly use which may be made of any material in my thesis.

Samuel Asante Afari

Date: 7/20/2023

ACKNOWLEDGEMENT

DEDICATION

First, I would like to dedicate this dissertation to the Almighty GOD for making this achievement possible. I would also like to dedicate this work to my late father, MR. WILLIAM AFARI. He would have been delighted to witness this day. Next, I express my gratitude to my mother, brother, and my in-laws. To my supportive and beautiful wife, BERTHA, and my lovely daughter, PHOEBE, this is dedicated to both of you. Thank you!

Executive Summary

Unconventional resources have been known to hold vast quantities of hydrocarbons. However, exploiting the oil and gas they hold was previously challenging due to their low permeabilities. Recent advances in horizontal well drilling and hydraulic fracturing have enabled oil and gas production from these reservoirs, leading to significant increases in energy supply to meet the growing energy demand. However, despite the relative technological success, considerable obstacles persist; oil production from unconventional wells often declines by more than 20% of their initial production rate within the first two years, leaving significant volumes of residual oil trapped in the formations. This overarching challenge warrants the need to develop techniques to improve recovery from these valuable resources.

Enhanced oil recovery (EOR) from unconventional resources has been a primary subject of interest among the research community. Gaseous solvent injection has been touted as promising to enhance recovery from unconventional resources. Although several small-scale laboratory experiments and field-scale simulation studies have corroborated the efficacy of gaseous solvents in improving oil recovery, recent field pilot tests have failed to yield the expected improvement in oil production. Hence, the technique has not been widely adopted by industry players. A major contributing factor to this lack of adoption is the gaps in understanding the underlying multiscale (i.e., pore, core, and well scales) recovery mechanisms by gaseous solvents during the injection. Furthermore, there is an apparent knowledge gap in understanding the influence of critical operating parameters on oil recovery (and gas utilization), the variable interaction between these parameters, and their optimal settings at the well scale.

This three-part project addresses some pertinent questions regarding gaseous solvent cyclic injection enhanced oil recovery in unconventional formations. The objective of the first part was

to determine the efficacy of select gaseous solvents for EOR, determine the influence of critical operating parameters and the variable interactions with gas composition and miscibility conditions, and deduce the underlying dominant mechanisms during gaseous solvent cyclic EOR. To this end, core-scale experiments that simulate matrix fracture interactions were conducted using CO_2 and ethane as gaseous solvents. The results showed that gaseous solvent huff-n-puff could achieve up to 87% recovery factor in small middle Bakken small core samples. The results also revealed the essential interactions of operating parameters with miscibility conditions and gas composition. Furthermore, the competition between diffusion and advection as a function of operating parameters was deduced from the results.

The second part aimed to examine the pore scale displacement efficiencies and corroborate the underlying mechanism responsible for enhancing recovery during gaseous solvent EOR. Nuclear magnetic resonance relaxometry was used to measure the fluid-filled pore size distribution to assess the pore level displacement effectiveness of the gaseous solvent huff-n-puff. The results reveal that gaseous solvent huff-n-puff could displace fluids down to the micropores in tight core samples. They also revealed the influence of diffusion and advective force on pore-level displacement efficiency.

The final phase consisted of well-scale studies to ascertain the large-scale effectiveness of gaseous solvents, the effects of the critical operating parameters and the interactions among them, and the optimization of these parameters for maximum recovery (and optimum gas utilization factor). Here, we leverage compositional reservoir simulation and response surface methodology (RSM) for this purpose. The result revealed the most important well-scale parameters for optimum recovery. Numerical optimization indicates that gaseous solvent huff-n-puff in the Bakken Formation can yield more than 7% incremental recovery with a gas utilization factor of

more than 2 bbl/Mscf. We believe the findings in this work can better guide operators to design efficient gaseous solvent huff-n-puff strategies in the Bakken Formation and other unconventional reservoirs.

Table of Contents

List of Figure

List of Tables

Chapter 1

Thesis Overview

1.1 Introduction

Unconventional reservoirs contain enormous quantities of hydrocarbons (Vedachalam et al., 2015). Prior to the early 2000s, these plays were commercially challenging to produce. However, horizontal drilling and hydraulic fracturing innovations have enabled the industry to recover vast quantities of hydrocarbons trapped in these oil reservoirs. Horizontal drilling has made it possible to contact large areas of hydrocarbon-bearing tight formations. Hydraulic fracturing, on the other hand, increases the permeability of these tight reservoirs, allowing fluids to flow into wells (Du & Nojabaei, 2019; Shelley, 2013). The process creates fractures in tight rocks by pumping fracking fluids into a horizontal well at predefined intervals. The pressure generates cracks, which are held open by proppants that act as fluid conductors. Advances in horizontal drilling and hydraulic fracturing have considerably expanded hydrocarbon output in the United States, enabling it to become energy self-sufficient (United States Energy Information Administration, 2013).

Despite these advances, hydraulically fractured horizontal wells frequently experience a substantial decline in production, typically after the first year of operation (Burrows et al., 2020). As a result, only between 3-5% of the large volume of oil in these reservoirs can be extracted (Lui et al.,2014). By way of illustration, the Bakken deposit holds substantial volumes of hydrocarbons in place. According to the North Dakota Geological Survey, an estimated 167,000 MM bbl of oil has been generated in the North Dakota section of the Bakken Formation (Energy and

Environmental Research Center, n.d.). However, according to a 2021 report, only approximately 4,288 MM bbl is recoverable from the Bakken and its underlying formations using current technology (United States Geological Survey, 2021). Given the massive amounts of oil that remain trapped, even a modest percentage of incremental recovery incentivizes the need for strategies to improve recovery.

Numerous investigations have been conducted to identify effective ways to increase recovery in unconventional reservoirs(Burrows et al., 2020). Naturally, water flooding and its variants, such as low salinity water floods, will be the initial candidates as they are simple to implement, inexpensive, and effective in conventional reservoirs(Ashraf et al., 2010; Morrow & Buckley, 2011; Tetteh et al., 2020). However, while a few small-scale laboratory experiments have shown some encouraging outcomes in applying waterflooding in unconventional reservoirs (Morsy et al., 2013; Nguyen et al., 2015; Teklu et al., 2018), it is evident that these findings cannot be used in the field due to issues about injectivity(Sheng, 2017a) and permeability reduction resulting from water-clay interactions(Chakraborty et al., 2017; Faulkner & Rutter, 2000).

Due to their low viscosity, gases are theoretically better at accessing the narrow pore spaces of tight formations and dislodging the trapped oil. Cyclic gaseous solvent injection, also known as Huff-n-Puff (H-n-P), has been identified as one of the best strategies to enhance recovery in tight formations based on several laboratory core scale studies. In one such study, Gamadi et al. (2014) conducted huff-n-puff on Eagle Ford and Mancos shale samples and obtained oil recovery factors of up to 95% from the oil-saturated samples. In another study of huff-n-puff performance in Wolfcamp shale core samples, Li et al. (2018) reported an improvement in oil recovery of up to 68%. Hawthorn et al. (2013) conducted oil extraction experiments on Bakken core samples and found that CO_2 huff-n-puff recovered nearly all the oil from the samples. Several authors have

conducted numerical modeling studies to investigate the method's feasibility in the field (Gala & Sharma, 2018; Jia et al., 2018; Sanchez-Rivera et al., 2015; Sun et al., 2019). Although these modeling studies reported lower recovery factors than the core-scale laboratory investigations, they generally support the feasibility of gaseous solvent huff-n-puff for enhanced oil recovery in tight formations.

Despite the encouraging laboratory and simulation studies results, gaseous solvent huff-n-puff has not received significant industry adoption in the Bakken area. At least seven EOR pilot projects in the Bakken have been completed during the previous decade. However, these tests show inconsistent results with regard to improvement in oil recovery (Hoffman & Evan, 2016). Numerous variables may contribute to the inability of positive laboratory experiments and numerical simulation results to be realized in the field. One possibility is that the mechanisms by which the gas promotes recovery are currently unknown. Additionally, the critical parameters affecting EOR performance and how to optimize them remain unknown.

For efficient performance of the huff-n-puff injection scheme, the effects of critical operational parameters such as injection pressure, injection rate, soak period, production period and bottom-hole pressure require some optimization. To this end, several attempts have been made to study influencing parameters that affect EOR performance and optimize these critical parameters. Gamadi et al. (2014) conducted an experimental study to determine the effects of operating parameters such as soak time, injection pressure, and the number of cycles. Although prolonged soaking times increased the recovery factor when miscible conditions existed, there was an optimum soak time beyond which there was no increment in oil recovery. Additionally, the authors noted that incremental oil recovery was significant after the first few cycles, after which no further rise in production was seen. In their numerical simulation study, Sheng (2017b)

optimized the injection (huff) time, production (puff) time, and soak time for a CO_2 huff-n-puff scheme. The optimal huff time was determined to be the time required for the pressure near the wellbore to reach the specified maximum injection pressure during the huff period. On the other hand, the optimal puff time was determined to be the time required for the pressure near the wellbore to reach the specified minimum production pressure. Also, the benefits of soaking may not be sufficient to offset the time lost in injection and output during the soaking phase. Li et al. (2016) conducted an integrated experimental and numerical analysis to determine the CO_2 huff-n-puff injection scheme's optimal operating parameters. They concluded in their studies that there is an optimal injection rate for the huff-n-puff process. Despite these efforts, further research is needed to study the influence of huff-n-puff operating parameters on oil recovery in unconventional, tight formations.

Furthermore, although CO_2 has been used as a model gas in several studies, there is no consensus on the choice of gas for huff-n-puff EOR in tight formation. Other gases, such as ethane and propane, have been reported to have superior diffusion, swelling, and component extraction abilities and may be more efficient at oil recovery than CO_2 (Burrows et al., 2020; Yang & Gu, 2006). However, data on the efficacy of these alternative gaseous solvents is relatively sparse in the current literature and needs further research.

1.2 Objectives

This research aims to investigate the multiscale effectiveness and underlying mechanisms of gaseous solvent EOR in unconventional formations and its optimization therein. To this end, the specific objectives can be summarized as follows:

1) To comprehensively review the extant literature on gaseous solvent injection in tight formations, which consists of laboratory experiments, numerical simulations, and field pilot tests.

2) To investigate the effectiveness of select gaseous solvents (CO_2 and ethane) in recovering oil from tight core samples. The recovery factor as a function of miscibility condition, gas composition, soak period, production period and rock surface area to volume ratio, and the interactions among these variables were a focus of this study.

3) To deduce the primary underlying recovery mechanisms at play during gaseous solvent cyclic injection in unconventional shale samples. Specifically, to ascertain the contributions of advection (viscous) forces and diffusive forces as a function of the above-mentioned design parameters.

4) To elucidate the pore-scale displacement efficiency during the gaseous solvent cyclic injection. In addition, the recovery efficiency in the various pore sizes was investigated as a function of the design parameters.

5) To corroborate the deductions on the primary underlying mechanism with observations from the pore scale investigations.

6) To investigate the well-scale feasibility and effectiveness of cyclic gaseous solvent injection in unconventional formations. In addition, the influence of the well-scale operation parameters on oil recovery (and gas utilization) and the variable interactions among them were also elucidated.

7) To determine the critical operational parameter settings that optimize the well-scale oil recovery (and gas utilization) during cyclic gaseous solvent injection in unconventional formations.

1.3   Summary of research approach

A systematic approach was used to achieve the goals mentioned above. To achieve objectives 2 and 3, core-scale laboratory cyclic injection experiments were carried out using Middle Bakken core samples collected from a representative well in the study area. The core dimensions and petrophysical properties were measured, and the cores were subjected to thorough cleaning and vacuum saturation. Then, laboratory cyclic injection experiments that simulate matrix-fracture interactions were carried out, and the results were analyzed. To achieve objectives 4 and 5, nuclear magnetic resonance relaxometry was employed to examine the fluid-filled pore size distributions of the core samples before and after cyclic injection experiments, allowing the recovery factors in different pore sizes to be determined and deduce underlying mechanisms. Finally, to achieve objectives 6 and 7, compositional reservoir simulation and response surface methodology were employed. We obtained well-scale data, including formation petrophysical properties, hydraulic fracture design data, production data and fluid PVT data from a representative study area. Then, a compositional reservoir model of the Bakken Formation was constructed and tuned by history matching with well production data. The performance of cyclic gaseous solvent injection was forecasted using the simulation model, after which the response surface methodology (RSM) was used to study the influence of critical operating parameters (and their variable interactions) on recovery and gas utilization factors. RSM also allowed us to optimize the recovery and utilization factors.

1.4   Significance and novelty

Early estimates of hydrocarbon generation in the Williston Basin indicated that the prolific areas and formations in the basin hold between 90 to 500 MMM bbl of oil (Schmoker & Hester, 1983; Webster, 1984; Energy and Environmental Research Center, n.d.). On the other hand, the

latest estimate of undiscovered resources estimated the fully risked estimated mean totals are 4.3 MMM bbl (United States Geological Survey,2021). This estimate indicates that only 1 to 5% is recoverable with current technology (Energy and Environmental Research Center, n.d.). Based on these numbers, a 2% increase in recovery factor by gaseous solvent EOR translates to 1.8 -10 MMM bbl of additional oil production. In perspective, approximately 5.6 MMM bbl of oil was produced in North Dakota between 1951 and 2020 (North Dakota Department of Mineral Resources, n.d.). At an average oil price of $60/bbl, this increment in oil production translates to $120 to $600 billion in revenue. However, this feat cannot be realized without the proper understanding of the underlying mechanisms of gaseous solvent injection for optimized design of recovery strategies. This thesis's results significantly contribute to the knowledge of the effectiveness and mechanism of gaseous solvent EOR in unconventional formations. We believe the results from this thesis will help engineers better understand and design effective EOR strategies in unconventional formations.

Specifically, the thesis makes the following novel contributions to the current literature.

1) The first part of the study compares the effectiveness of two potent gaseous solvents, CO_2 and Ethane, as solvents for EOR in Middle Bakken formation. The experimental design involved comparing their effectiveness normalized for their miscibility pressures. This experimental design enables us to deduce the primary underlying mechanisms, specifically the contribution of advection and diffusion. Our experimental design reveals the interactions between critical influential variables, introducing additional insights into the existing literature.

2) The second part of the study probes the pore-level mechanisms using NMR relaxometry. The mechanisms deduced from core scale experiments were confirmed at the pore level. The study of these pore-level mechanisms, as a function of miscibility condition, gas composition and operating parameters, bring another perspective to the current literature.

3) The final part of this thesis studies the impact of five critical operational parameters, namely, injection rate, injection period, soak period, production period and production bottom-hole pressure, on oil recovery and gas utilization. This part leverages compositional reservoir simulation and response surface methodology (RSM) for this purpose. The use of RSM enables the evaluation of the statistical significance of the influencing parameters and, most importantly, their interactions, which has often been neglected in the current literature. We also applied numerical and graphical techniques to find the combination of operating parameters that maximizes oil recovery and gas utilization.

1.5 Thesis structure

This thesis is partitioned into six (6) chapters.

1) Chapter 1 introduces the thesis. Here, we briefly discuss an overview of enhanced oil recovery in unconventional formations, the current challenges, and the problem statement. The objectives, methodology, significance and novelty of this thesis are also briefly discussed.

2) Chapter 2 includes an overview of the Bakken Petroleum System and a literature review of the previous numerical simulation, experimental work, and field pilot tests performed in Bakken.

3) Chapter 3 reports the core-scale investigation of cyclic gaseous solvent injection in Middle Bakken core samples. The chapter begins with a brief introduction, the materials, experimental setup, experimental procedure, the results (and discussions), and finally, the conclusions (and limitations).

4) Chapter 4 describes the pore-scale assessment of cyclic gaseous solvent injection in Middle Bakken core samples. The chapter also begins with a brief introduction to the context, followed by the materials, experimental setup, experimental procedure, results (and discussions), and concluding remarks (and limitations).

5) Chapter 5 presents the well-scale study and optimization of gas solvent EOR in the Bakken formation using numerical simulation and response surface methodology. This chapter begins with a brief background. It then outlines the methodology, which includes the simulation process, the study area, the fluid model, the reservoir model, sampling (and proxy model), and optimization. We then present the results (and discussions), which include simulation results, proxy model evaluation, the main effects, factor interactions and optimization.

6) Chapter 6 summarizes the dissertation findings and includes recommendations and future research that can be carried out.

Chapter 2

Literature Review

2.1 Overview of unconventional resources

The United States has recently seen an increase in oil production, primarily due to technological advances in extraction technologies from shale formations, particularly hydraulic fracturing and directional drilling. Owing to these technologies, oil and gas can now be produced economically from shale and other unconventional formations. The increase in production catapulted the US as the world's largest oil and natural gas producer in 2009; annual oil production increased over 2008 in 2009, the first increase since 1991, and has continued to rise each year since(Congressional Research Service, 2015). Between January 2008 and May 2014, monthly crude oil production in the US went up by 3.2 million barrels per day. About 85% of this increase was due to tight oil formations and shale in Texas and North Dakota(Congressional Research Service, 2015). Hence, developing several other unconventional oil fields will help the possibility of US energy independence in the near future.

According to the Society of Petroleum Engineers, "unconventional resources" are vast petroleum accumulations not considerably affected by hydrodynamic pressure. Also known as "continuous-type deposits" and "tight formations," they consist of fine-grained, organic-rich, sedimentary rocks, primarily shales and comparable rocks. Typically, in conventional petroleum systems, hydrocarbons are generated in the source rock (typically shales) and migrate to reservoirs such as sandstone and carbonate reservoirs that are permeable and porous and sealed by impermeable cap rocks. In contrast to conventional petroleum reservoirs, unconventional reservoirs are shale rocks that are both the source and reservoir of oil and natural gas. The term also encompasses tight formations that have served as reservoirs for nearby tight rocks (e.g., the

Middle Bakken formation). Unconventional formations have minuscule pore sizes and limited permeability, rendering them flow-resistant; thus, unless natural or artificial fissures occur, oil and gas usually remain in the source rock due to impermeability.

In the past, the oil and natural gas industry considered it uneconomical to extract hydrocarbons from unconventional resources. However, the development of directional well drilling and reservoir stimulation has drastically altered this narrative. Horizontal wells increase the reservoir contact area, while hydraulic fracturing provides high-conductivity flow pathways, which allow fluids to flow.

Unlike conventional resources, unconventional resources are relatively extensive and can extend several square miles in area. Major unconventional plays in the US include the Bakken, Eagle Ford, Permian, Marcellus, Woodford, Barnette, Fayetteville, and Niobrara, to mention a few. **Figure 1** shows a more exhaustive list and locations of US unconventional plays.
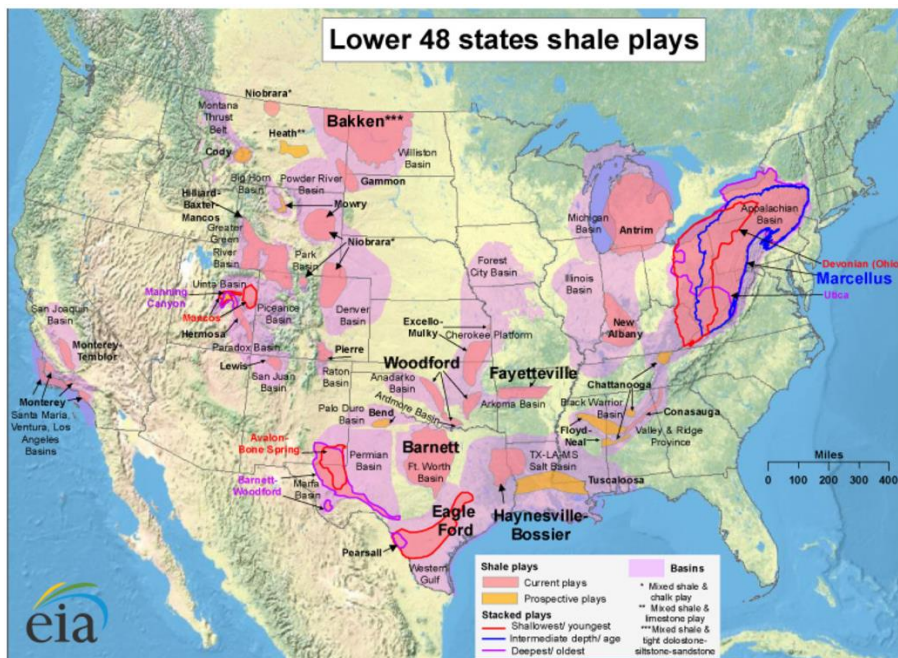
Figure 1: Unconventional resource plays in the US (source: US Energy Information Administration, 2011)

The Bakken Total Petroleum System (BTPS) is one of North America's most extensive oil-bearing tight formations located in the Williston Basin. This intracratonic basin straddles Montana, South Dakota, and North Dakota in the US and the provinces of Saskatchewan and Manitoba in Canada (**Figure 2**) (Gaswirth et al., 2013; Sonnenberg, 2018). The BTPS's strata range from the Upper Devonian Three Forks Formation, Upper Devonian to Lower Mississippian Bakken Formation, and the lowermost part of the Lower Mississippian Lodgepole Formation.
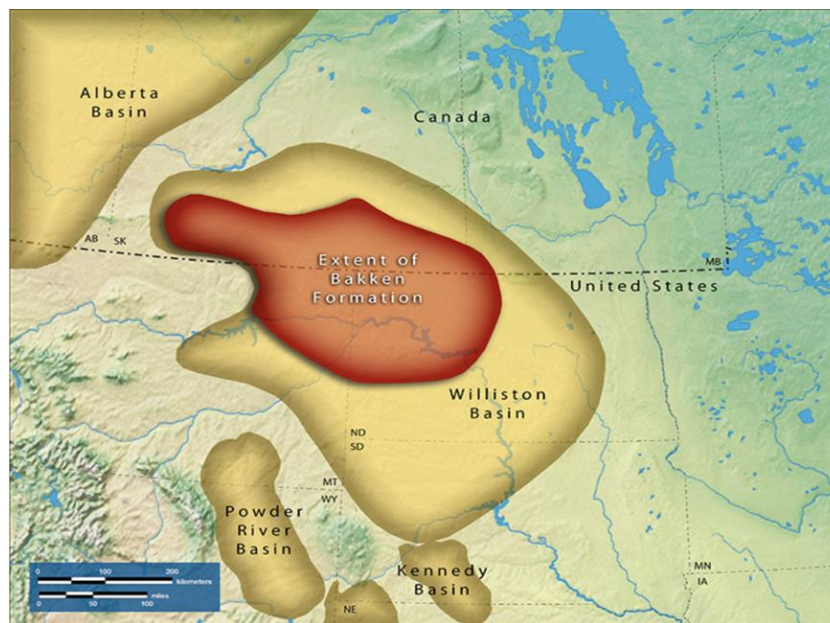
Figure 2: The extent of the Bakken Petroleum System(source: Energy and Environmental Research Center, n.d.)

The Bakken Formation consists of three main members: the Upper Bakken, Middle Bakken, and Lower Bakken, which are underlain by the Three Forks Formation. The upper and lower shale members are organic-rich and are the hydrocarbon source rocks. The upper shale member is the most regionally extensive and forms the outermost boundary of the continuous resource assessment units. The oil the upper and lower members generate has migrated into the Middle Bakken, the overlying Pronghorn, and the Three Forks Formation. However, the middle

member is the main horizontal drilling target within the Bakken Formation. The middle member is composed of sandstone, siltstone, dolomite, and mudstone. The Three Forks is a mix of dolomitic shale, siltstone, and dolostone, suggesting deposition within hypersaline marine, subtidal, and intertidal environments. Anhydrite nodules are common within lower sections of the Three Forks Formation(United States Geological Survey, 2021). **Figure 3** shows the stratigraphic cross-section of the BTPS.
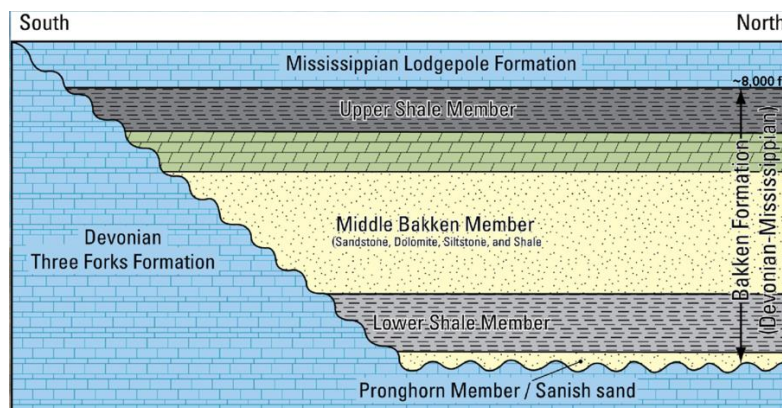
Figure 3: Stratigraphic cross-section of the Bakken Petroleum System(Gaswirth et al., 2013)

Early estimates of hydrocarbon generation in the Williston basin indicate that the productive areas and formations in the basin hold between 90 to 500 MMM bbl of oil (Schmoker & Hester, 1983; Webster, 1984). As of 2021, more than 17,500 wells had been drilled into the Bakken and the Three Forks Formations, and approximately 4 MMM bbl of oil had been produced from these units (United States Geological Survey, 2021). In 2021, The USGS evaluated the BTPS for undiscovered, technically recoverable continuous oil, gas, and natural gas liquid resources in the Bakken and Three Forks Formations of North Dakota and Montana's Williston Basin. The agency reported the fully risked mean totals of 4.3 MMM bbl of oil, 4.872 MMM CF of gas, and 0.417 MMM bbl of natural gas liquids (United States Geological Survey, 2021).

2.2 Challenges of enhanced oil recovery in unconventional reservoirs

Despite the vast quantities of hydrocarbons, only a fraction of the reserves is recoverable. Based on the estimated oil generated and the undiscovered technically recoverable reserves stated above, only 1% to 5% of the oil in the Bakken Formation can be extracted with current technologies. The average recovery factor for the industry is usually well below 10% (Von Flatern, R., 2017). After drilling and hydraulic fracturing, oil production often drops to less than 15% of the original rate after three years. **Figure 4** shows the production characteristics of a typical shale oil well. Because there are no options for extending the well's life, operators have to drill more wells to maintain production(Burrows et al., 2020).
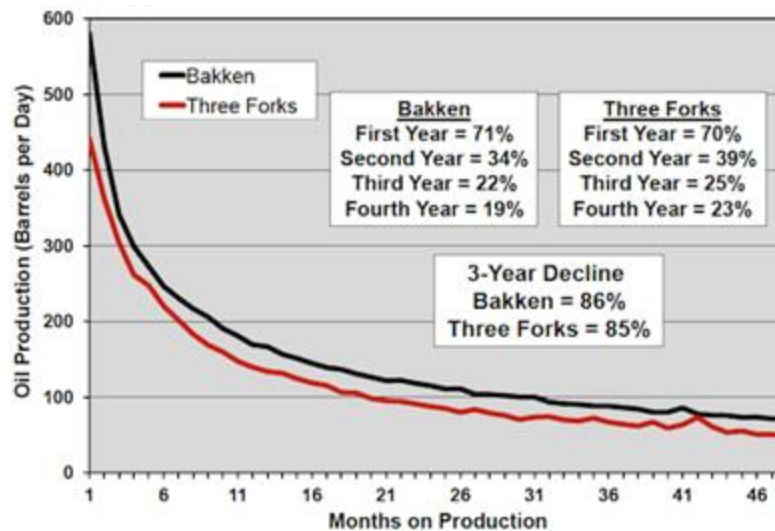
Figure 4: Production type curves of the Bakken and Three Forks formation. (Source: Reverse Engineering the North Dakota Bakken Data – Peak Oil Barrel, 2014)

Deploying feasible EOR strategies in unconventional formations could unlock the vast volume of oil trapped in the formations. Even a modest fractional increase in recovery factor translates to huge revenue turnovers for companies and state (and federal) governments.

Unfortunately, EOR strategies that have been successful in conventional formations are not nearly as successful in unconventional formations. Examples of EOR strategies utilized in conventional formations include waterflooding, immiscible and miscible gas flooding, polymer flooding, and chemical flooding, to mention a few. These strategies are effective because fluids can easily flow through pores and extract the residual hydrocarbons throughout the reservoir. Flow through the matrix is difficult or impossible in tight and shale formations due to the formation's limited permeability. The injection pressure required to establish flow through an unfractured shale or tight formation would be exceedingly high.

Conventional formations will typically have permeabilities between 0.1 and 100 mD. On the other hand, the permeability of unconventional formations can be below 0.001 mD, which is several magnitudes times lower than that of conventional formations (Loucks et al., 2012). At the pore level, unconventional formations have a considerable proportion of nanopores, with pore sizes ranging between 1nm and 1μm. In contrast, conventional formations have a significant proportion of pore sizes greater than 2 μm. The presence of nanopores further complicates the physics of flow through tight formations as fluid phase behavior in nanopores differs from that of larger pores. In addition, while the pores in conventional formations are mostly interconnected, the pores in unconventional formations have a significant proportion of isolated pores. Furthermore, organic matter in unconventional formations may render most shale formations intermediate to oil-wet, unlike conventional formations that are water to intermediate-wet (some carbonates are oil-wet). Oil wetness implies that the pore surfaces have an affinity for oil, and oil adheres to the surfaces. These properties of unconventional formations explain the difficulties involved in producing from unconventional formations.

2.3 Injection modes for enhanced oil recovery in unconventional reservoirs

Because of the characteristic differences between unconventional and conventional formations, injection strategies that have been successful in conventional formations will be challenging to deploy in unconventional formations. Burrows et al.(2020) identified the three main injection modes as 1) Continuous, 2) Multi-well cyclic, and 3) Huff-n-puff. **Figure 5** depicts the various injection modes for EOR.

The continuous injection mode is the most common mode of injection. The mode involves at least two wells where the injection fluid is injected from one well, and the reservoir fluids are produced from the other well. This injection mode is best suited for reservoirs with high permeability and well connectivity, as is commonly used in conventional reservoirs.   In unconventional formations, this mode may be considered if there is good interconnectivity between the wells, usually because of natural fractures. The downside of this interconnectivity is that when low-viscosity fluids are used as injection fluid, the natural fractures act as high-conductivity flow, causing conformance issues.

For situations with limited well interconnectivity, huff-n-puff is the preferred injection mode. Unlike the continuous injection mode, huff-n-puff only requires a single well that cyclically acts as both producer and injector. The fluid is injected, allowed to soak for some time, and produced from the same well. This model is a stripping process that relies on highly conductive flow pathways to reach the shale matrix's surfaces (Burrows et al., 2020). Upon reaching exposed surfaces, the injected fluid slowly imbibes the matrix by diffusion. This injection mode is the most used mode for unconventional formations, with gas as the injection fluid.
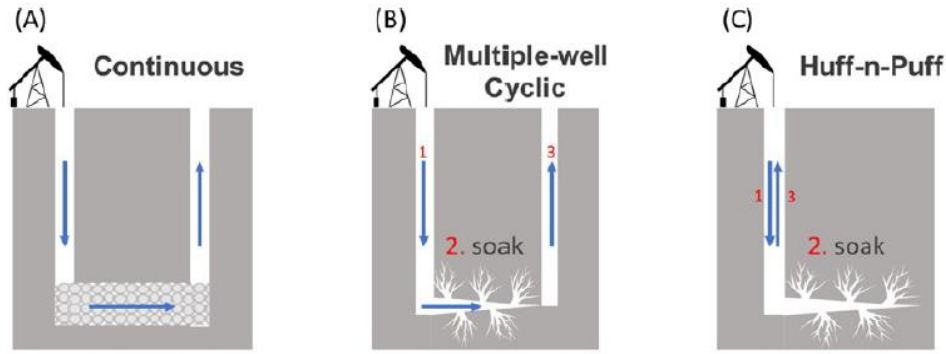
Figure 5: Fluid injection modes for EOR (Burrows et al.,2020)

Multi-well cyclic mode combines the multi-well feature of continuous injection mode and the cyclic feature of huff-n-puff. As seen in **Figure 5**, two wells (an injector and a producer) are required. In this mode, the injection fluid is injected through the injector and then allowed to soak for some time. Then, the reservoir fluid is produced from the producer well. In unconventional formations, this injection mode is rarely used, usually due to the lack of interconnectivity between wells. This mode of injection is also known as asynchronous injection mode and can involve multiple injectors and producers in parallel. Using this mode with multiple parallel wells has been shown to work well (Kong et al.,2016).

2.4 Enhanced oil recovery methods in unconventional Reservoirs

Various EOR methods have been considered in unconventional formations. The main methods include water injection, surfactant injection, foam injection and gas injection. In this review, we will limit our scope to water injection and gas injection since these are the most common EOR techniques that have been considered in unconventional reservoirs. Readers should refer to Burrows et al. (2020) and Sheng et al. (2020). for a detailed review of the other techniques.

17

2.4.1 Water injection

Owing to the low permeabilities of unconventional formations, the injectivity of water has been the main concern for operators. Surprisingly, the available data shows that injectivity is not an issue. In a 2014 field pilot test in the Montana(MT) portion of the Bakken formation, operators successfully injected approximately 1200 bbl/day of water into the formation for over a month, showing there were no problems with water injectivity(Hoffman & Evan, 2016).

Another issue of concern is formation damage during and after water injection. The interaction of water with water-sensitive clay minerals present in shales can cause swelling of the clays, which may reduce the already-low permeabilities of the shale formation. Zhou et al. (2016) observed a significant permeability reduction in shale samples from the Niobrara, Woodford and Horn River samples when imbibed with water-based hydraulic fracturing fluids. The findings from other authors have corroborated this observation (Behnsen & Faulkner, 2011; Duan & Yang, 2014; Faulkner & Rutter, 2000). However, water-clay interactions may positively impact permeability by creating microfractures during and after injections. Wang et al. (2017) observed that macroscopic swelling of shales after water exposure was limited (less than 2%), plausibly due to the presence of non-swelling inclusions in the shales. After water exposure, microcracks were observed under an environmental scanning electron microscope (ESEM).

Despite these limitations and uncertainties, field pilot tests have been carried out to examine the efficacy of water as a recovery agent in unconventional formations. In 2006, Crescent Point Energy Corp. tested the effectiveness of waterflooding projects in the Bakken Formation. The results indicated that oil production peaked at 550 bbl/d from the initial 50 to 100 bbl/d from four producer wells (Wood & Milne, 2011). In the MT-Bakken field pilot mentioned earlier, no increase in oil rate was observed during the injection. Water broke through in an offset well after

one week of injection. However, when the offset well was closed and reopened after some months, the oil rate increased (Hoffman & Evan, 2016). Meridian Oil Co. successfully injected 13,200 bbl of fresh water into a horizontal well in the Upper Bakken Shale for 50 days and then shut it in for 60 days. After reopening the well, no increase in oil production was observed (J. Sorensen & Hamlin, 2016).

Water huff-n-puff has also been suggested as a viable technique to improve recovery from unconventional formations. The idea behind water huff-n-puff is that the injected water preferentially invades large pores and then imbibes into small pores to displace oil. In a study to study oil recovery by water imbibition, Yu and Sheng (2015) observed that water huff-n-puff could achieve up to 21% oil recovery when pressure was increased to 5000 psi. In 2012, a field pilot test was conducted in the North Dakota portion of the Bakken Formation, where water was injected in a cyclic mode. Water was injected at a rate of 1200 bbl/d for a month, after which a soak period of two weeks was allowed. There was no evidence of a water injectivity issue. The well was then opened for production for 90-120 days, but no increase in oil rate was observed (Hoffman & Evan, 2016). In the same year, a similar test was conducted in the Parshall Field. Approximately 40,000 bbls of produced water was injected according to a 30-day injection and 10-day soak schedule. Again, no incremental oil production was observed (J. Sorensen & Hamlin, 2016). These findings highlight the general discrepancy between laboratory scale experiments and field tests.

2.4.2 Gas injection

Gases are the most used in unconventional formations among the currently used injection fluids due to their low viscosities and densities, as they can invade the micropores in shale formations and dislodge residual fluids from the pores. Sheng and Chen (2014) compared gas flooding to water flooding in their simulation studies. Their results showed that gas flooding

outperformed water flooding in tight formations. They observed that the average pressure during water injection could not be increased much higher than the starting reservoir pressure, as the pressure increased only near the injector. This inability to increase the average reservoir pressure is due to the relatively high viscosity of water and the high water-oil interfacial.

As with water injection, gases can also be injected in continuous or cyclic mode (huff-n-puff or multi-well cyclic). The evidence for the efficacy of gas flooding is conflicting in the literature. In one study, the authors observed that in low permeability formations, it is difficult for the gas and the pressure to propagate from an injector to a producer when gas is injected, thus lower recovery than huff-n-puff (Sheng & Chen, 2014). Sorensen et al. (2016) conducted a comprehensive study that included field-scale simulations of the Middle Bakken interval in the Bailey and Grenora fields. The team used a comprehensive dataset including well logs, core analysis, fluid analysis, CT scanner and electron microscope. In that study, the authors estimated that CO_2 could improve the oil production rate by up to 50%. They observed that multi-well continuous injection performed better than single-well cyclic injection. The study also suggested that this EOR technique can store up to 3.2 billion tons of CO_2 while recovering an additional 4 to 7 bbl of oil from the Bakken formation.

In a field pilot test conducted in the Song-Fang-Dun Field in China, the operators observed a 3-times increase in oil production rate after CO_2 injection. Also, the operators observed that CO_2 had 6.3 times higher injectivity than water. The field had an average permeability of 0.8mD and a porosity of 12% (Jiang et al., 2008). Another field pilot test was conducted in the Yu-Shu-Lin field, Daqing, with an average permeability of 0.96mD. In this test, the injection was started six (6) months ahead of production. The estimated recovery factor was approximately 21%, which is remarkable for a tight oil reservoir (Wang et al., 2010). We note that for the two field tests, the

wells were unfractured. Based on the reported permeabilities, the formations could be classified as 'tight' reservoirs rather than 'ultra-tight' formations, such as the upper and lower Bakken formations, which could explain the high recovery factor. These studies show that gas flooding could be viable in certain tight formations depending on the permeability and presence (or absence) of fractures.

Huff-n-puff has been the favored injection mode for gas EOR in unconventional reservoirs. Gamadi et al. proposed the injection mode and first tested the concept with CO_2 in small core samples. The team examined the effectiveness of huff-n-puff on tight Eagle Ford and Mancos shales samples and reported recovery factors between 33% to 85% (Gamadi et al., 2014). In another experimental study, Tovar et al. (2014) coupled laboratory experimental huff-n-puff studies with x-ray computed tomography to examine the effectiveness of CO_2 huff-n-puff on confined tight core samples. The authors reported between 18 to 55% recovery from the sample. Sennaouie et al.(2022) conducted an experimental investigation of huff-n-puff on Three Forks tight core samples using various gases. The authors reported up to 88% recovery factor depending on the gas composition, soak period and injection pressure. Several other authors have corroborated these results at the laboratory scale, providing overwhelming support for the effectiveness of gas huff-n-puff (Hawthorne et al., 2013; Jin, Hawthorne, et al., 2016; Song & Yang, 2017; Yu et al., 2016; Zhao et al., 2021). A comprehensive list of extant experimental work on gas huff-n-puff reviewed is provided in Table 1.

In order to scale up the huff-n-puff strategy for use at the field scale, it is necessary to examine the strategy using field scale simulations; thus, several authors have conducted field scale numerical simulations to ascertain the effectiveness of the technique. Notable amongst them is the work by Torres et al. (2018), who conducted a field scale simulation to assess the mechanisms

controlling CO_2 EOR in the Bakken formation. The authors reported incremental recovery factors between 0.6% to 5.4%. Gamadi et al.(2014) conducted field-scale compositional simulation studies to evaluate the effectiveness of natural gas huff-n-puff as an EOR technique in the Eagle ford formation. The results revealed that natural gas huff-n-puff could achieve between a 3 to 5% recovery factor. These and many other findings, as listed in **Table 2 ,** point to the potential efficacy of huff-n-puff in conventional formation, albeit generally lower recovery factors compared to laboratory core scale experiments.

Several field-scale pilot tests have evaluated the effectiveness of gas huff-n-puff with inconclusive results. In 2008, a CO_2 huff-n-puff field pilot test was conducted in the Elm Coulee field located in the North Dakota part Bakken formation. In this test, 1 MMSCF/day of CO_2 was injected at a pressure between 2000 to 3000 psi for 30 days. There were no issues with injectivity, but the oil rate did not improve (Hoffman & Evan, 2016; Sheng, 2017a). In another test in the same year, EOG Resources Inc. injected CO_2 in a cyclic mode in the Parshall field's Middle Bakken interval. The test well was a horizontal well with a six-stage hydraulic fracture treatment. The operators injected approximately 30 MMSCF of CO_2 for 11 days. The oil rate increased after the injection period. However, CO_2 breakthrough was observed in a nearby offset well. This breakthrough of CO_2 was attributed to the high degree of natural fracturing, which allowed the highly mobile to bypass the rock matrices. This result demonstrates the potential conformance issues that need to be considered when injecting gas in a fractured tight formation (Sheng, 2017a; J. Sorensen & Hamlin, 2016). A comprehensive list of field pilot tests is presented in **Table 3.**

Table 1: Review of extant core-scale experimental studies of gas huff-n-puff in unconventional formations.

Reference	Formations	Solvent Composition	Some key findings
Gamadi et al.(2014)	Mancos, Eagle Ford	CO_2	Recovery factor was between 33-85%. Miscible CO_2 injection affects recovery factors more than immiscible injection. Injecting CO_2 above MMP has little effect on recovery factor.
Li et al. (2019a)	Eagle Ford	CO_2, N_2	The recovery factor was between 34-62%. CO_2 huff-n-puff is more effective than N_2. The First huff-n-puff cycle had the highest oil recovery. CO_2 had superior injectivity in ultra-low permeability shale than N_2.
Tovar et al.(2014)	N/A	CO_2	Oil recovery was 18-55% of OOIP. CT scans demonstrated that oil vaporization into carbon dioxide is the principal oil recovery mechanism.
Adel et al. (2018)	Eagle Ford	CO_2	Recovery factor was between 1-50%. Recovery factor is primarily affected by injection pressure. Increase in pressure increases recovery factor even beyond the MMP.
Tovar et al. (2018)	Barnette, Wolfcamp, Bakken, Eagle Ford	CO_2	Recovery factor was between 2-40%. Both injection pressure and soak period had significant impact on recovery factor. Further

			pressure increases beyond MMP increased recovery factor.
Li et al. (2017)	Wolfcamp	CO_2	Recovery factor was between 40-70%. Under the MMP, the injection pressure significantly increased oil recovery. Above the MMP, the increased pressure enhanced oil recovery until the injection pressure was approximately 200 psi above the MMP.
Hawthorne et al.(2013)	Bakken	CO_2	The recovery factor was between 40-95%. Higher surface area significantly improves hydrocarbon recovery rates.
Alharty et al. (2015)	Bakken	$CO_2,$ $CH_4,$ $N_2,$ C_2H_6	The recovery factor was between 40-90%. Gas injection mobilizes matrix oil through miscible mixing and solvent extraction in a small region along the fracture/matrix interface, hence encouraging countercurrent flow of oil from the matrix as opposed to oil displacement through the matrix.
Jin et al. (2016)	Bakken	$CO_2,$ $CH_4,$ $N_2,$ C_2H_6	Recovery factor was between 18-95%. CO_2 and C_2H_6 resulted in the highest recovery factors. The enhancement in oil recovery could partly be explained by reservoir conditions that create high gas diffusivity, causing miscible gas extraction in experiments.
Jin et al. (2016 b)	Bakken, Three Forks	CO_2	The recovery factor was between 58-100%. Lower TOC content (<0.5 wt.%) and moderate pore size (approximately 8–80nm) provide a favorable flow condition for CO_2 and

			hydrocarbons. Oil mobilization is significantly influenced by diffusion.
L.Li et al (2016)	Wolfcamp	CH_4	Recovery factor was between 9-39%. The optimal strategy is to increase the pressure gradient during huff and puff phases to attain the largest average pressure gradient in the matrix in a predetermined amount of time, which can be achieved by increasing the injection pressure or decreasing the production pressure. Extending the soak period is detrimental to oil recovery.
Meng et al. (2019)	Eagle Ford	CH_4	The recovery factor was between 23-53%. High injection pressure during the huff period could vaporize the liquid condensate produced during the puff period. However, a high injection pressure above the dew point does not significantly affect oil recovery.
Sennouie et al.(2022)	Three Forks	$CO_2,$ $C_2H_6,$ C_3H_8	Up to 88% recovery in the Upper Three Forks formation. Injection pressure, soak period, and gas composition significantly impacted the recovery factor. Ethane was the most effective gas in both formations, followed by propane and CO_2.
Gamadi et al. (2013 b)	Barnette, Mancos, Eagle Ford	N_2	Recovery factor was between 10-50%. Repressurization is the primary oil recovery mechanism for the N_2 huff-n-puff process in shale oil reservoirs.

Ellafi & Jabbari(2019)	Bakken	CO_2	The recovery factor was between 8-55%.
			Oil recovery by CO_2 injection increases as the temperature and pressure increase until it reaches an optimum. The number of cycles and soaking time are crucial design parameters. Oil production increases as the contact surface area increases.
Yu et al. (2016)	Eagle Ford	N_2	The recovery factor was between 12-26%.
			A higher injection pressure is beneficial for oil recovery. The ultimate recovery factor can be achieved with fewer operating cycles at higher injection pressures. A soak period is critical to recovering oil effectively, but too long a soaking period does not affect the recovery factor. Increasing the pressure depletion rate can improve the incremental RF from each cycle.

Table 2: Extant simulation studies on gaseous solvent-enhanced oil recovery in unconventional formations.

Reference	Formations	Solvent Composition	Simulator (Model)	Some key findings
Alharty et al. (2015)	Bakken	CO_2, NGL,	CMG (dual porosity)	The incremental field recovery after CO_2 injection was up to 5.1%, whereas the incremental stimulated reservoir volume (SRV) recovery was 22.3%. Increasing the injection rates by twofold increased the field and SRV recovery by more than

				fifty percent. Due to poor matrix permeability, the soaking period has minimal effect, confirming that miscibility occurs in a narrow region along the fracture-matrix contact.
Gamadi et al. (2014)	Eagle Ford	Natural gas	ECLIPSE 300 (n/a)	Natural gas injection can achieve an incremental recovery factor between 3 % to 5%. The ultimate recovery factor is affected by injecting natural gas at pressures higher than MMP. The soaking period substantially impacts the ultimate recovery factor, the longer the soaking period, the higher the ultimate recovery. Repressurization is a key oil recovery mechanism.
Torres et al. (2018)	Bakken	CO_2,	CMG (single and dual porosity)	CO_2 huff-n-puff can achieve recovery factors ranging between 0.6% and 5.4%. The presence of natural or induced fracture networks could improve CO_2 sweep efficiency and oil mobilization.
Wan et al. (2014)	Eagle Ford	Lean gas, Rich gas CO_2	CMG (dual porosity)	Recovery factors were between 5-70%. Natural fracture spacing has a significant impact on enhanced oil recovery.
Chen et al. (2013)	Bakken	CO_2	UT-COMP (n/a)	The recovery factor was up to 7%. CO_2 huff-n-puff recovery depends significantly on reservoir heterogeneity.

Li et al. (2017)	Wolfcamp	CO_2 CH_4 N_2	CMG (dual porosity)	The recovery factors ranged from 6 to 17%. CO_2 EOR yielded the best results, followed by N_2 and $CH_4.$ The mechanism of gas huff-and-puff EOR is comprised of pressure and gravity gradients, swelling, miscibility, and molecular diffusion, which will result in a decrease in hydrocarbon density, viscosity, and interfacial tension.
Sanchez-Rivera et al. (2015)	Bakken	CO_2	CMG (single porosity)	CO_2 injection achieved up to 2.7% incremental recovery. Beginning Huff-and-Puff operations too early in the well's lifetime reduces the treatment's effectiveness. A shorter soaking period is better than more extended soaking periods. Huff-and-Puff works well in reservoirs with natural fractures.
Yu et al. (2019)	Eagle Ford	CO_2	CMG (embedded-discrete-fracture-model)	The relative increase in cumulative oil production after 20 years of CO_2 injection was approximately 12%. CO_2 molecular diffusion and nanopore confinement are essential mechanisms that affect oil recovery during CO_2 huff-n-puff. Both mechanisms positively affected the CO_2 huff-n-puff effectiveness.
Yu et al. (2015)	Bakken	CO_2	CMG (n/a)	The incremental oil recovery factor after 30 years of gas injection is 2.43%.

				Longer fracture, half-length, and more heterogeneity favor the CO_2 huff-n-puff process.
Sanaei et al. (2018)	Bakken	CO_2	CMG (n/a)	CO_2 injection resulted in an additional 30% oil recovery. The injection period has an optimum duration based on reservoir pressure in the near-wellbore region and surface gas injection rate. Prolonging soaking had a negligible effect on incremental oil recovery. An extended production period increased oil recovery, but only at later cycles. Beginning gas cycling operations too early in the well's life will reduce the effectiveness of huff-n-puff.
Wang et al. (2019)	Bakken	CO_2	CMG (single and dual porosity)	Optimal CO_2 injection achieved 58% incremental oil recovery. The presence of natural fractures significantly impacts the recovery factor. CO_2 diffusion has no significant impact on the recovery factor. Additionally, the injection gas composition does not significantly affect the recovery factor.
Cudjoe et al. (2016)	Chattanooga	CO_2	CMG (dual porosity)	Cyclic CO_2 injection increased the final recovery from 10% to 53% of the OOIP in the SRV region. The permeability of natural fracture impacted oil production

				most, especially in later production times.
Alfarge et al. (2017)	Bakken	CO_2, Lean gas, Rich gas,	CMG (dual porosity)	Up to 3% incremental recovery. Molecular diffusion has a significant role in EOR by gas injection in the Bakken shale reservoir. However, CO_2 needs a high molar-diffusivity in oil to enhance oil production in tight formations. Lean and rich gas require less molar diffusivity to be effective as EOR fluid.
Wan et al. (2018)	Eagle Ford	CO_2	CMG(n/a)	CO_2 huff-n-puff process is more effective in the presence of fracture networks compared to planar fractures. Fracture network spacing is more critical for recovery efficiency than fracture conductivity, but the network must meet an optimal conductivity requirement.
Phan et al. (2018)	Wolfcamp	CO_2	CMG (dual porosity)	An optimal soaking time is crucial to maximizing recovery. However, a soak period longer than optimal impairs overall productivity. Also, the larger the number of huff-n-puff cycles, the higher the incremental oil recovery.
Akita et al. (2018)	Eagle Ford	CO_2	CMG (single porosity)	Total recovery is a function of the fluid diffusivity coefficient. The choke effect at the fracture-matrix interface could lead to a loss in pore connectivity, which may impede production. Thus, a slow

				production rate is advised to maximize the recovery factor.
Kong et al. (2016)	Cardium	CO_2	CMG(n/a)	CO_2 Huff-and-Puff is sensitive to the injection and production periods. Therefore, prolonging the injection and production periods of each consecutive huff and puff cycle can improve its performance compared to a fixed cycle length huff and puff. The soaking period does not significantly impact the recovery factor.
Phi et al. (208)	Eagle Ford	CO_2	CMG (dual porosity)	CO_2 huff-n-puff yielded up to 22% incremental recovery. Compared to continuous injection, CO_2 huff-n-puff recovers the most incremental oil but also requires the least CO_2 to be injected.

Table 3:Comprehensive list of gas injection for enhanced oil recovery pilot projects.

Company (Year)	Formation (Location)	Solvent Composition/ Injection mode	Results	*Reference*
EOG Resources (2008)	Bakken (Mountrail County, North Dakota, USA)	CO_2 H-n-P	No issues with CO_2 injectivity. No significant increase in oil production was observed.	Hoffman et al. (2016)
N/A (2008)	Daqing (Yushulin, China)	CO_2 Cont. Inj.	Gas injection led to a 21% increase in recovery	Wang et al. (2015)
EOG Resources (2009)	Bakken (Richland County, Montana, USA)	CO_2 H-n-P	No issues with CO_2 injectivity. No significant increase in oil production was observed.	Hoffman et al. (2016)
Lightstream Resources (2011)	Bakken (View Field, Saskatchewan, Canada)	Natural Gas Cont. Inj.	Oil production increased by approximately 120% at the peak in the 12 months following the start of the injection.	Schmidt et al. (2014)

EOG Resources (2012)	Eagle Ford (n/a)	Natural Gas H-n-P	The estimated recovery increment was between 1.3–1.7 times the primary recovery.	Wang et al. (2017)
EOG Resources (2012)	Eagle Ford (Gonzales County, Texas, USA)	Natural Gas H-n-P	Each cycle resulted in oil production increases. However, the introduction of more lease wells complicated the interpretation of the data.	Hoffman et al. (2016)
EOG Resources (2014)	Bakken (Mountrail County, North Dakota, USA)	CO_2 Cont. Inj.	The objective was to study gas injectivity. CO_2 injectivity was good but experienced an early breakthrough.	Hoffman et al (2016)
EOG Resources (2014)	Bakken (Mountrail County, North Dakota, USA)	CO_2 Cont. Inj.	Results are unavailable	Sorensen & Hamlin (2016)
Whiting Petroleum Corp. (2014)	Bakken (Mountrail County, North Dakota, USA)	Natural Gas Cont. Inj.	All offset wells exhibited increased oil output. However, frac hits and activities in surrounding wells confounded the interpretation of the favorable results.	Hoffman et al (2016)
EOG Resources (2014)	Bakken (Mountrail County, North Dakota, USA)	Water/Field Gas Cont. Inj.	Increased production	Sorensen & Hamlin (2016)
EOG Resources (2015)	Eagle Ford (Gonzales County, Texas, USA)	Natural Gas H-n-P	Gas injection led to a 17% increase in total production after 1.5 years.	Hoffman et al. (2018)
EOG Resources (2015)	Eagle Ford (Gonzales County, Texas, USA)	Natural Gas H-n-P	Gas injection led to a 20% increase in total production after 2.5 years.	Hoffman et al. (2016)
EOG Resources (2015)	Eagle Ford (La Salle County, Texas, USA)	Natural Gas H-n-P	Gas injection led to a 30% increase in total production.	Hoffman et al. (2016)
EOG Resources (2015)	Eagle Ford (Atascosa County, Texas, USA)	Natural Gas H-n-P	Potential increase in production, albeit obscured by production from nearby wells.	Hoffman et al. (2016)
EOG Resources (2015)	Eagle Ford (Atascosa County, Texas, USA)	Natural Gas H-n-P	Inconclusive	Hoffman et al. (2016)
EOG Resources (2016)	Eagle Ford (Gonzales County, Texas, USA)	Natural Gas H-n-P	The reports on incremental oil recovery were encouraging.	Hoffman et al. (2016)
XTO Energy/EERC (2017)	Bakken (Dunn County, North Dakota, USA)	CO_2 Cont. Inj.	Low CO_2 injectivity. Lighter hydrocarbons were preferentially produced.	Sorensen et al. (2018)

2.5   Mechanisms of enhanced oil recovery in unconventional reservoirs

The mechanisms by which injected gas enhances oil recovery from unconventional formations has been a subject of interest as it could determine the best ways to deploy EOR strategies. Hoffman and Rutledge (2019) identified at least nine of the major mechanisms that underly gas huff-n-puff, namely vaporization, viscosity reduction, secondary solution gas drive,

interfacial tension reduction, wettability alteration, oil swelling, pressure support, rock/fluid interactions and injection-induced fractures. The authors quantified the contributions of the first five (5) of the mentioned mechanisms based on a black oil reservoir simulation model (**Figure 6).** The simulation allowed the authors to switch on (and off) the parameters that controlled these mechanisms. The contributions of the mechanisms were evaluated as a function of gas-oil-ratio(GOR). The authors reported that vaporization was the most significant of the five mechanisms examined in this study for high-GOR reservoirs, while oil swelling was the most important for low-GOR reservoirs. In most instances, the role of pressure support was minor and independent of GOR, while the effect of viscosity reduction was only remarkable for low GOR reservoirs but negligible for other types of reservoirs.

The study mentioned above did not include molecular diffusion, possibly because current black-oil simulators are incapable of implementing diffusion. However, diffusion has been identified as one of the primary mechanisms of transport into the low permeability matrix of tight formations. Jia et al. (2018) and W. Yu et al.(2015) observed in their independent reservoir simulation studies that molecular diffusion played a significant role in oil recovery. Jin et al.(2016) in their experimental study, proposed that diffusion was the sole mechanism responsible for CO_2 penetration into the rock matrix, while advection is responsible for transporting gas through the fractures. The team noted other mechanisms, such as oil swelling, also play a role.

It is worth mentioning that several mechanisms work in synergy to improve recovery during CO_2 huff-n-puff. Burrows et al.(2020) and Hawthorne et al.(2013) proposed an integrated mechanism responsible for oil recovery during CO_2 huff-n-puff. They divided the huff-n-puff cycle into four stages, which include injection, early soak, late soak, and production stages. During the injection stage, CO_2 is transported by a high-pressure gradient (viscous forces) through the

fracture networks. Although CO_2 does not penetrate the rock matrices at this stage, secondary fractures may be created during the injection. In the early soak stage, the CO_2 at the matrix-fracture interface penetrates the pores and microfractures due to high pressure. Where the injection pressure is sufficiently high, a low CO_2-oil interfacial tension (IFT) may develop, causing CO_2 to dissolve in the oil phase. The dissolution of CO_2 in the oil phase causes oil swelling (and viscosity reduction), which, in turn, increases the pressure in the pores, creating a local gradient that drives oil into the fractures. Other secondary mechanisms, such as wettability alteration, may also be active at this stage. The authors also noted that diffusion plays a minimal role in this stage. In the late soak period, CO_2 permeates deeper into the pores of the matrix by molecular diffusion as the injection pressure diminishes. Molecular diffusion is driven by the concentration gradient of CO_2 near the fractures and deeper in the matrix. The transport of CO_2 by diffusion at this stage is a slow process that requires long soak periods to observe its effects in the field. In addition, because CO_2 has been in contact with oil for a prolonged time, the vaporization of the lighter hydrocarbons in the oil becomes significant. Furthermore, oil extraction from pores and fractures is still aided by oil swelling and viscosity reduction. Finally, in the production stage, pressure reduction enables CO_2 dissolved in the oil to flow to the fractures and toward the wellbore. When the pressure drops below the bubble point pressure, CO_2 exsolves from the oil, facilitating production by solution gas drive. In addition, because of relative permeability hysteresis, the gas relative permeability is lower during this production step compared to the injection step (at the same gas saturation), allowing for the easier transport of the oil phase.

In summary, molecular diffusion, vaporization, oil swelling, oil viscosity reduction, and pressure support may be the most important primary mechanisms that work synergistically to

recover oil. Although the mechanisms described refer to CO_2, they may also be applicable to other gases as well.
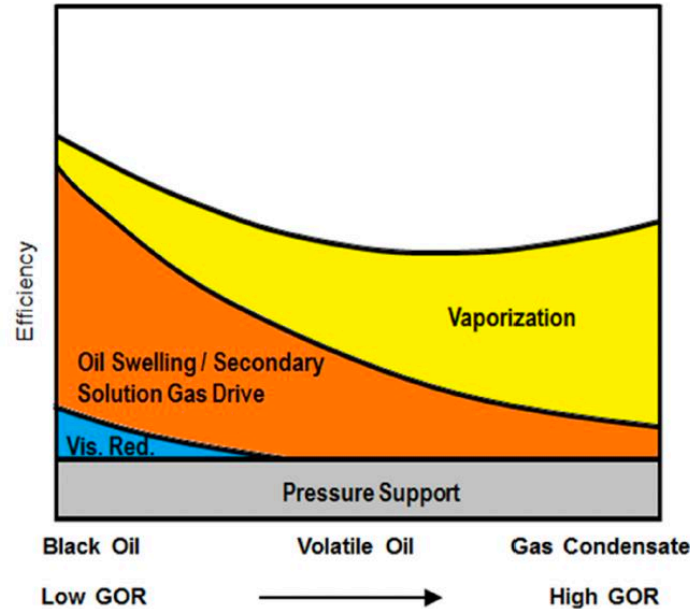
Figure 6: Recovery mechanisms for huff-n-puff gas injection (Hoffman & Rutledge, 2019)

2.6 Pore-scale phenomenon during gaseous solvent huff-n-puff

Understanding the pore scale mechanisms during gaseous solvent huff-n-puff is key to designing better strategies for improving oil recovery from unconventional formations. However, this aspect of the subject has yet to receive widespread attention compared to macro-scale observations. This lack of attention is partly attributed to the challenge in studying shale pores due to their small pore sizes, with average sizes that fall below the resolution of current in-situ imaging technologies. Researchers have thus relied on indirect techniques such as NMR to study pore-scale phenomena in unconventional formations.

Wei et al. (2020) employed NMR to study CO_2 cyclic injection in rock samples from the Lucaogou formation in China. CO_2 injection was conducted at 35MPa and 80°C while

continuously monitoring the oil desaturation process using an online NMR scanner. They reported that CO_2 mainly recovered oil from the large pores while oil in the small pores was not mobilized. The authors deduced from observations of the NMR signals that the primary mechanism varied with the injection cycle. The recovery by the first cycle was driven by diffusion, while recovery by the second stage was mainly due to the pressure gradient during the puff stage.

Zhao et al. (2021) also utilized NMR to investigate the pore scale displacement of oil in tight sandstone cores during CO_2 huff-n-puff. The core samples were obtained from the Chang 8 reservoir in the Henshui field in China. The permeabilities of the core samples ranged between 0.47 and 5.93mD. The authors reported that CO_2 could mobilize crude oil from all pore sizes, although oil could be recovered more quickly from macropores and medium pores. The oil recovery was a function of injection volume and the soak period. When the soak period was increased, the recovery in all pore sizes improved. The authors also indicated that below a threshold injection volume of 1.5 PV, it is nearly impossible to mobilize the oil in the small and micropores. However, above this threshold, CO_2 could effectively extract oil from all pore sizes.

In another study, Ma et al. (2015) investigated the influence of operating parameters on oil distribution in different pore sizes during CO_2 huff-n-puff using NMR technology. The core samples were collected from the Xinjiang Lucaogou formation with permeabilities ranging between 0.03-0.47 mD. An online NMR was used to study the dynamic displacement of fluids during CO_2 injection. The experiments were conducted at a pressure of 43MPa and a temperature of 81°C. The results revealed that oil extraction from the pores occurs sequentially during CO_2 huff-n-puff. During the first cycle of injection, oil is first produced from the macro and medium pores, followed by the small pores, while the oil in the micropores is barely mobilized. In subsequent cycles, production from the macro to medium pores decreases while that from the small

and micropores increases. These studies are examples of the valuable insight that can be gained from studying the pore-scale mechanisms during gaseous solvent huff-n-puff, which warrants applying such techniques to better understand the EOR strategy in unconventional formations.

2.7 Critical operational controls of cyclic gaseous solvent EOR in unconventional formations

Compared to continuous injection, the huff-n-puff mode has several parameters to optimize EOR performance. Some of the critical operating parameters include injection pressure (or volume), soaking time, production period, production bottom-hole pressure and hydraulic fracture properties. In addition, some authors have also investigated the effects of porosity, permeability, and heterogeneity.

2.7.1 Effect of injection pressure

The injection pressure is one of the most important parameters to consider in the design of the gas huff-n-puff for EOR. This is because the interaction of the injection gas with oil is predominantly a function of pressure and temperature. The performance of injected gas is determined by whether it is miscible or immiscible with the oil. Thus, the determination and consideration of the minimum miscibility pressure (MMP) of the gas is a key component in the design of the injection strategy. The MMP is the pressure above which the gas is completely miscible with oil.

Several authors have investigated the effect of injection pressure on gas huff-n-puff EOR performance, both at laboratory and field scales. Li et al. (2017) studied the effect of the injection pressure on CO_2 huff-n-puff EOR in Wolfcamp shale cores. The injection pressures were varied to include pressures below and above the CO_2-Wolfcamp oil MMP. The authors reported that

below the MMP, recovery increased with increasing pressure. However, above the MMP, the recovery tends to level off with increasing pressure. Gamadi et al.(2014) performed huff-and-puff experiments on Mancos and Eagle Ford shale cores. They investigated a myriad of factors, including the effect of injection pressure. They observed that oil recovery increased as pressure increased up to the MMP, and only modest improvements were observed at pressures above the MMP. Hawthorne et al. (2017) and Adel et al. (2018), in similar independent studies, both reported that oil recovery increased with increasing pressures, even beyond the MMP. These reports show the lack of consensus on the effect of pressure on recovery by gas huff-n-puff, especially beyond the MMP.

In a simulation study to investigate CO_2 huff-n-puff in the Bakken formation by Song et al.(2017), a series of simulations with various injection pressures (12.0 MPa, 15.0 MPa, 18.0 MPa, and 21.0 MPa) were studied. The authors reported the recovery factors to be 5.1%, 10.8%, 13.5% and 15.9% of OOIP, respectively. The results indicated that a higher injection pressure leads to higher oil; however, the improvement in oil recovery becomes less significant as the injection pressure is increased beyond 15 MPa. In summary, it is generally agreed that increasing the pressure increases recovery. This increase in recovery with pressure could be due to the increased tendency for the injection gas to invade the small pore. In addition, the solvent strength of injected gas generally increases with pressure, thus the increase in recovery with pressure.

2.7.2 Effect of soak period

The effect of the soak period has been debated in the literature. Some researchers report that a short soak period benefits recovery, while others opined that a long soak period is beneficial to oil recovery. In the study by Gamadi et al.(2014) mentioned earlier, the authors observed that increasing the soaking period increased the recovery factor in both Mancos and Eagle Ford core

samples. This increase in recovery was attributed to the increased mass transfer of CO_2 into oil due to molecular diffusion. In another laboratory core scale study, Song et al.(2017) observed an increased oil recovery when the soak period was increased up to 6 hours, beyond which there was no further benefit. Sanchez-Rivera et al.(2015) conducted a series of reservoir simulations with soak periods of 1, 30 and 100 days. The authors reported that the case with the shortest soak period yielded the highest incremental recovery, which indicates that a longer soak period has little to no benefit on oil recovery. Chen et al. (2013) and Yu et al.(2014) also corroborated this observation. These conflicting results could be attributed to the difference in the length scales studied by the various authors. It appears the effect of the soak period is remarkable at the core scale and less so at the field scale. Secondly, there could be significant variable interactions between the soak period and the parameters such as injection pressure, gas composition and surface area, which have not yet been considered by researchers.

2.7.3 Effect of number of cycles

There appears to be a consensus that the recovery factor per cycle decreases as the number of cycles increases. Thus, there is an optimum cycle number beyond which the oil recovery may not warrant the amount of gas injected economically. In a simulation study by Artun et al.(2011), the authors reported that this optimum cycle number was two to three cycles based on the calculated net present value (NPV). On the contrary, Yu and Chen (2015) observed that oil production continuously increased with more cycles. We note that these two studies were of different length scales and different gas compositions, which may suggest that the effect of cycle number may have interactions with gas composition, length scale, injection pressure, and soak period. The relationship between the number of cycles and the soak period has been considered

in the literature. It has been reported that for a given time length, increasing the number of cycles at short soak periods increases recovery relative to long soak periods (Gamadi et al., 2014).

2.7.4   Effect of production period and depletion rate

A few papers have investigated the influence of the production period on the recovery factor. At the field scale for a fixed total cycle period, prolonging the soak period will mean a shorter production period and vice versa. As mentioned, some authors have reported that a shorter soak and longer production periods benefit oil recovery. Sheng et al. (2016) studied the effects of production time in a reservoir simulation study. Several simulation runs were conducted for 100, 300,350,440 and 600 days while keeping the huff time at 300 days. The authors observed that the oil recovery factor increased when the puff time was increased from 100 to 300 days. However, when the puff time was increased to 350, 450 and 600 days, the additional recovery factors were negligible. The authors observed that, at 100 days, the length of the puff time was insufficient for the reservoir pressure near the well to reach the set bottom hole pressure. After 300 days, the near-well average pressure reached the set bottom hole pressure, leading to incremental recovery. However, prolonging the production time does not benefit further pressure decline, thus no benefit to recovery. The authors concluded that the optimum puff time is the time required for the near-well pressure to reach the set bottom hole pressure.

In a core-scale N_2 huff-n-puff study using Wolfcamp core samples, Yu and Sheng(2015) observed that bleeding the gas at a faster rate (short production period) improved oil recovery from the cores. The researchers noted that shortening the production time implies that more cycles can be performed, leading to increased recovery. In contrast, in a core-scale investigation, Akita et al. (2018) reported that a faster depletion rate resulted in a lower recovery. These contrasting findings

demonstrate the need for further research on the influence of the production period on recovery factors and interactions with other variables.

2.7.5   Effect of exposed surface area

Horizontal well drilling and hydraulic fracturing are the two technological advancements that have made production from unconventional reservoirs possible; both help increase the contact area with the producing formation. Hence, understanding the effect of exposed surface area on recovery by solvent gas injection is critical in designing better EOR strategies.

In laboratory core-scale experiments, the exposed surface area is controlled by the dimensions of the core samples. Mathematically, the smaller the core samples' size, the larger the surface area exposed.   In the literature, gaseous solvent huff-n-puff has been conducted on various core sample sizes ranging from crashed cores to 4-inch diameter cores. Burrows et al.(2020) compiled the EOR performance of CO_2 as a function of exposed surface area for samples from various unconventional formations. The results showed that the larger the exposed surface area, the higher the recovery. For middle Bakken crushed core samples, CO_2 could recover more than 80% of hydrocarbons within two (2) to four (4) hours of exposure and 100% recovery after 24 hours of exposure. However, for larger core samples (1.5-inch diameter and 2-inch length), the recovery factor was reduced to 65-75% with the 24-hour exposure.   Li and Sheng (2016) studied the influence of core size on the performance of CH_4 huff-n-puff in Wolfcamp shale samples. The recovery factors were reported as a function of core diameter (with the length held constant) and core length (with the diameter held constant).   Their results showed that the recovery factor decreased as the core diameter increased. Interestingly, there was no change in the recovery factor as a function of the core length. A plausible explanation for this observation is that the surface

area-to-volume ratio is more sensitive to the diameter of the core than the length of the cores, hence the less impact of the length on the recovery factor.

Yu et al. (2014) performed a field-scale simulation to study the influence of the number of hydraulic fractures on CO_2 huff-n-puff performance. The authors performed sensitivities for one (1) to four (4) fracture stages. Interestingly, their results showed a nonlinear relationship between the fracture stages and recovery factor; the highest recovery factor was achieved with two fracture stages. These surprising results warrant the need for further investigations into the impact of surface area on huff-n-puff EOR performance.

2.7.6   Effect of gas composition

The choice of gas composition is arguably the most important huff-n-puff design parameter. Before reviewing extant literature on gas choice for EOR strategies, it is key to review the properties of gases that make them desirable as EOR agents in unconventional formations.

Fundamentally, gases are preferred to liquids as EOR agents in unconventional formations because of their molecular size. Compared to liquids, the small size of gas molecules allows them to penetrate the nanopores in shales to dislodge the oil trapped in these pores. For perspective, the kinetic diameters of CO_2, methane, ethane, and nitrogen have been measured to be 0.33nm, 0.376 nm, 0.44nm and 0.364nm, respectively. This allows them to easily invade shale nanopores with less than 1nm in size. In addition, their small sizes mean that they have high diffusivity coefficients (according to Knudsen), which further enhances their ability to penetrate small pores in the presence of an occupying fluid (oil). Thus, in general, the smaller the gas molecule, the better its oil extraction potential.

Secondly, gases are preferred to liquids because of their low viscosity, facilitating flow through hydraulic fractures and small pores. For perspective, the viscosities of CO_2 and ethane are about one-seventh that of water. Methane has a lower viscosity than CO_2 and ethane. This low viscosity will allow the gases to flow easily into shales for dislodging trapped oil. However, the viscosity of gases may have the undesirable effect of potentially causing conformance issues during injection.

Third, the ability of the EOR agent to dissolve in the residing oil is critical for EOR in unconventional formations. Therefore, gases that dissolve in oil relatively easily are preferred for enhancing recovery in unconventional formations. The MMP measures the ease with which gases dissolve in oil; the lower the MMP, the easier the gas dissolves in oil and the higher its solvent strength. Although the MMP of the gas varies significantly with oil composition, the MMPs for common EOR gases trend as ethane $< CO_2 <$ methane $<$ nitrogen (Hawthorne et al., 2020). According to this trend, ethane and CO_2 make better EOR agents in unconventional formations than others.

As gases dissolve in oil, secondary effects such as oil swelling and viscosity may arise. Oil swelling facilitates oil recovery by creating a local pressure gradient, causing oil to flow from the pores to the fractures. It has been shown at the laboratory scale that the dissolution of CO_2 and hydrocarbon gases causes significant swelling of oil (Habibi et al., 2017; Mansour et al., 2019). The viscosity reduction of the oil-gas mixture also facilitates the flow of fluids from the pores into nearby fractures. Different gases have different viscosity-reducing effects when dissolved in oil. Li & Luo (2017), in a laboratory study, demonstrated that CO_2 had the largest viscosity-reducing effect on live Bakken oil compared to enriched natural gas, natural gas and nitrogen.

Based on the properties described above, it is expected that different gases will perform differently as EOR agents in unconventional formations. To this end, several authors have conducted experimental and simulation studies to compare the performance of various gases for EOR. Notable amongst them is the work by Jin et al.(2017), who conducted laboratory oil extraction experiments using Lower and Middle Bakken cores and various gases. The goal was to compare the performance of the gases as EOR agents. After 24 hours of exposure, ethane recovered the most oil, followed by CO_2 and methane/ethane mixture. N_2 performed the poorest among the gases. In the Middle Bakken cores, ethane was able to recover 100% of oil within 24 hours of exposure. CO_2, methane, and methane/ethane blend all recovered more than 90% after 24 hours, while N_2 recovered less than 30% of oil from the core samples. In the tighter upper Bakken core samples, CO_2 recovered approximately 30%, methane/ethane blend recovered approximately 25%, methane recovered about 20%, and N_2 recovered a little under 10% (the recovery factor for ethane was not reported for lower Bakken core samples).

Li et al. (2017) compared the effectiveness of N_2, methane and CO_2 as EOR fluids in Wolfcamp shales using laboratory experiments and numerical simulations. In the laboratory experiments, CO_2 resulted in the highest recovery with close to 70% recovery factor. Interestingly, N_2 recovered more oil than methane in both the laboratory experiments and core-scale simulations. However, field-scale numerical simulations showed that N_2 was the worst-performing gas and CO_2 performed best among the three gases.

Alfarge et al. (2018) conducted field-scale simulation studies to compare the recovery performance of rich gas, lean gas, and CO_2 in the Bakken Formation. The authors indicated that the performance of the gases was significantly dependent on the molar diffusivities of the gases in oil since diffusion

was the dominant EOR mechanism. Where field conditions predict higher CO_2 molar diffusivity, it outperformed lean gas and rich gas; otherwise, rich gas was the best choice for EOR.

2.7.7 Effects of petrophysical properties

The influence of petrophysical properties, such as porosity, permeability and lithology, on recovery performance by gas injection is important but has received little attention compared to the aforementioned.

The main petrophysical properties that distinguish conventional from unconventional formations are permeability and, to a lesser extent, porosity. In experimental studies that have used core samples for different formations, there is a clear trend in the recovery factor as a function of permeability (and porosity). One example is the work by Hawthorne et al. (2013), who performed CO_2 oil extraction experiments on middle Bakken, lower Bakken, upper Bakken, and conventional core samples. The conventional core sample had a permeability range between 800 to 1100 mD and 25% porosity. The middle Bakken core samples had permeabilities between 0.002 and 0.04 mD and a porosity range between 4.5 to 8.1%. The lower and upper Bakken samples are the tightest, with permeabilities between 0.001 to 0.0001mD. The experiments were conducted on core samples with various geometries. CO_2 recovered nearly 100% of the oil from the conventional core samples within 4 hours of exposure for cylindrical-shaped core samples. At the same time, CO_2 recovered approximately 70% from the middle Bakken core sample and less than 20% from the lower and upper Bakken core samples. In another experimental study, Jin et al.(2016) conducted extraction studies on lower middle and upper Bakken core samples using different gases. Referencing their results with methane gas, the gas extracted approximately 90% of the oil from the middle Bakken cores, less than 20% from the lower Bakken, and less than 25%

from the upper Bakken samples. These results show that the recovery factor will likely increase with increased permeability, irrespective of the gas composition used.

The trends in the recovery factor mentioned above could also be attributed to lithology. In a follow-up study, Hawthorne et al. (2019) conducted CO_2 extraction experiments on the upper, middle, and lower Bakken and the Three Forks formations from 10 wells. The authors applied statistical data analysis to find the correlation between the various lithological properties and the recovery factor. The authors reported that when all four formations were analyzed as a single population, the total organic content (TOC) and the pore throat radii were sufficient predictors of the recovery factor. The high TOC in the upper and lower Bakken formations makes the rocks hydrophobic. This hydrophobicity implies that oil will be tightly bound to the surfaces of the kerogen and require sufficient energy to dislodge the molecules. The degree of hydrophobicity is also related to the degree of maturity of the kerogen in the formation. Investigations have revealed that the upper and lower Bakken formations have a significant proportion of immature kerogens with relatively higher hydrophobicity than other kerogens(Jin et al., 2017). The middle Bakken, on the other hand, has a negligible proportion of TOC. The higher proportion of immature kerogen and smaller pore throat sizes could explain the low recovery factor in the lower and upper Bakken formations compared to the Middle Bakken.

Another petrophysical property worth mentioning is the presence of natural fractures. Although most tight formations have low permeability matrices, there is often the presence of natural fractures. The natural fractures act as high-conductive pathways through which injected fluid can easily flow and bypass the matrix. Due to the high mobility of gases, the natural fractures cause early breakthrough during solvent injection in nearby wells if these natural fractures are connected to those wells. A 2018/2019 multi-well cyclic gas injection pilot test conducted by

Liberty Resources LLC, in partnership with the Energy and Environmental Research Center (EERC), indicated no significant increase in oil production due to the early breakthrough of the injected gas through nearby offset wells (Katiyar et al.,2019). This early breakthrough could cause an ineffective oil sweep in the matrix (poor conformance). Thus, although gaseous solvent injectivity may be high in the field, there is a need to have some conformance control strategies for effective oil recovery. Some conformance control strategies that have been proposed in the literature include gas-in-water foam injection, co-injection of water and gas, and gels (Salman et al.,2020; Katiyar et al.,2019; Enick et al.,2012).

Chapter 3

Experimental Investigation of Gaseous Solvent Huff-n-puff in the Middle Bakken Formation

3.1　Background

Following the seminal study by Gamadi et al.(2014), several attempts have been made to study influencing factors and understand the underlying recovery mechanism during H-n-P. Optimizing recovery by adjusting operation parameters, such as injection pressure and soak time, has also been a major research priority. Most investigations agree that increasing injection pressure positively impacts oil recovery (Hawthorne et al., 2017; L. Li, et al., 2017; L. Li et al., 2018). However, the same cannot be said about the soak period, and results have been mixed. Studies by Yu and Sheng (2015), Tovar et al. (2014) and Song and Yang (2017) all support the observation that a long soak period improved recovery when CO_2 was used. On the other hand, Shilov et al. (2019) and Sanchez-Rivera et al. (2015) have noted that shorter soak time is more beneficial to oil recovery by CO_2 than more prolonged periods. Although we acknowledge that discrepancies between these results could be due to different rock samples and length scales, it also exposes the lack of understanding of the underlying by which H-n-P enhances recovery. In addition, other influencing factors, such as depletion rate and production period, have not received the needed attention compared to the soak period and injection pressure. It is thus not surprising the H-n-P has not been widely adopted by shale oil producers. Moreover, the few field pilot projects conducted have not yielded encouraging results (Hoffman & Evan, 2016).

A thorough investigation of the existing literature has suggested that CO_2 has been the primary focus of most studies (Burrows et al., 2020). The gas has been favored due to environmental concerns as a greenhouse gas coupled with other favorable properties such as its

solubility in oil and its oil swelling properties. However, alternative gaseous solvents such as ethane (C_2H_6) have shown promise as a recovery agent. Burrows et al.(2020) noted that C_2H_6 possesses superior miscibility properties compared to CO_2. Favorable diffusion coefficients and swelling factors have also been reported (Yang & Gu, 2006). Despite these properties, only a handful of studies have been done to assess the efficacy of C_2H_6 thoroughly. Jin et al.(2017) observed a 100% recovery from a pulverized core sample when C_2H_6 was used as an extraction solvent. Clearly, these results overestimate recovery from tight formations and are likely due to the unnaturally large surface area exposed during extraction; thus, more studies on intact core plugs are warranted.

With CO_2 as the model gas for H-n-P in tight formations in several studies, its performance has been correlated to the injection pressure relative to its minimum miscibility pressure (MMP), and injection above the MMP leads to higher recovery. The question then arises: Can one inject any other gas and expect a similar performance to CO_2 so long as the injection pressure is above the MMP? What is the role of composition-dependent interactions in H-n-P EOR? Are the effects of operating parameters dependent on miscibility conditions and gas composition? These are pertinent questions that need answers for H-n-P EOR to gain widespread adoption.

To this end, in this chapter, we aim to study the viability of CO_2 and C_2H_6 as H-n-P gaseous solvents for enhancing recovery in the Middle Bakken formation. We compare the recovery enhancement performance of the two gases in tight formations in the same set of cores. To the best of our knowledge, a comprehensive comparison of the two solvents in the same set of cores in the Middle Bakken is sparse in the literature. Based on laboratory H-n-P experiments, we investigate the influence of injection pressure (miscibility condition), soak period, surface area to volume ratio and production period on oil recovery. It is worth mentioning that experimental studies on the

effect of the production period in tight formation are lacking, especially for the Middle Bakken formation. The influence of the above-mentioned design parameters is studied, taking into consideration the miscibility conditions of the gases. By so doing, the dependency of the effects of the design parameters on miscibility conditions, the gas composition, and the role of gas composition-dependent mechanisms are better assessed. Again, we know of no extant work in literature that has studied such relationships, and we believe such an approach helps elucidate the recovery mechanism in gaseous solvent H-n-P in unconventional reservoirs.

3.2 Materials and Methodology

3.2.1 Study area and experimental materials

The Bakken Formation is a prolific oil-bearing unconventional formation in the Williston basin. Its area straddles the states of North Dakota, Montana (in the USA), and the province of Saskatchewan (Canada). The formation has been a significant economic resource for these regions. The formation has three principal members: The upper and lower members, which are organic-rich black shales, have extremely low permeabilities(LeFever et al., 1991). The middle member has a lower total organic content and relatively higher permeability, thus the primary target formation for field developments in the Williston Basin.

All core samples used in this study are from the Middle Bakken Formation. Five (5) core plugs were drilled from larger slabs obtained from the Titan F-WP 32-14-H well in the Mondak Field. Core plugs were selected to ensure minimal fractures and fissures that could have been artificially induced. The properties of the cores used in this work are summarized in **Table 4.**

A dead oil sample from the Bakken Formation was used in this study. The dead oil sample has a density of 0.86 g/cc, API gravity of 46.7 and a viscosity of 2.4 cp at 72 °F and 14.7 psi.

The CO$_2$ used in the huff-n-puff experiments is industrial grade with a purity of 99.99% and at a tank pressure of 1000 psi, while C$_2$H$_6$ was obtained at 99.99% purity and a tank pressure of 750 psi. Both gases used were procured from Red River Welder Supply.

Table 4: Identity and petrophysical properties of core samples used in this work.

Core ID	Depth ft.	Diameter cm.	Length cm.	Porosity %	Permeability mD.
MB1	10731	2.5	6.3	7.58	0.261
MB2	11617	2.5	6.7	5.70	0.356
MB3	10716	2.5	6.5	4.00	0.114
MB4	10930	3.81	4.1	3.60	0.457

3.2.2 Experimental procedure

3.2.2.1 *Core cleaning*

After obtaining the core plugs, they were cleaned in a Dean-Stark apparatus. The procedure involves immersing the cores in a toluene vapor for approximately five (5) days to strip off any residual oil and other oil-soluble impurities from the core plugs. Next, the cores were immersed in a vapor of isopropanol to rinse off any toluene. The cores were then dried in an air bath at a temperature of 150°F for 24 hours, after which the core samples' dry weights (W$_{dry}$) were recorded.

3.2.2.2 *Vacuum saturation*

The vacuum saturation setup is illustrated in the schematic in **Figure 7**. The system consists of a high-pressure sample chamber connected to a vacuum pump and an accumulator. The accumulator is connected to a syringe pump, which discharges distilled water below a piston in the accumulator. The accumulator is filled with the dead oil sample above the piston.

As illustrated, the cleaned core samples are placed in the saturation chamber and sealed tightly. The chamber is then vacuumed for six (6) hours to evacuate air from the sample chamber and the core samples' pores. Next, the dead oil is transferred to the evacuated chamber with the aid of the syringe pump until the cores are fully immersed. The pressure in the chamber was increased gradually to 6000 psi and held constant while we monitored the flow rate. The samples were kept under saturation pressure until the flow rate was stabilized, at which point the cores were assumed to be thoroughly saturated. At a pressure of 6000 psi, it takes two to five (2-5) days for the crude oil to adequately saturate the core samples. After the core samples are thoroughly saturated, the saturated weights (W_{sat}) are measured and recorded. The total volume of oil imbibed into the core samples was calculated by taking the difference between the dry weight (W_{dry}) and the saturated weight (W_{sat}) of the core plugs and dividing by the oil's density.
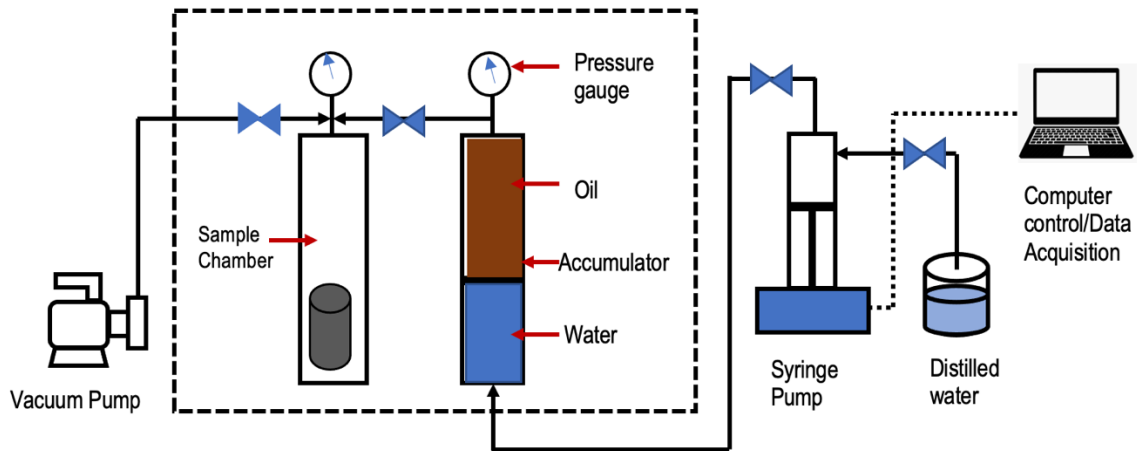
Figure 7: Schematic of the vacuum saturation apparatus used in this work.

3.2.2.3 Huff-n-puff experiments

The H-n-P experiment is designed to simulate matrix-fracture interaction in tight formations. A core sample is placed in the center of a pressure vessel (sample chamber), leaving some annular space around the core. Gas is injected into the annulus such that the core is fully immersed in the injected gas. The core sample simulates the matrix, while the annulus simulates the fractures.

Figure 8 is a picture(a) and schematic (b) of the H-n-P experimental setup and mainly consists of a high-pressure sample chamber, an accumulator, a syringe pump, a gas reservoir, and a temperature-controlled air bath. In addition, pressure gauges are placed at the inlet (top) of the sample chamber and the accumulator to monitor pressure during the experiments.

For one H-n-P cycle, the core sample is positioned in the center of the sample chamber, tightly sealed, and connected to the remainder of the system in the temperature-controlled oven. A sufficient volume of gas is then delivered from the gas tank to the accumulator using the syringe pump. The system temperature is set to 215°F (the reservoir temperature) and allowed to equilibrate for approximately one (1) hour. Once the system is sufficiently equilibrated, additional gas is injected, and the pressure is increased to the design pressure. Next, the inlet valve is closed, and the pressure is held constant for the design soak period. After the design soak period elapses, the accumulator is steadily stepped down to atmospheric pressure over the design production period while the oven is cooled gradually to room temperature, with careful pressure monitoring. The core is then removed, and its weight is recorded as W_i.
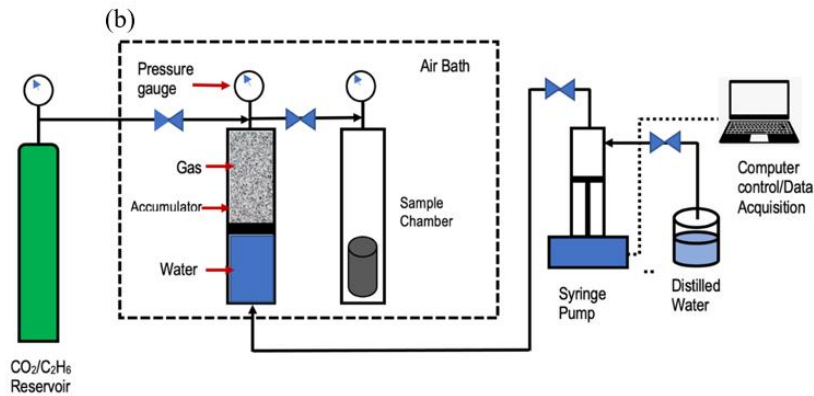
Figure 8: a) Picture and b) Schematic of setup for the solvent huff-n-puff experiments

3.2.2.4 *Summary of workflow*

The apparatus and methods described were used alternately to assess the H-n-P performance of CO_2 and C_2H_6. The workflow is summarized below:

1) The core is cleaned with solvents, dried, and the dry weights (W_{dry}) recorded.

2) The core is vacuum-saturated with dead oil at 6000 psi for 2 -5 days, after which the saturated weight (W_{sat}) is recorded.

3) An H-n-P cycle is conducted at the design injection pressure, soak period, production period, surface-to-volume ratio, and solvent composition.

4) At the end of the cycle, the weight of the core sample is recorded as W_i. The cumulative oil recovery factor (CRF) after each cycle is calculated as follows:

$$CRF = \frac{Wsat - Wi}{Wsat - Wdry} \times 100\%$$

5) Steps 4-6 are repeated for all four (4) cycles for each set of design parameters.

6) Steps 1 and 2 are repeated for another set of experiments after all four (4) cores have been used. The theoretical injection-soak-production cycle is illustrated in **Figure 9**

Table 5: Table of experimental design used in this work.

Experiment ID	Core Sample	Solvent	Miscibility Condition	Soak Period hours	Production Period hours
1	MB1	CO_2	BM	6	6
2	MB2	CO_2	NM	6	6
3	MB3	CO_2	AM	6	6
4	MB1	C_2H_6	BM	6	6
5	MB2	C_2H_6	NM	6	6
6	MB3	C_2H_6	AM	6	6
7	MB1	CO_2	BM	12	6
8	MB2	CO_2	NM	12	6
9	MB3	CO_2	AM	12	6
10	MB1	C_2H_6	BM	12	6
11	MB2	C_2H_6	NM	12	6
12	MB3	C_2H_6	AM	12	6
13	MB1	CO_2	BM	6	12
14	MB2	CO_2	NM	6	12
15	MB3	CO_2	AM	6	12
16	MB1	C_2H_6	BM	6	12
17	MB2	C_2H_6	NM	6	12
18	MB3	C_2H_6	AM	6	12
19	MB4	CO_2	BM	6	6
20	MB4	CO_2	NM	6	6
21	MB4	CO_2	AM	6	6
22	MB4	C_2H_6	BM	6	6
23	MB4	C_2H_6	NM	6	6
24	MB4	C_2H_6	AM	6	6
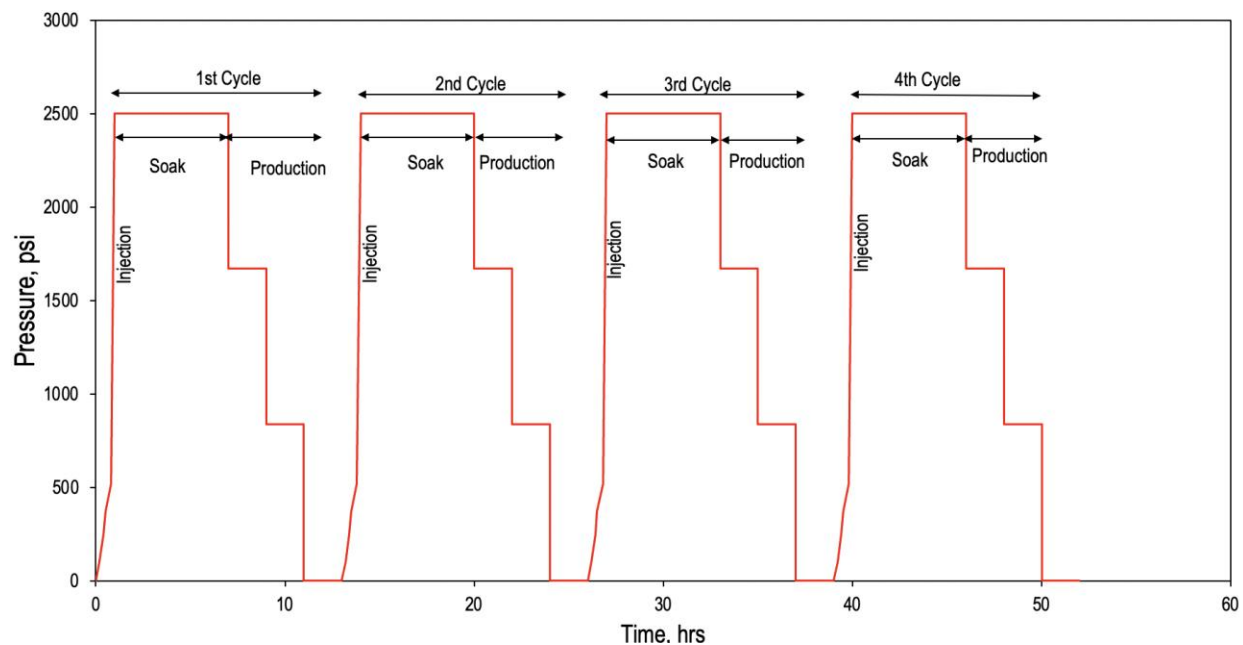
Figure 9: Theoretical pressure profile showing cyclic injection, soak, and production cycles

3.3   Results and Discussions

3.3.1   Recovery factor as a function of miscibility condition and gas composition

Six (6) H-n-P experiments were done to investigate the effects of the miscibility condition and its interaction with gas composition. The operating pressures were chosen to represent the conditions' Below miscibility' (BM), 'Near miscibility' (NM), and 'Above miscibility' (AB), as shown in **Table 4**. The injection pressures will, therefore, depend on the gas compositions. We obtained the MMPs of CO_2 and C_2H_6 from Hawthorne et al. (2017), which are presented in **Table 6**. It is worth noting that we set these parameters based on the first contact miscibility of the gases. The multiple contact miscibility for these gases with Bakken oil has been measured to be lower than the chosen pressures (Green & Wilhite, 2018, p. 288). The soak and production times are constant at 6 hours each, and the cycle number for all experiments is fixed at four (4) cycles.

Table 6: Minimum miscibility pressures and conditions defined for the gases used in this study.
*Obtained from Hawthorne et al. and measured at 230ºF.

Solvent	MMP	Below Miscibility	Near Miscibility	Above Miscibility
	psi	psi	psi	psi
CO_2	2521*	1000	2500	3500
C_2H_6	1358*	500	1500	2500

Figure 10 shows the results of the measured recovery factors for the H-n-P experiments. The results show several vital observations. Firstly, As expected, the recovery factor generally increases with an increase in pressure for both CO_2 and C_2H_6. The recovery factor at AM > NM > BM, irrespective of the gas composition. This observed trend corroborates with results reported by several other authors (Gamadi et al., 2014; L. Li et al., 2017; Meng et al., 2019). As pressure increases, while below the MMP, the injected gas can invade smaller pores with high entry capillary pressure thresholds. Increased pressure to and above the MMP results in a significant drop in IFT to zero and complete gas dispersion in oil. This mixing also results in several secondary mechanisms taking effect, which include oil swelling (Yang & Gu, 2006), viscosity reduction (H. Li et al., 2013) and lighter component extraction (Hawthorne et al., 2013).

As seen more clearly in **Figure 11,** our results also show that, for both gases, an increase in pressure from BM to NM led to a larger increment in recovery factor than from NM to AM. When CO_2 is injected, an increase in the pressure from BM to NM results in ≈18% improvement in the recovery factor, whereas an increase in pressure from NM to AM results in ≈13% increase in the recovery factor.
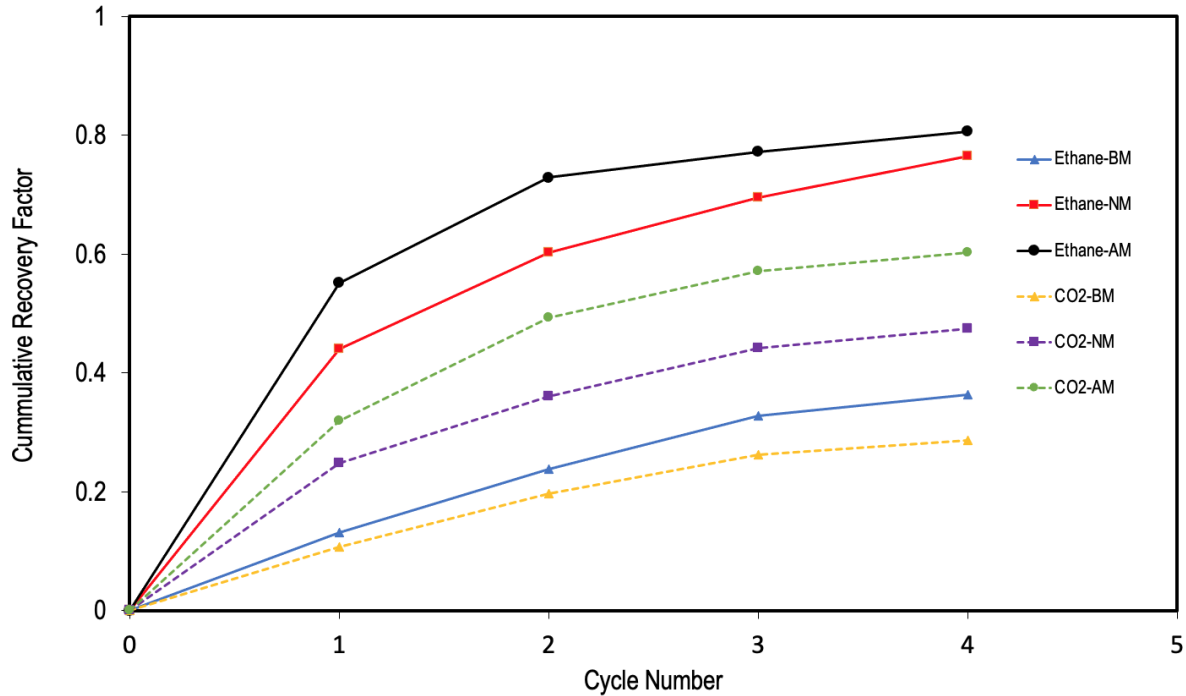
Figure 10: Recovery performance of ethane and CO₂ as a function of miscibility condition. All experiments are conducted with 6 hours soak period, 6 hours production period and a temperature of 215°F.

For C_2H_6, going from BM to NM resulted in a ≈40% increase in recovery factor, but only a modest ≈5% improvement in recovery factor was realized when the pressure was increased from NM to AM. The increase in recovery factor per psi pressure has been a subject of interest in H-n-P studies. In their H-n-P studies in Wolfcamp core samples, Li et al.(2018) observed an improvement in recovery factor with increased pressure for pressure ranges below the MMP. Beyond the MMP, oil recovery leveled off or improved modestly depending on the permeability of the cores. In other studies, Hawthorne et al. (2017) and Tovar et al. (2018) reported a continuous recovery increase as the pressure increases beyond the MMP. The former attributed this observation to the low permeability of the core sample, which causes a substantial pressure drop on the surface of the core. The results support this theory. Thus, even at or beyond the MMP, miscibility is not achieved

uniformly throughout the core sample. As a result, the residual oil at the center of the core becomes inaccessible despite any further increase in pressure.
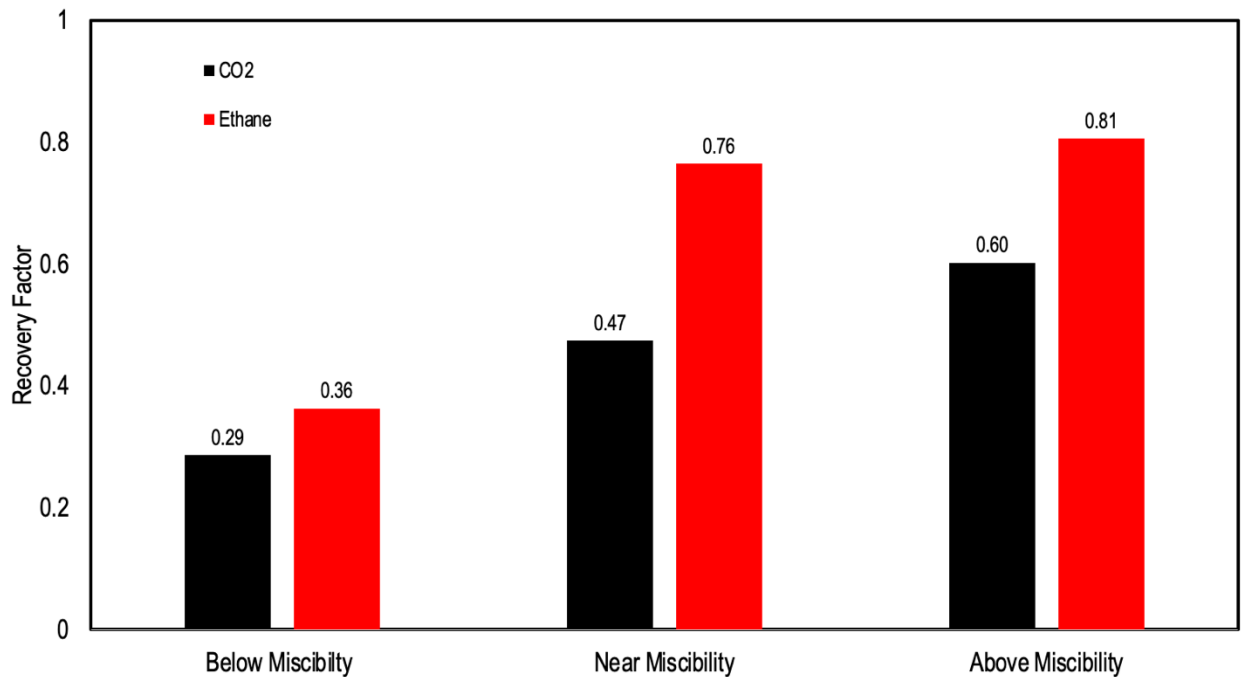
Figure 11:Terminal recovery factors for CO_2 and C_2H_6 at various miscibility conditions over a 6-hour soak and production period.

Although C_2H_6 performs better under all miscibility conditions, the performance difference varies with the miscibility condition. At BM conditions, C_2H_6 recovered only $\approx 7\%$ more oil than CO_2. Contrarily, C_2H_6 recovered around 30% more oil than CO_2 under NM conditions and about 20% more oil than CO_2 under AM conditions. This finding implies that, under BM conditions, the effect of gas composition is diminished. Under BM conditions, the injected gas displaces the oil immiscibly, and the principal forces at play during immiscible displacement are advective forces provided by the piston-like displacement from pore to pore. Due to the high interfacial tension, there are limited molecular interactions between the displacing gas and the displaced oil (except at the interface). Therefore, the composition of gas becomes irrelevant. At

NM conditions, the distinction between the gases becomes apparent as the effect of molecular interactions begins to become relevant. The mechanism of recovery by which CO_2 varies from that of C_2H_6. CO_2 may interact with oil by extracting lighter oil components from the pores, facilitating oil recovery.

3.3.2 Influence of the number of cycles and its dependency on miscibility condition

The number of cycles is essential to optimizing the H-n-P injection scheme as it directly relates to the volume of gas utilized. Sensitivity analysis was not carried out specifically to study the effect of the number of cycles, as the number of cycles was fixed at four (4) cycles for all experiments. However, specific key observations are worth mentioning.

Figures 12 a through c are presented to identify observable trends in the relation between the cycle number and recovery at different miscibility conditions. The cycle number is plotted against the normalized recovery (as bar graphs) and cumulative normalized recovery (as line graphs). It is to be noted that the normalized recovery here is defined as the volume of oil recovered during the cycle as a proportion of the total volume of oil recovered. These definitions are to be differentiated from the recovery factor, which is the volume of oil recovered as a proportion of the total pore volume.

First, we observe that the first cycle recovered the most oil while recovery continuously decreased with successive cycles. This trend was observed for both gases and under all miscibility conditions. The behavior has also been reported in extant literature (Gamadi et al., 2014; L. Li et al., 2019b). Initially, the injected gas contacts and displaces oil in easily accessible pores, which consist of large to medium-sized pores. Since these pores contain a large volume fraction of the

oil, the initial cycle interacts with and displaces the large volume. In subsequent cycles, the injected gas would have to access more difficult-to-reach pores containing a smaller fraction of the oil.

Figure 12a reveals that the behavior described above under BM conditions is less apparent, and the oil recovery rate is gradual compared to NM and BM conditions for both. However, under NM and AM conditions, the initial cycles recover significantly more oil than subsequent cycles. For example, for CO_2 under BM conditions, the first two cycles recovered ≈68% of recoverable oil, but under AM conditions, the first two cycles recovered ≈81% of the total volume recovered. A similar observation was made for C_2H_6, as shown in **Figure 12b and c**. This observation indicates that the injected gas can only penetrate a limited pore volume per cycle under BM conditions. Because there is no mixing, the injected gas merely displaces the amount of oil it immediately contacts. On the other hand, under NM and AM conditions, owing to dispersion and molecular diffusion, the injected gas can contact a wider range of pore sizes, thus displacing a larger volume of oil in the first few cycles compared to BM conditions.

In addition, we note that CO_2 and C_2H_6 behaved similarly in terms of oil recovery per cycle under BM conditions. Under AM conditions, the distinction between the two gases is more pronounced. C_2H_6 recovered more oil (≈90% normalized recovery) during the first two cycles compared to CO_2(≈81% normalized recovery). This observation may imply that C_2H_6 has superior recovery-enhancing properties at miscibility conditions compared to CO_2. Yang and Gu (2006) noted that C_2H_6 has superior oil swelling and diffusion properties in oil than CO_2. These properties could partly explain the ability of C_2H_6 to recover more oil than CO_2.
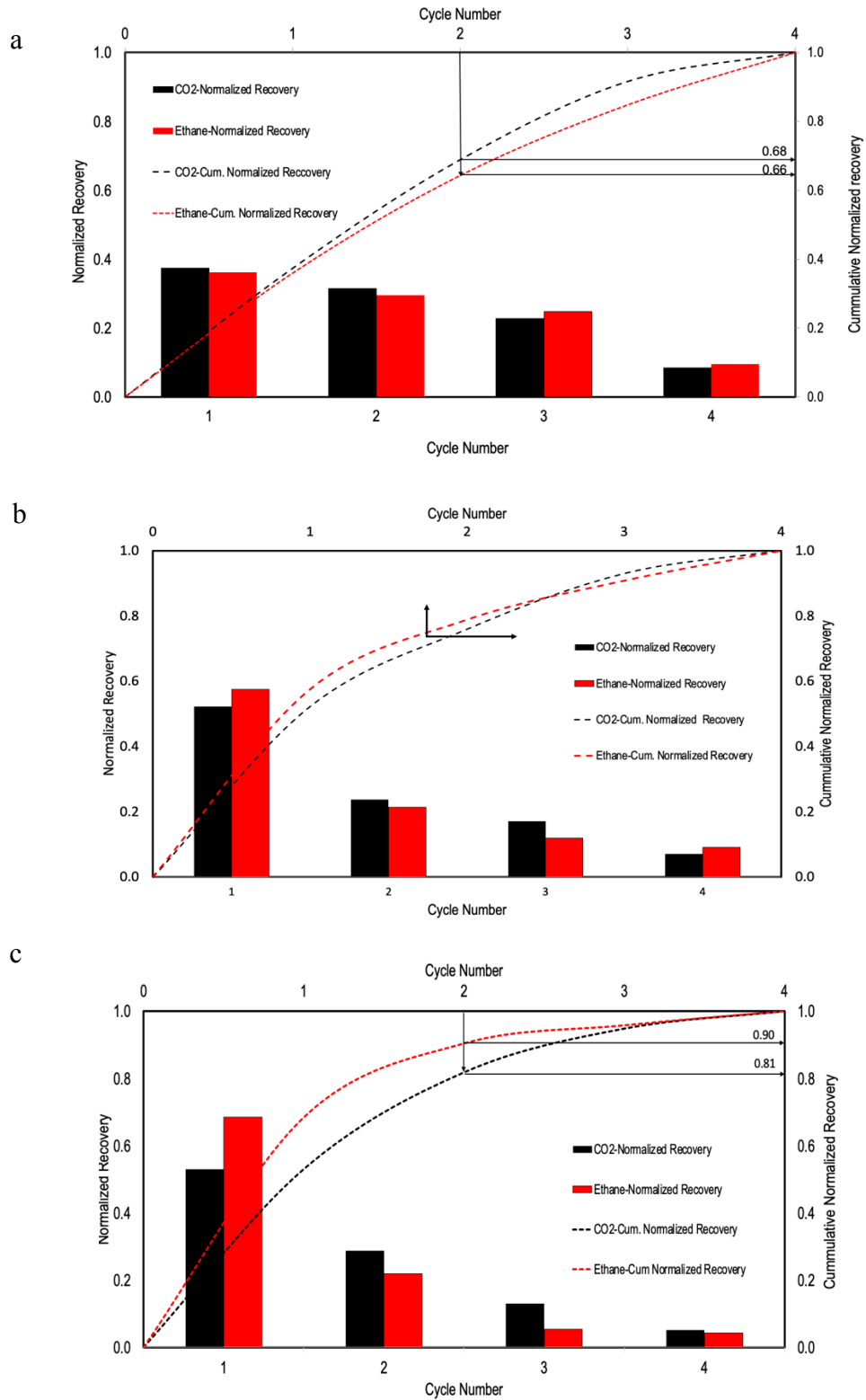
Figure 12: Normalized and cumulative normalized recovery versus cycle number for different miscibility conditions. a) Below b) Near c) Above miscibility conditions.

3.3.3 Influence of soaking period and its dependency on miscibility condition

As already mentioned, the effect of the soak period on cyclic gas injection performance has been a subject of interest in several studies, and results have been mixed. To investigate the impact of the soak period and its dependency on miscibility condition (and gas composition), six (6) laboratory scale H-n-P experiments were carried out with soak periods set to 12 hours for CO_2 and C_2H_6 at BM, NM and AM conditions. The production periods were all fixed at 6 hours.   The data is then compared to previously described experiments conducted at 6-hour soak periods.

The results are presented in **Figure 13.** As seen from the figure, there are no remarkable differences in the recovery factor for short (6 hours) and long (12 hours) soak periods under BM conditions. This finding holds for both the CO_2 and C_2H_6 experiments. On the other hand, there is a significant difference in recovery factor at NM and AM conditions (compared to shorter soak periods for the same gas compositions). For CO_2, there was $\approx5\%$ improvement in recovery factor under NM conditions and $\approx10\%$ under AM conditions. For C_2H_6, there was an improvement of $\approx4\%$ under NM conditions and $\approx7\%$ under AM conditions.

The increase in recovery factor with prolonged soak periods has been attributed to diffusion (Gamadi et al., 2014; Jin et al., 2017). When gas molecules contact oil at the fracture-matrix interface (surface of the core sample), the molecules move from the region of higher concentration to a region of lower concentration until a dynamic equilibrium is established. The movement of molecules allows the gas to access deeper pores within the matrix, which will otherwise not be directly accessible. Diffusion is time-dependent; thus, the longer the contact time, the further the molecules can travel. This implies that a longer soak time allows molecules to diffuse deeper into oil-filled pore spaces and enhance the microscopic sweep. The results at BM conditions show that

diffusion is negligible. For molecular diffusion (differentiated from self-diffusion) to be initiated, the gas and oil should be miscible, which doesn't happen under BM conditions. It is evident from the findings that a prolonged soak period results in a superior microscopic sweep under NM and AM conditions where oil and gas become miscible, and the influence of diffusion is noticeable.

Under NM and AM conditions where diffusion mechanism plays a significant role, C_2H_6 outperformed CO_2 at extended soak periods; C_2H_6 achieved ≈80% and ≈88% under NM and AM, versus ≈52% and ≈70% by CO_2 under NM and AM, respectively. In fact, injection C_2H_6 at AM condition for 24 hours achieved the highest recovery among all experiments. As indicated, the literature has already reported that C_2H_6 has a superior diffusion coefficient than CO_2. In our opinion, this may partly contribute to ethane's superior performance during prolonged soak times. However, given that CO_2 had a better recovery factor (over a shorter soak period for the same gas composition), a more extended soak period will be economically more beneficial for CO_2 than C_2H_6.
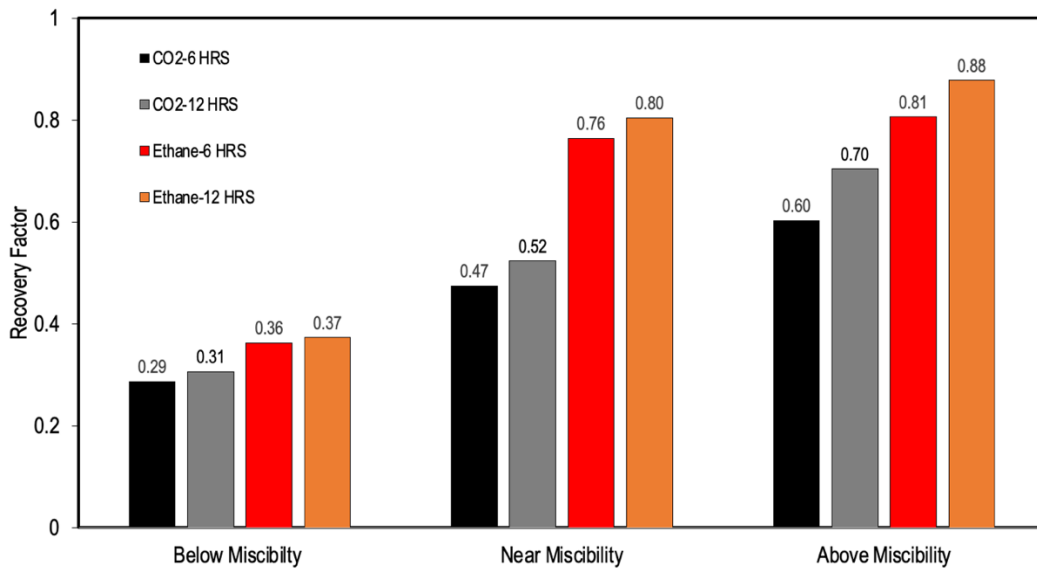
Figure 13: Effect of soak period under different miscibility conditions and gas compositions

3.3.4 Influence of production period and its dependency on miscibility condition

Although the production (puff) period has been recognized in literature to influence H-n-P performance at the field scale, there is a paucity of experimental data on its influence at the core scale (Fragoso et al., 2018; Kong et al., 2016). Therefore, to study the effect of the production period in this work, six experiments were carried out at 12-hour production period under BM, NM, and AM conditions and for CO_2 and C_2H_6. At the end of the design soak period, the pressure in the accumulator is stepped down at a rate of three equal pressure steps per time. This was done to replicate the pressure reduction in the field as closely as possible. The results are presented in **Figure 14.**

The results show that, at the core scale, the recovery factor was not affected by the puff period under BM and NM conditions, irrespective of gas composition. Surprisingly, under AM conditions, the influence of the puff period was quite noticeable. Under AM conditions, CO_2 achieved $\approx$4% higher recovery factor at 12 hours puff time compared to 6 hours puff time, while C_2H_6 achieved $\approx$5% higher recovery factor.

Under miscible conditions, gas is dissolved in oil. As the pressure declined, the expansion of the gas drives oil to the surface. Under AM conditions, a larger volume of gas is dissolved in oil, requiring more time for complete exsolution from the bulk oil phase. Thus, the more time that is allowed, the more oil is recovered.   In their work, Akita et al. (2018) also reported an increase in recovery factor when the depletion rate was reduced (i.e., increased puff period). They attributed this finding to the so-called "choke effect," which describes the loss of pore connectivity after a sudden pressure drop caused by physical closure and two-phase blockage. A gradual reduction in pressure may prevent the choke effect and enhance production. Sheng (2020, p. 24) proposed a gas bubble nucleation mechanism to explain the direct relationship between depletion rate and

recovery factor. Under miscible conditions, as pressure is depleted, exsolution of the gas is initiated, and small gas bubbles begin to nucleate in the bulk oil phase. These droplets then diffuse in the bulk oil phase until they coalesce with other droplets to form larger gas bubbles. The authors explain that this coalescence into large gas bubbles is detrimental to recovery as large gas bubbles are likely to bypass oil. This phenomenon could explain the lack of improvement in recovery with pressure decline from the NM pressure condition. At AM conditions, a similar mechanism may be playing a role. However, during pressure decline from a pressure value higher than the MMP, the fluid is still in a condition where IFT is still low. Sohrabi et al.(2008) reported that at low oil-gas IFT conditions, when large gas bubbles bypass oil-containing pores, oil could still be transferred to the gas and be produced to the surface. We believe this mechanism may also contribute to high recovery at AM; however, we recommend further studies to ascertain this mechanism in tight formations.
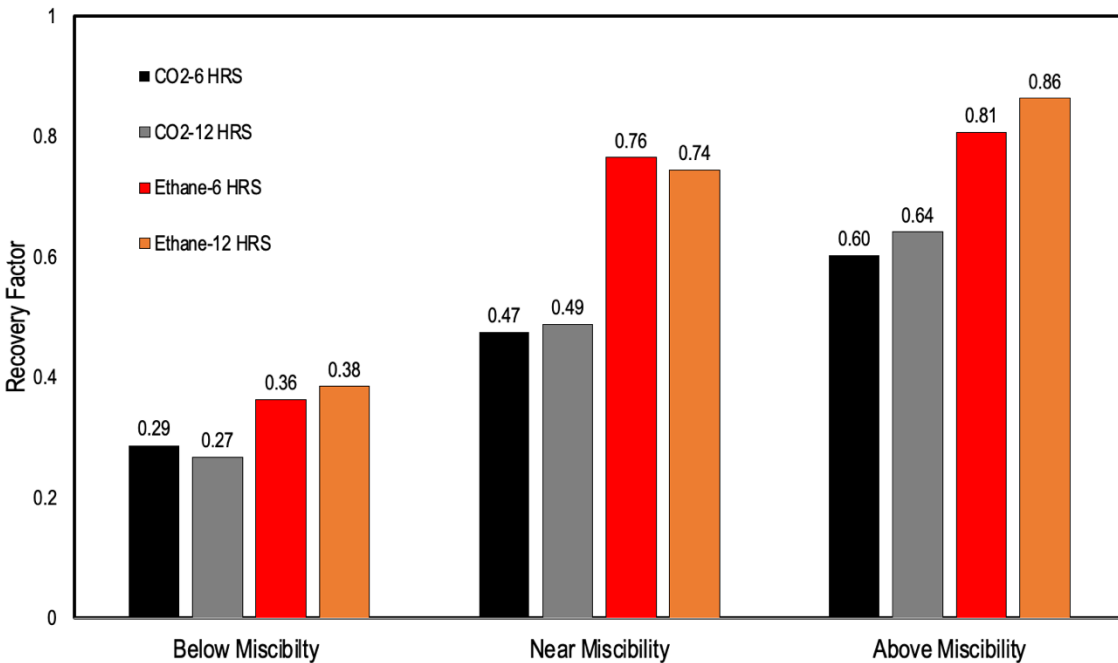
Figure 14: Effect of production time on recovery at different miscibility conditions and gas compositions

3.3.5 Influence of rock surface area-to-volume ratio and its dependency on miscibility condition

Production from tight formations primarily depends on the matrix volume exposed to hydraulic fractures. Therefore, as much as possible, tremendous effort is dedicated to ensuring that a high fracture surface area is achieved in the hydraulic fracture operation and design. Questions have often arisen about the effect of exposed rock surface area-to-volume ratio (SA/V) on EOR performance, which may also determine if refracturing is required for efficient recovery (Hejazi et al., 2017). In laboratory core-scale experiments, the SA/V is controlled by the core size (Chaisoontornyotin et al., 2019; L. Li & Sheng, 2017). We use two core sizes in this work, as presented in **Table 4.** Six (6) experiments using core sample MB4 with a SA/V of 3.6 in^2/in^3 were conducted under BM, NM, and AM conditions with both CO_2 and C_2H_6 to better understand the impact of rock surface area-to-volume ratio on EOR performance.

As seen from the results in **Figure 15,** the core samples with lower SA/V generally resulted in a decreased oil recovery factor. Under BM and NM conditions, there is a considerable difference in recovery factors. Under BM conditions, the recovery was reduced by $\approx$8% and $\approx$4% for CO_2 and $C_2H_6,$ respectively, compared to recovery from 4.8 in^2/in^3. Likewise, under NM conditions, the recovery factors decreased by $\approx$4% and $\approx$2% for both CO_2 and $C_2H_6,$ respectively. Under AM conditions, the effect of SA/V is less conspicuous; recovery by CO_2 was reduced by a meager $\approx$2% and by $\approx$1% with $C_2H_6.$ These observations also indicate that the effect of SA/V seems to diminish with increased injection pressure. In addition, the impact of SA/V is much more significant for CO_2 than for $C_2H_6.$

According to Darcy's flow model, the flow rate is expected to increase as the flow area increases, thus the increased recovery at high SA/V. In radial flow geometry, as present in our

core-scale experiment, a reduction in the radius (increase SA/V) results in an increased pressure gradient (dP/dr), which increases flow out of the core. Second, according to Fick's law, a decrease in surface area impacts the diffusive flux of gas molecules into the core. Under BM conditions, diffusion tends to play a minimal role in the recovery; thus, we can deduce that the reduction in recovery may be primarily due to the increased pressure gradient. However, although diffusion plays a role at NM and AM, gas dissolution in oil also occurs. Other mechanisms, such as oil swelling, lighter component extraction and viscosity reduction, may play significant roles. The surface area less influences these mechanisms and may explain the lack of significant difference in recovery under AM conditions since these mechanisms have a more considerable influence. Our results suggest that injecting gases at higher pressure may compensate for a reduced simulated reservoir volume (SRV) in the field. However, more studies at the field-scale are recommended to ascertain this conclusion.
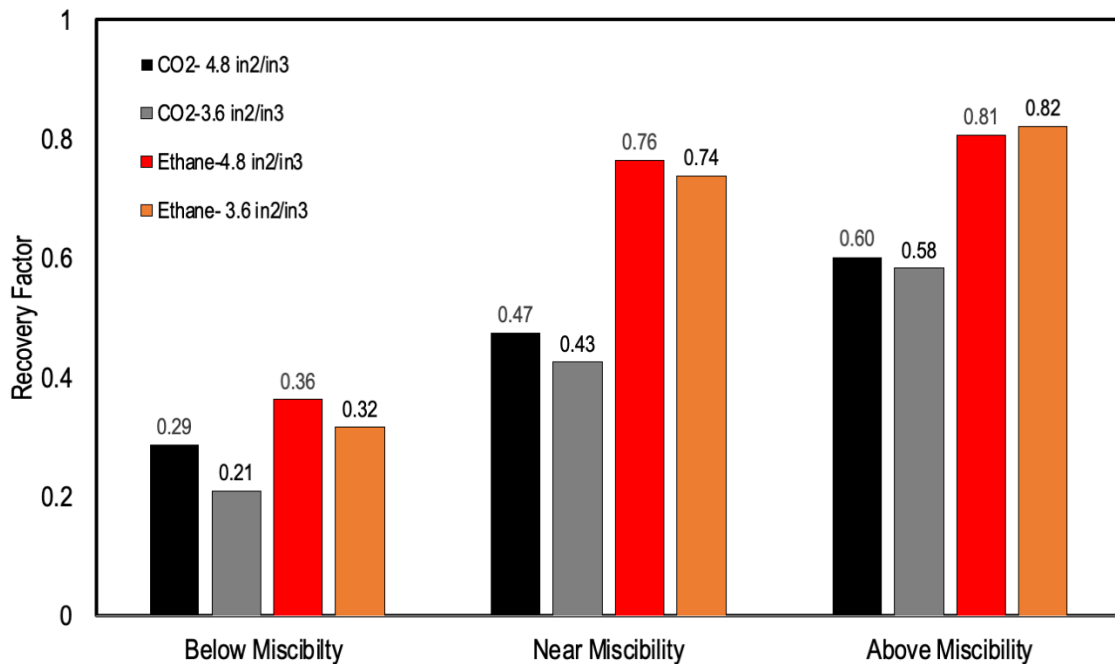
Figure 15: Influence of surface area on recovery at different miscibility conditions and gas composition

3.4 Conclusion

A core-scale study has been conducted to investigate the efficacy of CO_2 and C_2H_6 as H-n-P gaseous solvents for improving recovery in the Middle Bakken Formation. First, we investigated the recovery improvement performance of the two gases in the same set of tight formation cores. In addition, the effect of injection pressure, soak time, surface area to volume ratio, and production time on oil recovery was investigated. Some of the key findings are summarized as follows:

1)   For both CO_2 and C_2H_6, the recovery factor generally increases as pressure increases. Regardless of gas composition, the recovery factor at AM > NM > BM increases, though this increase is not linear. The results show that increasing the pressure from BM to NM increased the recovery factor more than increasing the pressure from NM to AM.

2)   Although C_2H_6 performed better under all miscibility conditions, the performance gap differed depending on the miscibility condition. The disparity in performance was least under BM conditions and largest under AM conditions.

3)   The initial cycles recovered the most oil for all experiments, while recovery continuously decreased with successive cycles. The behavior was less pronounced under BM conditions but was more noticeable under NM and AM conditions.

4)   The influence of the soak period was dependent on the miscibility condition and gas compositions. The soak period had a minor impact under BM and NM conditions but a remarkable influence under AM conditions, where a prolonged soak period significantly increased recovery.

5)   The influence of the production period was also dependent on miscibility at the core scale. Our results indicated that the recovery factor was not affected by puff period under BM and NM

conditions, irrespective of gas composition. However, under AM conditions, the influence of the puff period was quite noticeable.

6)   In general, core samples with lower SA/V generally resulted in a decreased oil recovery factor, although the influence of SA/V is dependent on miscibility conditions; there is a pronounced effect under BM and NM circumstances but a less remarkable impact under AM conditions.

7)   Finally, C_2H_6 outperforms CO_2 even if miscibility conditions are factored in. These findings suggest that unique gas-oil interactions (such as diffusion rates, oil swelling, component extraction etc.) that are solely dependent on gas composition may play an essential role in recovery by gas huff-n-puff.

It is worth mentioning that there were some limitations to this work. First, although the core samples were selected in close vicinity of each other, heterogeneities are present, as shown by the variations in the porosity and permeability values in **Table 4**. These heterogeneities may influence the conclusions of this work. In addition, the re-use of core samples and the cyclic saturation and desaturation may alter core properties due to hysteresis and physical damage to the samples, which could affect the conclusion of this work (Badrouchi et al., 2022). Secondly, we used a dead oil sample with a different composition than live oil at reservoir conditions; thus, we caution against extrapolating the results presented to the reservoir scale. Thirdly, cooling the core samples from reservoir temperature to room temperature to allow for weight measurements is not representative of field conditions. In reality, the reservoir temperature remains constant during production. Finally, this experimental procedure does not include confining pressure to simulate the subsurface stresses, which may also impact recovery. These limitations notwithstanding, we believe the

results can help better understand and design enhanced oil recovery strategies in unconventional

reservoirs.

Chapter 4

A Pore Level Experimental Investigation of Gaseous Solvent Cyclic Injection for Enhanced Oil Recovery in the Bakken Formation Using Nuclear Magnetic Resonance Relaxometry

4.1   Introduction

Understanding the pore-level mechanisms is critical in elucidating the mechanisms by which any EOR strategy improves recovery. Recent advances in rock imaging technologies, such as MicroCT technology, have enabled pore scale studies in conventional formations. Using MicroCT technology, Akindape et al. (2022) used the technology to study the mechanism by which carbonated water injection enhances recovery in carbonate reservoirs. By studying the pore-level fluid occupancy during carbonated injection and directly measuring contact angles in situ, the authors deduced that wettability alteration was a dominant mechanism for enhancing recovery. Several other authors have also applied such advanced techniques to study various EOR strategies (Ekechukwu et al., 2021; Igwe et al., 2022; Mohamed et al., 2020). However, it is worth noting that the modern MicroCT has a resolution between 50-100μm (Reedy & Reedy,2022). The typical shale constitutes a wide distribution of pore sizes ranging from nano to micro to macropores, and a large portion of the pores may fall below the resolution. Therefore, it is apparent that the MicroCT is inadequate to study mechanisms in shales and tight samples. Nuclear magnetic resonance (NMR) technology provides an alternative means to study pore scale phenomena in tight formations.

NMR is typically used to examine the dispersion of fluids containing hydrogen in porous media (Xiao et al., 2018). When a fluid containing hydrogen is placed in a porous medium, the nucleus of hydrogen in the fluid undergoes transverse relaxation (Cannon & Minh, 1998). The

length of the transverse relaxation time (T_2) corresponds to the pore size. Consequently, the T_2 spectrum distribution also reflects the pore size distribution; thus, the NMR method can be utilized to determine the pore size distribution. The technique has been applied to study the pore level sweep efficiency of CO_2 in Henshui reservoir sandstone in China (Zhao et al., 2021). Song et al. also used NMR relaxometry to compare the EOR potential of CO_2 and N_2 in tight samples in the Songliao Basin.

In this work, we employ NMR relaxometry to investigate the pore scale sweep efficiency of two gaseous solvents, CO_2 and ethane, in the Bakken formation. To the best of our knowledge, a comparison of CO_2 and ethane in Bakken formation at the pore level using indirect NMR relaxometry is sparse in the current literature. Tight core plugs from the Middle Bakken formation were collected, cleaned and vacuum-saturated with oil from the same formation. Then, their initial pore size distributions (PSD) were measured using NMR. Following initial PSD measurement, CO_2 and ethane H-n-P experiments were carried out in the cores at different miscibility conditions and operating parameters. All investigations are conducted at the reservoir temperature of 215°F. Then, the cores' fluid distribution (PSD) is measured by recording the NMR T_2 distribution after the H-n-P experiments. By comparing the initial PSD and the PSD after H-n-P, the recovery efficiency of the H-n-P experiment in specific pore sizes can be ascertained. In addition, the effects of miscibility condition (injection pressure), soak period, production period and rock surface-to-volume ratio on pore-level sweep efficiency are assessed and discussed.

4.2   Materials and Methodology

4.2.1   Materials

The Bakken Formation in the Williston Basin is a prolific oil-bearing unconventional formation. It is a crucial economic resource that straddles the states of North Dakota and Montana in the USA and the province of Saskatchewan in Canada. The formation consists of three primary members: the Upper and Lower members, which are organic-rich black shales with low permeabilities (LeFever et al., 1991), and the middle member, which has lower total organic content and significantly greater permeability. Owing to their relatively higher permeability, the middle member has been the target formation for field operations in the Williston Basin.

All of the core samples utilized in this research are from the Middle Bakken Formation. Three (3) core plugs were drilled from larger slabs obtained from the Mondak Field Titan F-WP 32-14-H well. The core plugs were carefully selected to ensure that the chosen plugs have minimal artificially induced fractures and fissures. **Table 7** summarizes the properties of the cores used in this research.

A dead oil sample from the Bakken Formation was utilized for this study. The density of the dead oil sample is 0.86 g/cc, its API gravity is 46.7, and its viscosity at 72 °F and 14.7 psi is 2.4 cp.

The gaseous solvents used in this work were supplied by Red River Welder Supply Co. The CO_2 had a purity of 99.99% and a tank pressure of 1000 psi. The ethane was obtained with a purity of 99.99% and a tank pressure of 500 psi.

Table 7: Identity and petrophysical properties of core samples used in this work.

Core ID	Depth ft.	Diameter cm.	Length cm.	Porosity %	Permeability mD.
MB1	10731	2.5	6.3	7.58	0.261
MB2	10716	2.5	6.5	4.00	0.114
MB3	10930	3.81	4.1	3.60	0.457

4.2.2 Experimental Procedure

4.2.2.1 Core cleaning

After drilling out the core plugs, they were cleaned using a Dean-Stark apparatus. First, the cores are submerged in toluene vapor for approximately five(5) days to remove any remaining oil and other oil-soluble impurities from the core plugs, after which the cores are submerged in isopropanol vapor to remove any remaining toluene. Finally, the core samples are dried in an air bath at 150°F for approximately 24 hours.

4.2.2.2 Vacuum saturation

After the core plugs are cleaned and dried, they are saturated with oil in a vacuum saturator. The schematic for the vacuum saturation apparatus is depicted in **Figure 7.** The system includes a high-pressure sample chamber, a vacuum pump, and an accumulator. The accumulator is connected to a syringe pump that dispenses distilled water beneath the accumulator's piston. The accumulator is filled with the dead oil sample above the piston.

The core samples are placed in the saturation chamber and sealed tightly. The chamber is then evacuated for approximately two (2) hours. Next, the dead oil is transferred to the evacuated chamber with the aid of the syringe pump until the cores are fully immersed. Then, the pressure in the chamber is increased gradually to 6000 psi and held constant while the flow rate is continuously monitored. The samples were kept under saturation pressure until the flow rate was stabilized, at

which point the cores were assumed to be thoroughly saturated. At a pressure of 6000 psi, it takes two to five (2-5) days for the crude oil to saturate the core samples adequately.

4.2.2.3 *Huff-n-puff experiments*

The purpose of the H-n-P experiment is to simulate matrix-fracture interaction in tight formations (Iraji et al., 2015). The core sample simulates the matrix, while the annulus represents the fractures. First, the core sample is placed in the middle of a pressure vessel (sample chamber), leaving annular space around the core. Then, gas is injected into the annulus to submerge the core in the injected gas fully. **Figure 8** is a schematic of the H-n-P experimental setup, which mainly consists of a high-pressure sample chamber, an accumulator, a syringe pump, a gas reservoir, and a temperature-controlled air bath. In addition, pressure gauges are placed at the inlet (top) of the sample chamber and the accumulator to monitor pressure during the experiments.

For one H-n-P cycle, the core sample is positioned in the center of the sample chamber, tightly sealed, and connected to the remainder of the system in the temperature-controlled oven. A sufficient volume of gas is then delivered from the gas tank to the accumulator using the syringe pump. The system temperature is set to 215°F (the reservoir temperature) and allowed to equilibrate for approximately one (1) hour. Once the system is sufficiently equilibrated, additional gas is injected, and the pressure is increased to the design injection pressure. Next, the inlet valve is closed, and the pressure is held constant for the design soak period. After the design soak period elapses, the accumulator is steadily stepped down to atmospheric pressure over the design production period while the oven is cooled to room temperature with careful monitoring of vessel pressure. The core sample is removed, and its NMR T_2 distribution spectrum is measured.

4.2.2.4 Nuclear magnetic resonance

As previously stated, NMR is utilized to determine the distribution of pore fluids in porous media. The NMR apparatus initially applies a permanent magnetic field that polarizes the hydrogen nuclei in the sample. This source of the hydrogen nuclei is typically the fluids contained within the pores. Then, a series of high-frequency magnetic pulses are used to realign the nuclei, which creates a magnetic moment or spin (Coates et al., 1999). The spinning protons emit magnetic signals as they return to their original state after being stimulated by an applied magnetic field. A receiver detects the decay of this magnetic signal in the transverse direction and quantifies the transverse magnetization decay signal, $M_{i(t)}$, at discrete time slots and for constant time spacing. Then, the sum of the decaying signals, $M_{i(t)}$, is computed by the exponential decay formulation.

$$M_{i(t)} = \sum_{i=1}^{N} A_i e^{\left(\frac{t}{T_i}\right)}$$

Equation 2

Where N is the number of T_2 relaxation values, A_i, is the amplitude of each relaxation (depending on the number of protons in the pores of the sampled size), and T_i, is the decay time constant.

The measured T_2 signal is a composition of the three relaxation mechanisms in a magnetic field, which are bulk relaxation, surface relaxation, and diffusion-induced relaxation (D), as expressed as

$$\frac{1}{T_2} = \frac{1}{T_{2\_bulk}} + \frac{1}{T_{2\_surface}} + \frac{1}{T_{2\_D}}$$

Equation 3

Where T_{2_bulk} is the transverse relaxation time due to bulk relaxation of the pore fluid, $T_{2\_surface}$ is the transverse relaxation time due to surface relaxation, and T_{2_D} is the relaxation time due to diffusion in the magnetic field gradient. The relaxation mechanisms relate to the fact that

the signal decay depends on the location of the hydrogen nuclei. The nuclei in the bulk of the fluid decay at a different rate than the nuclei at the fluid-rock interface. While bulk relaxation is related to the fluid type and depends on the fluid properties, surface relaxation occurs at the fluid-solid interface and is a function of rock mineralogy. Although light oil exhibits substantial diffusion-induced relaxation, it is safe to neglect this mechanism at short inter-echo spacing as applicable in this experiment (Coates et al., 1999). Likewise, bulk relaxation can be safely ignored at short inter-echo spacing, coupled with the tight nature of the sample. With these assumptions, the T_2 signal will solely be composed of a surface relaxation component. Studies have shown that, in the fast diffusion limit, the T_2 surface relaxation can be related to the ratio of pore surface to fluid volume. **Equation 3** can be re-written as

$$\frac{1}{T_2} = \frac{1}{T_{2\_surface}} = \rho_2 \left(\frac{S}{V}\right)_{pore}$$

<p align="right">Equation 4</p>

Where ρ_2 is the T_2 surface relaxivity (T_2 relaxing strength of the grain surfaces) and, $\left(\frac{S}{V}\right)_{pore}$ and is the ratio of pore surface to fluid volume. For simple shapes, this ratio is a measure of pore size via the relationship:

$$\left(\frac{S}{V}\right)_{pore} = \frac{F_s}{r}$$

<p align="right">Equation 5</p>

Where F_s is the pore shape factor, and r is the pore radius. Given that in a specific core ρ_2 and F_s are constant, the T_2 and the pore size are related via the relationship.

$$T_2 = Cr$$

<p align="right">Equation 6</p>

Where C denotes a conversion constant for a given fluid in a specific core.

NMR relaxation measurements were acquired using a Geo spec2/53 (Oxford, England) with an operating frequency of 2.0 MHz set at room temperature. Before T_2 measurements, the system was calibrated with a standard calibration sample. The NMR T_2 distributions were acquired at the desired signal-to-noise ratio of 100.

4.2.2.5 Summary Workflow

The apparatus and methods described were used alternately to assess the pore scale H-n-P performance of CO_2 and C_2H_6. The workflow is summarized below:

7) First, the core is cleaned with solvents and dried.

8) Next, the core is vacuum-saturated with dead oil at 6000 psi for 2-5 days.

9) A pre-injection NMR T_2 measurement is obtained to assess the initial PSD at 100% fluid saturation.

10) Then, H-n-P cycles are conducted at the design injection pressure, soak period, production period, surface-to-volume ratio, and solvent composition for two (2) cycles.

11) After the two (2) cycles, a post-injection NMR T_2 spectrum distribution measurement is conducted to evaluate the fluid distribution of the residual oil in the core sample.

12) Using the T_2 spectrum before and after H-n-P, the pore level recovery factors in different pore sizes are calculated using the expression

$$R = \frac{A_O - A}{A} \times 100\%$$

Equation 7

where R represents the recovery factor after the H-n-P, Ao depicts the area covered by the original T_2 spectrum and the x-axis before H-n-P, and A is the area covered by the T_2 spectrum and x-axis after solvent H-n-P.

13) Steps 1 through 6 are repeated for all experiments, as presented in the design of the experiment in Table 8.

Table 8: Table of experimental design used in this work.

Experiment ID	Core Sample	Solvent	Injection Pressure psi.	Soak Period hours	Production Period hours
1	MB1	CO_2	BM	6	6
2	MB2	CO_2	AM	6	6
3	MB1	C_2H_6	BM	6	6
4	MB2	C_2H_6	AM	6	6
5	MB1	CO_2	BM	12	6
6	MB2	CO_2	AM	12	6
7	MB1	C_2H_6	BM	12	6
8	MB2	C_2H_6	AM	12	6
9	MB1	CO_2	BM	6	12
10	MB2	CO_2	AM	6	12
11	MB1	C_2H_6	BM	6	12
12	MB2	C_2H_6	AM	6	12
13	MB3	CO_2	BM	6	6
14	MB3	CO_2	AM	6	6
15	MB3	C_2H_6	BM	6	6
16	MB3	C_2H_6	AM	6	6

4.3 Results and Discussions

4.3.1 Preliminary concepts

One popular application of NMR is quantifying the bound volume irreducible (BVI) in formations. Traditionally, the BVI is calculated based on a fixed $T_{2cutoff}$ (Coates et al., 1999). In this method, the NMR T_2 distribution is divided into two components, one consisting of pore sizes containing bound fluids and the other consisting of pore sizes containing free fluids. The T_2 value that defines this partition is termed as $T_{2\ cutoff,}$ and it divides the spectrum into BVI and the free fluid index (FFI), as shown in **Figure 16**. This method assumes that all the bound fluids reside in small pores, the producible fluids reside in large pores, and that pore throats and pore bodies are

often not differentiated. Given the small pore sizes and lack of pore connectivity between them within the matrix of the rocks, the fluids in these pores may never be recoverable, regardless of the recovery technique used(Tomomewo et al., 2019). This bound fluid fraction is akin to what is measured by relative permeability or capillary pressure curves. It is a function of rock-fluid properties such as wettability(Al-Mahrooqi et al., 2003). The $T_{2cutoff}$ is therefore assumed to be an intrinsic rock property that can be measured in the laboratory. In special core analysis (SCAL), core samples are analyzed for NMR characteristics under two conditions: at 100% water saturation and irreducible water saturation established by centrifugation or a porous plate technique at a specified capillary pressure. The NMR T_2 signals can display incremental porosity (IP) and cumulative porosity (CP). The CP at a given T_2 is the integral of the IP for all T_2 values that are less than or equal to the given T_2. It is noteworthy that the $T_{2\,cutoff}$ is estimated from the CP. On the T_2 relaxation time versus CP plot, the $T_{2\,cutoff}$ is obtained by horizontally projecting the endpoint CP at irreducible saturation to the CP curve at 100% water saturation. At the intersect, the vertical line is projected downward to determine the $T_{2\,cutoff.}$
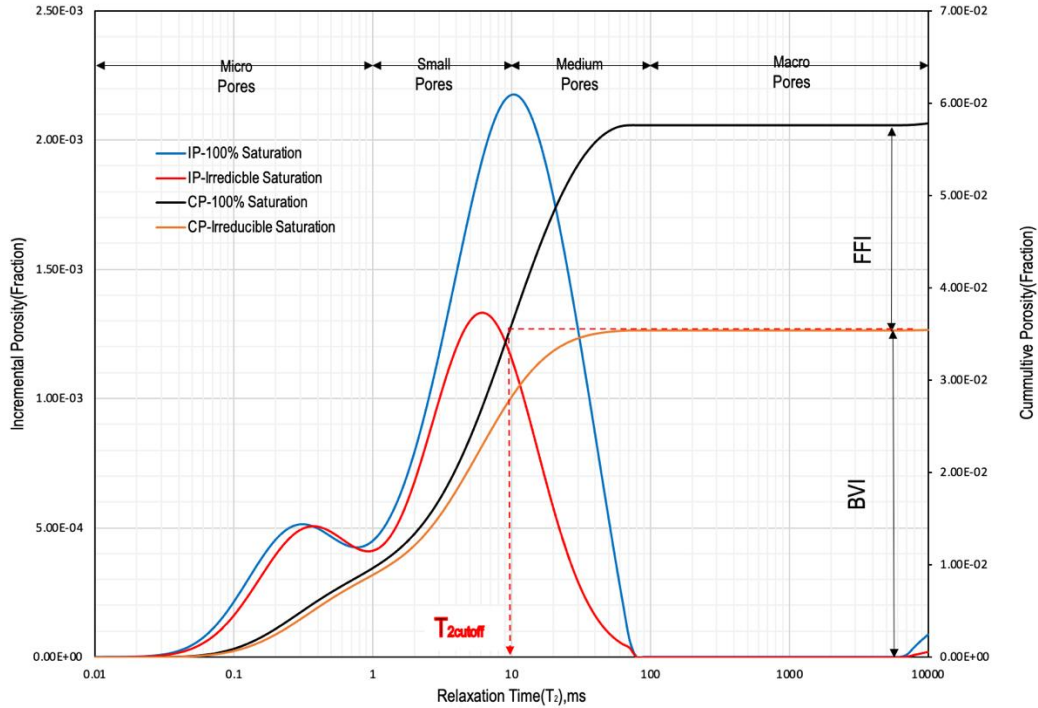
Figure 16: Theoretical characteristics of NMR T₂ distribution

As mentioned, the cutoff method assumes that all bound fluid is contained in the small pores and free fluids are contained in the large pores. However, in natural porous media, pores are not simple geometrical shapes like cylinders or spheres but may have very complex geometries. In addition, the walls may be rough and contain intricate irregularities, which adds further complexities when trying to analyze them. When a non-wetting fluid displaces a wetting phase, it is easiest for the non-wetting phase to occupy the center of the medium to large pores(Ekechukwu et al., 2021). Therefore, the irreducible wetting phase will usually remain in the small pores and the corners and crevices of the medium to large pores. Thus, there will be some bound wetting fluid across all sizes of pores. A given pore can, therefore contain both bound and free fluid. Therefore, although it is still valid to interpret the $T_{2cutoff}$ as a property of the rock, it should not be construed as physical pore size below which residing fluids are not producing, irrespective of

the recovery technique applied. Experimental results of several authors support this concept and form the basis for interpreting the results in this work.

It is also worth noting that the $T_{2cutoff}$ can shift along the T_2 axis depending on the centrifugation speed or pressure, even in standard measurements. It is, therefore, valid to expect a shift in $T_{2cutoff}$ depending on the recovery method applied to the formation in non-standard laboratory scale experiments. Thus, although NMR $T_{2cutoff}$ measurements have been primarily applied with water as the wetting phase, the concepts described in the preceding paragraph have allowed the technique to be used to investigate EOR effectiveness in core samples.

Several studies have compared the T_2 pore size distribution and pore size distribution as measured by mercury injection capillary pressure (MICP) measurements(Jácomo et al., 2019; Müller-Huber et al., 2018; Zhao et al., 2021). The T_2 distribution showed a remarkable correlation with the pore throat size distribution. Based on this correlation, T_2 value ranges have been defined for commonly encountered pore size ranges. We adopt the classification by Zhao et al. (2021). In this classification, micropores have a relaxation time between 0 and 1 milliseconds. Small, medium and macro pores have relaxation times of 1–10 ms, 10–100 ms, and greater than 100 ms, respectively. These T_2 ranges correspond to the pores sizes as follows: micropores (> 0-007 μm), small pores (0.007-0.07 μm), medium pores (0.07-0.7 μm), and macropores (>>0.7 μm) on the scale of T_2, as shown in **Table 9.**

These pore size delimitations allow us to probe the BVI and FFI in the various pore size ranges. The initial saturation, S_i, in each pore size range, can be computed via the expressions:

$$S_i = \frac{CP_{T2,u} - CP_{T2,L}}{CP_{T2,max}}$$

Equation 8

where $CP_{T2,u}$ is the cumulative porosity at the upper bound T_2 value of the pore size range at 100% fluid saturation, $CP_{T2,L}$ is the cumulative porosity at the lower bound T_2 value of the pore size range at 100% fluid saturation, and $CP_{T2,max}$ is the total porosity at 100% saturation. The FFI in each pore size range is also computed via the expression:

$$FFI = 1 - \frac{CP_{T_2,u,irr} - CP_{T_2,L,irr}}{CP_{T_2,u,100\%} - CP_{T_2,L,100\%}}$$

Equation 9

Where $CP_{T_2,u,irr}$ is the cumulative porosity at upper bound T_2 value of pore size rang at irreducible saturation; $CP_{T_2,L,irr}$ is the cumulative porosity at the lower bound T_2 value of pore size range at irreducible saturation; $CP_{T_2,u,100\%}$ is the cumulative porosity at upper bound T_2 value of pore size rang at 100% saturation; $CP_{T_2,L,100\%}$ is the cumulative porosity at the lower bound T_2 value of pore size rang at 100% saturation. Finally, the overall FFI, FFI$_{total,}$ can be calculated using the expression

$$\text{FFI}_{total} = 1 - \frac{CP_{T_2,max,irr}}{CP_{T_2,max,100\%}}$$

Equation 10

Where $CP_{T_2,max,irr}$ is the total porosity at irreducible saturation; $CP_{T_2,max,100\%}$ is the total porosity at 100% saturation.

Table 9: Pore size classifications used in this work.

T_2 Relaxation Time, ms	True Pore Size, μm	Pore Class
0.01-1	0-007	Micropores
1-10	0.007-0.07	Small Pores
10-100	0.07-0.7	Medium Pores
100-1000	>0.7	Macropores

4.3.2 Influence of Miscibility condition and its interaction with gas composition

In this section, we examine the effects of the miscibility condition and its interaction with gas composition on the pore-level recovery factor in Middle Bakken core samples. Four (4) H-n-P experiments were conducted at operating pressures representing "Below miscibility" (BM) and "Above miscibility" (AM) with CO_2 and ethane. Consequently, the injection pressures were selected with reference to the minimum miscibility pressures (MMP) of the gases shown in **Table 6**. The first contact MMPs of CO_2 and C_2H_6 were obtained from Hawthorne et al.(2017). The soak and production times are constant at 6 hours each, and the cycle number for all experiments is fixed at two (2) cycles.

MB1 and MB2 were used for these experiments, and initial PSD measurements were conducted on the samples after they were fully saturated with crude oil to assess the initial pore level fluid occupancy before H-n-P. Then, the H-n-P experiments are performed at the design operating parameters. **Figure 17** shows an example of the core sample (MB2) before and after CO_2. The results are presented in **Figure 18** and **Figure 19**.

As seen in **Figure 18** (solid blue plot), the initial scan shows that core MB1 is composed of two remarkable peaks on the T_2 spectrum based on the classifications described. These peaks are predominantly in the small and medium pore regions. Quantitative conversion of the areas covered by the PSD (blue bars in **Figure 19**) shows that $\approx 17\%$ of the initial fluid saturation is contained

in the micropores. The small and medium pores have $\approx 46\%$ and $\approx 37\%$ of the initial fluid saturation, while there was a negligible volume of large pores in this core. Sample MB2, on the other hand, shows a unimodal distribution with a peak in the small pore region. Quantitative conversion shows that the micro, small, medium, and macro pores contained $\approx 15\%, 54\%,$ $29\%, and\ 2\%$ of the initial fluid saturation, respectively. The proportion of micropores found here corroborates with the reported results by Tomomewo et al.(2019).
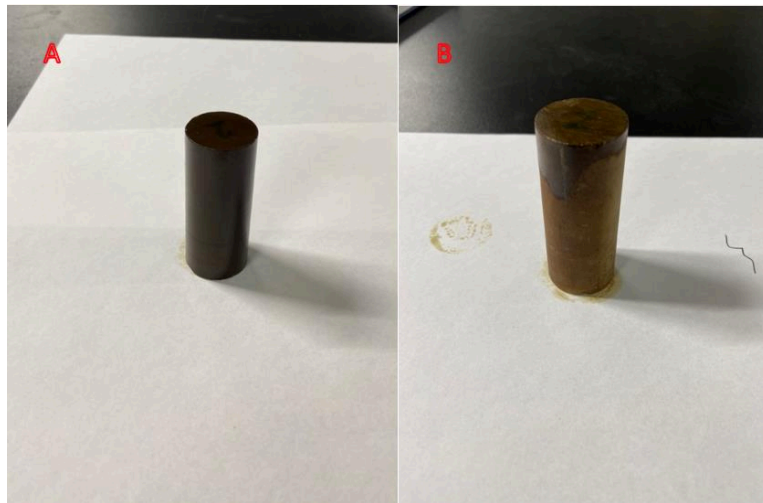
Figure 17: Core sample MB2 (A) before full saturation and (B)after CO_2 H-n-P.
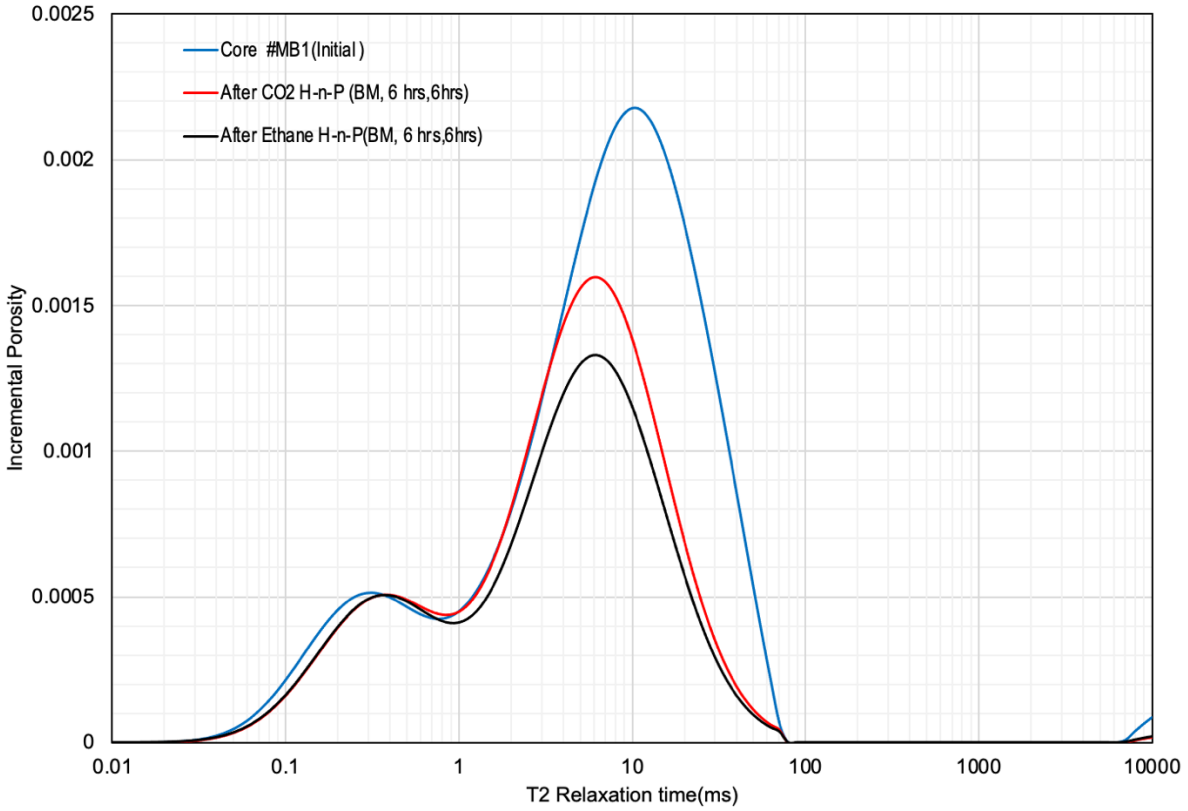
Figure 18:Comparison of T_2 spectrum distributions of #MB1 before and after H-n-P under BM condition, 6-hour soak period and 6-production period.
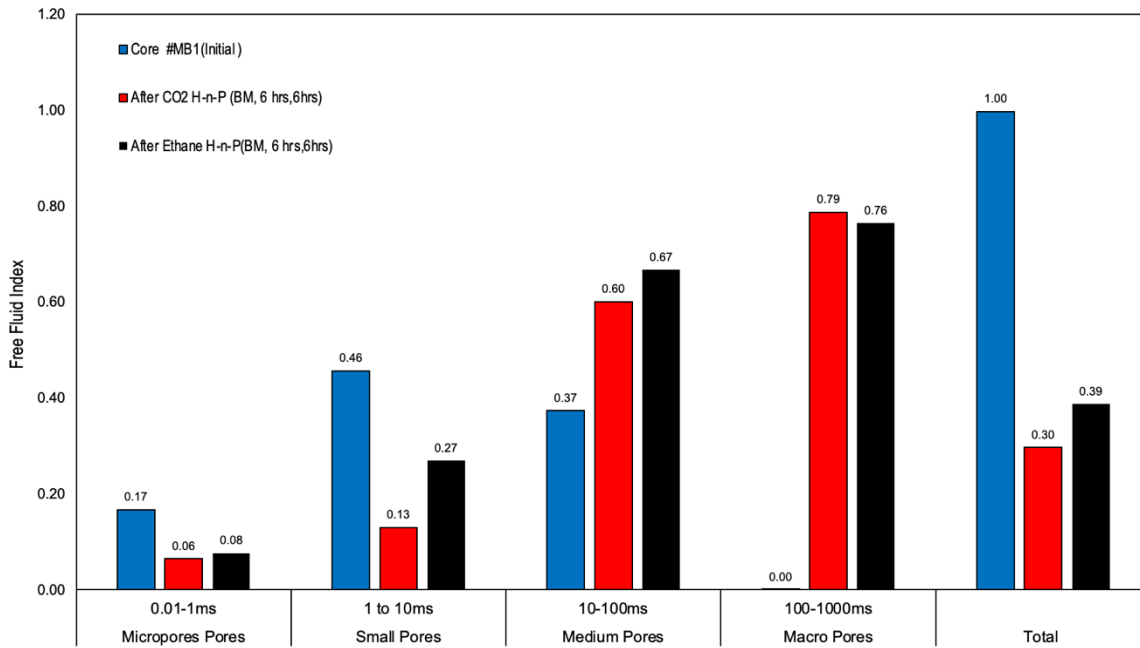
Figure 19: Comparison of free fluid indices in various pore sizes (and overall FFI) for core #MB1 under BM condition, 6-hour soak period and 6-hour production period.

After initial saturation with crude oil, core sample MB1 was subjected to H-n-P experiments with CO_2 and ethane under BM conditions. In contrast, core sample MB2 was subjected to CO_2 and ethane under AM conditions. **Figure 18** also compares the T_2 spectrum distributions of MB1 at 100% saturation (solid blue line) and after H-n-P with CO_2 (solid red line) and ethane (solid black line) under BM conditions. Compared to the spectrum at 100% saturation, the areas covered by the PSDs after H-n-P experiments are significantly reduced, indicating less volume of fluids in the pores after H-n-P. Remarkably, the area reduction for ethane is more significant than CO_2, suggesting that ethane could sweep more oil from the pores than CO_2 under BM conditions. Also conspicuous was the decrease in the area under both curves at the right peak of the distributions. Conversely, there was no significant change in the area covered in the left peak. This evidence indicates that the oil sweep was mainly from the small and medium pores and a less substantial sweep in the micropores.

The computed FFIs (**Figure 19**) show that when the saturated core sample was subjected to CO_2 at BM conditions, the gas recovered $\approx 7\%, 13\%, 60\%$ and 100% from the micro, small, medium, and macro pores, respectively. On the other hand, ethane swept $\approx$ $8\%, 27\%, 66\%$ and 100% from the micro, small, medium, and macro pores, respectively. Overall, CO_2 recovered $\approx 30\%$ of oil while ethane swept 39%.

Figure 20 and **Figure 21** depict the results for CO_2 and ethane H-n-P under AM conditions. **Figure 20** compares the T_2 spectrum distribution of core sample MB2 at initial saturation and after CO_2 (and ethane) huff-n-puff. As observed, the area reduction of the spectrums after H-n-P under AM was more significant compared to BM condition, irrespective of the gas composition. Again, the area reduction for ethane was more remarkable than that of CO_2, indicating that ethane

outperformed CO_2 under AM conditions. In addition, the PSD corresponding to ethane shows a relatively uniform distribution, while the spectrum for CO_2 exhibits skewness to the left. This evidence indicates that ethane could access all pore sizes at AM conditions, while CO_2 assessed pores down to small pores but failed to assess the micropores. Interestingly, the region of the graph corresponding to micropores displays fluid inflow, suggesting that CO_2 displaced a portion of the in-place fluids toward the micropores rather than sweeping them toward the surface. This phenomenon was also reported by Badrouchi et al. (2022).

Figure 20: Comparison of T_2 spectrum distributions of #MB2 before and after H-n-P under AM condition, 6-hour soak period and 6-production period.

Figure 21:Comparison of free fluid indices in various pore sizes (and overall FFI) for core #MB2 under AM condition, 6-hour soak period and 6-hour production period.

According to **Figure 21,** CO_2 could recover 79%, 89% and 89% of the fluids in the small, medium, and macro pores, respectively. The fluid volume in the micropores increased by 18%. Ethane could recover 59%, 84%, 90% and 76% from the micro, small, medium and macro pores, respectively. Overall, CO_2 could recover 67% of fluids in the pores, while ethane swept 82% of fluids in the pores.

Two predominant forces have been reported to be responsible for oil recovery during solvent H-n-P: advective and diffusive forces(Hoffman & Rutledge, 2019). Advective forces involve the movement of bulk fluid driven by a pressure gradient. On the other hand, diffusion forces are driven by a concentration gradient. In a matrix-fracture system, advective forces are believed to be predominant in the fractures, while diffusion is the principal mechanism in the matrix. It is worth mentioning that for molecular diffusion to occur, the participation molecules should be in the same phase (miscible). Given this constraint, we do not expect molecular diffusion

to be predominant under BM conditions. Hence, the sweep in the small to macro pores can be attributed to the mainly advective force. These results indicate that advective forces may also play a role in the matrix. Under AM conditions, miscibility occurs between oil and injected gas. The introduction of diffusive forces enables the gas molecules to invade the micro pores to displace the residing fluids from them. This explains the higher sweep efficiency in the micro pores under miscible conditions.

We believe the superior performance of ethane over CO_2 is due to their different diffusivities in crude oil. Molecular diffusion is a function of time and the intermolecular forces between the interacting molecules. Ethane has been reported to have superior diffusivity in oil compared to CO_2; thus, given the same time, ethane could penetrate to greater distances than CO_2(Yang & Gu, 2006). It is plausible that the base case soak period was insufficient for CO_2 to penetrate the small pore for efficient displacement.

4.3.3 Influence of soak period and its dependency on miscibility condition

In this section, four (4) H-n-P experiments were conducted with 12-hour soak periods for CO_2 and ethane under BM and AM conditions, after which PSD measurements were conducted to ascertain the pore level fluid occupancy. These experiments were conducted to investigate the influence of the soak period on the pore level sweep efficiency and its dependence on miscibility conditions (and gas composition). The production period was set at 6 hours. The results are then compared to previously described experiments with 6-hour soak periods. Like the preceding section, cores MB1 and MB2 were used for the experiments. Core MB1 was used for H-n-P experiments under BM conditions (and a 12-hour soak period), while core MB2 was subjected to H-n-P under AM (and a 12-hour soak period).

The PSDs compared before and after H-n-P under BM conditions are presented in **Figure 22 and Figure 23.** According to the results, subjection to H-n-P under BM conditions for a prolonged soak period reduced the areas covered by the PSD, showing some degree of sweep from the pores by the injected gas. However, just like the T_2 spectrums for 6 hours under BM conditions, the reduction in the area was only remarkable at the right peak, that is, regions corresponding to medium and small pores. There was no significant change in the area corresponding to micropores, which implies that even a prolonged soak period does not significantly benefit pore scale sweep efficiency under BM conditions. A change in the gas composition does not considerably improve sweep efficiency in the micropores either. The improvement in the sweep by ethane was only in the regions corresponding to the small to medium, and there was no remarkable change in the micropores.

As seen in **Figure 23**, under BM conditions for the prolonged soak periods, CO_2 recovered $\approx 22\%, 73\%, and\ 100\%$ from the small, medium, and macro pores, respectively. There was a $\approx 3\%$ inflow of fluids into micropores. On the other hand, ethane recovered $\approx 3\%, 38\%, 61\%\ and\ 100\%$ from the micro, small, medium, and macro pores, respectively. Overall, CO_2 recovered 37% of pore fluids, and ethane recovered 41% under BM conditions and for prolonged soak periods.
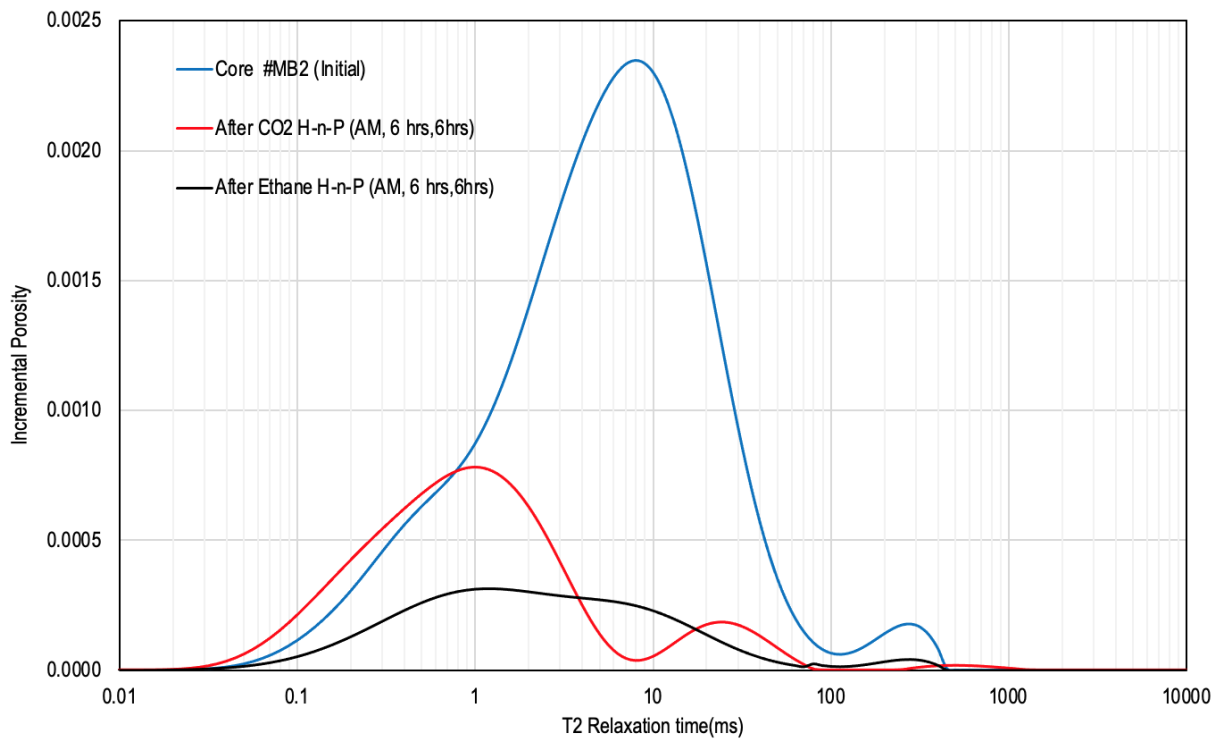
Figure 22: Comparison of T_2 spectrum distributions of #MB1 before and after H-n-P under BM condition, 12-hour soak period and 6-production period.
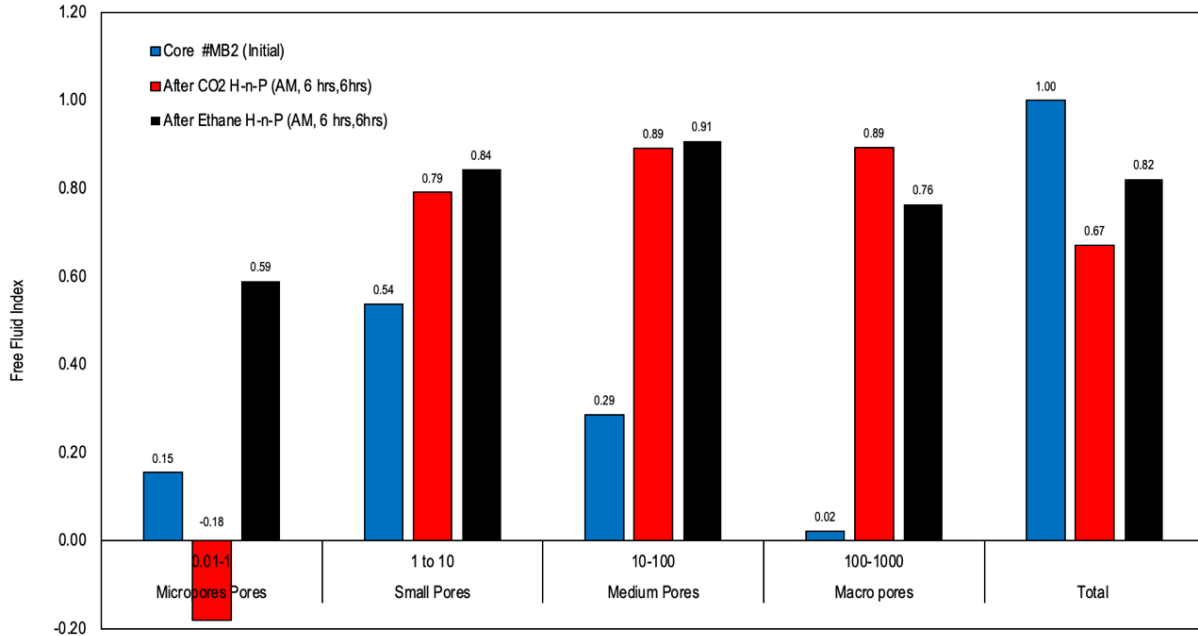

Figure 23: Comparison of free fluid indices in various pore sizes (and overall FFI) for core #MB1 under BM condition, 12-hour soak period and 6-hour production period.

Figure 24 compares the initial T_2 distribution of core sample MB2 and the distribution after H-n-P experiments with a 12-hour soak period and under AM conditions. The figure shows a remarkable reduction in the areas under the distributions, indicating a significant sweep of the residing fluids. The decrease in the area is uniform across all sizes of pores for both CO_2 and ethane, suggesting that the injected gas could assess all pore sizes when the injection was under AM conditions with a prolonged soak period. According to **Figure 25**, CO_2 recovered $\approx$ $32\%, 78\%, 94\%$ and 100% from the micro, small, medium, and macro pores, respectively, for a long soak period and under AM conditions. Ethane recovered $\approx 55\%, 94\%, 93\%$ and 100% from the micro, small, medium, and macro pores, respectively. Overall, CO_2 swept 76% of the residing fluids, and ethane recovered 87% under AM conditions and for prolonged soak periods.

The increase in recovery factor with prolonged soak periods has been attributed to diffusion (Gamadi et al., 2014; Jin et al., 2017). Diffusion is time-dependent; thus, the longer the contact time, the further the molecules can travel, which implies that a longer soak time allows molecules to diffuse deeper into oil-filled pore spaces and enhance the microscopic sweep. The insensitivity of recovery to longer soak periods under BM condition justifies our interpretation that diffusion is insignificant under immiscible conditions. Under AM conditions, an extended soak period results in a superior microscopic sweep noticeable in the micro pores since diffusion becomes significant. Furthermore, the significant improvement in the displacement effectiveness in the micro pores by CO_2 indicates that prolonging the soak period improves the effectiveness of solvents with relatively low diffusivities.

Figure 24: Comparison of T₂ spectrum distributions of sample #MB2 before and after H-n-P under AM condition, 12-hour soak period and 6-production period.

Figure 25: Comparison of free fluid indices in various pore sizes (and overall FFI) for core #MB2 under AM condition, 6-hour soak period and 6-hour production period.

4.3.4 Influence of production period and its dependency on miscibility condition

The influence of the production period on the pore-level sweep efficiency and its dependency on miscibility was examined. To the best of our knowledge, the effect of production period on pore scale sweep efficiency has not been studied in extant literature. To this end, four (4) H-n-P experiments were conducted with prolonged production periods of 12 hours under BM and AM conditions and for CO_2 and ethane. Core samples MB1 and MB2 were exposed to both gases under BM and AM, respectively. The soak periods were fixed at 6 hours. At the end of the design soak period, the pressure in the accumulator is stepped down at a rate of three equal pressure steps per time. This schedule was designed to replicate the pressure reduction at the field-scale as closely as possible.

Figure 26 compares the PSD of core sample MB1 before and after exposure to CO_2 and ethane under BM conditions. The results with prolonged production period at BM show no remarkable difference with other observations at BM condition. That is, although there is evidence of the residing fluid being displaced, the displacement only occurs in areas corresponding to small to medium pores. Thus, the micropores are not easily assessed by prolonging the production period when the cores are subjected to H-n-P under BM conditions, irrespective of the gas composition. According to **Figure 27**, with a 12-hour under BM conditions, CO_2 swept $\approx$ $9\%, 7\%, 58\%$ and 100% from the micro, small, medium and macro pores, respectively. Overall, CO_2 recovered 27% of the residing fluid, and ethane recovered 38%, which is not significantly different from the case with the 6-hour production period under BM conditions.
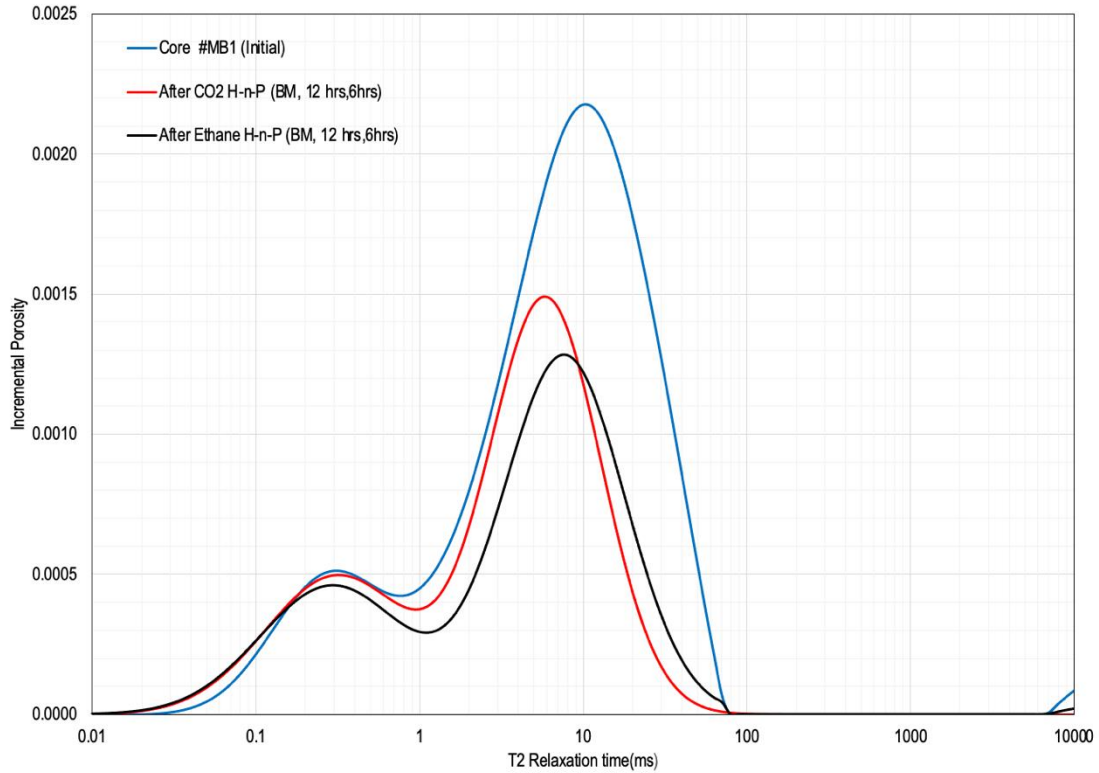
Figure 26: Comparison of T₂ spectrum distributions of sample #MB1 before and after H-n-P under BM condition, 6-hour soak period and 12-production period.
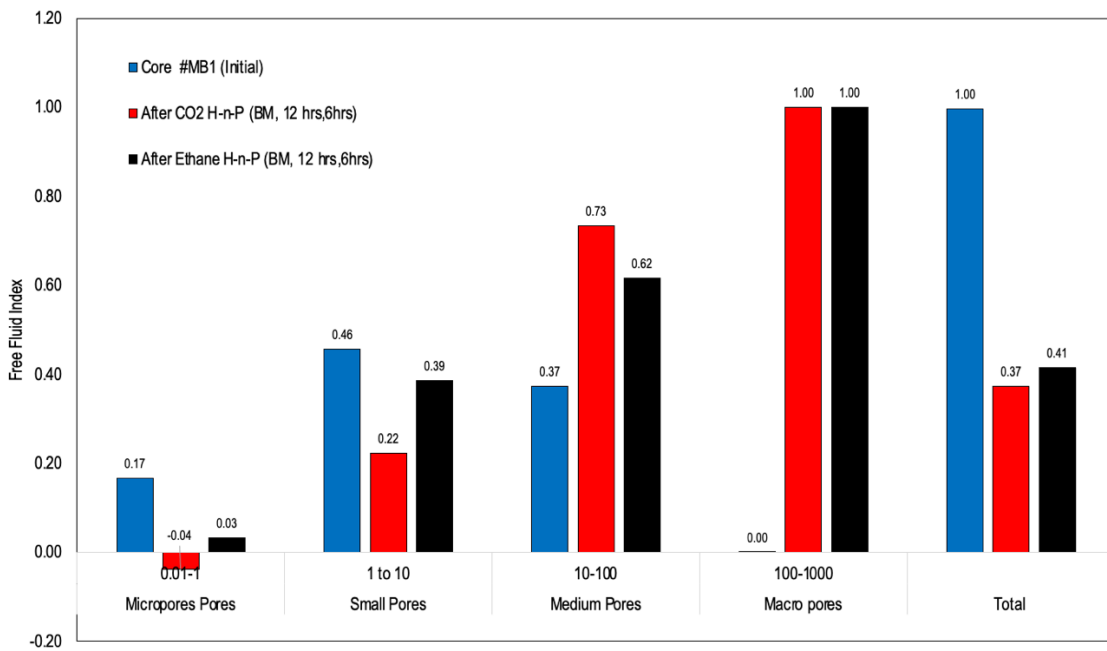

Figure 27: Comparison of free fluid indices in various pore sizes (and overall FFI) for core #MB1 under BM condition, 6-hour soak period and 12-hour production period.

Figure 28 and Figure 29 depict the result with a prolonged production period under AM conditions. As expected, the PSD suggests a significant sweep of the residing fluids. The influence of the production period under AM conditions is observed when **Figure 28** is compared with **Figure 20.** For CO_2, it is noticed that there is an improved performance in the region corresponding to micropores. This evidence indicates that, under AM conditions, increasing the production period may improve recovery performance. According to **Figure 29**, CO_2 recovered $\approx$ $39\%, 72\%, 91\%$ *and* 100% of the fluids in the micro, small, medium and macro pores. Similarly, ethane recovered $\approx 39\%, 72\%, 91\%$ *and* 100% from micro, small, medium and macro pores, respectively. Overall, CO_2 recovered 73%, and ethane recovered 84% of the residing fluids.

Figure 28:Comparison of T_2 spectrum distributions of sample #MB2 before and after H-n-P under AM condition, 6-hour soak period and 12-production period.

Figure 29: Comparison of free fluid indices in various pore sizes (and overall FFI) for core #MB1 under AM condition, 6-hour soak period and 12-hour production period.

A comparison of the above-mentioned overall FFIs with the case with a 6-hour production period under AM condition indicates that both gases swept more fluids with the 12-hour production period. Under AM conditions, a larger volume of gas diffuses through the oil into the micro pores. This diffused gas will require more time for complete exsolution from the bulk oil phase during production. Thus, the more time that is allowed, the more oil that is recovered.

Another plausible explanation for the increase in displacement effectiveness with a prolonged production period is that a slow depletion rate extends the period under which the gas is pressurized in the oil. In other words, a slow depletion rate extends the soak period, albeit at declining pressure levels over time. Hence, the effect of a prolonged production period is similar to that of the soak period, as evident from the improved sweep in micropores by CO_2.

4.3.5 Influence of rock surface area-to-volume ratio and its dependency on miscibility condition

In unconventional oil production, the matrix volume exposed to hydraulic fractures is a primary determinant of the production rate; thus, every effort is made to maximize fracture surface area in the operation and design of hydraulic fractures. However, concerns have frequently been raised regarding the effect of exposed rock surface area-to-volume ratio (SA/V) on EOR performance, which can also determine if refracturing is necessary for efficient recovery (Hejazi et al., 2017). Typically, the SA/V in laboratory core-scale experiments is characterized by the core size (Chaisoontornyotin et al., 2019; L. Li & Sheng, 2017). Hence, to evaluate the effect of SA/V on pore level performance of gas H-n-P, four (4) experiments were conducted using core sample MB3 with an SA/V of 3.9 in^2/in^3 under BM and AM conditions. The dimensions of the cores used are presented in **Table 7**. The experiments were conducted with CO_2 and ethane to better comprehend the effect of rock surface area-to-volume ratio on the pore scale sweep performance.

As shown in **Figure 31** (blue bars), initial NMR scans on 100% saturated core sample MB3 indicate that it is composed of 50% micropores, 41% small pores, 3% medium pores and 5% macro pores. In addition to the volume differences, the NMR T_2 distribution suggests a different pore structure from MB1 and MB2. **Figure 30** compares the PSDs after H-n-P under BM conditions with initial PSDs. As expected, the results show that both fluids predominantly displaced fluids in the small to macro pores. CO_2 swept $\approx$37% from the small pores, $\approx$35% from the medium pores and 100% from the macro pores (**Figure 31**). There was a $\approx$12% inflow of fluids into the micropores. Ethane, on the other hand, displaced $\approx 3\%, 41\%, 94\%$ and 100% from the micro, small, medium and macro pores, respectively. The calculated total FFIs indicate that CO_2 displaced $\approx$19% of the total pore volume and ethane swept $\approx$31% of the fluids. Compared to the

case with 4.8 in²/in³ at BM conditions, the solvent recovered less fluids with the 3.9 in²/in³ core
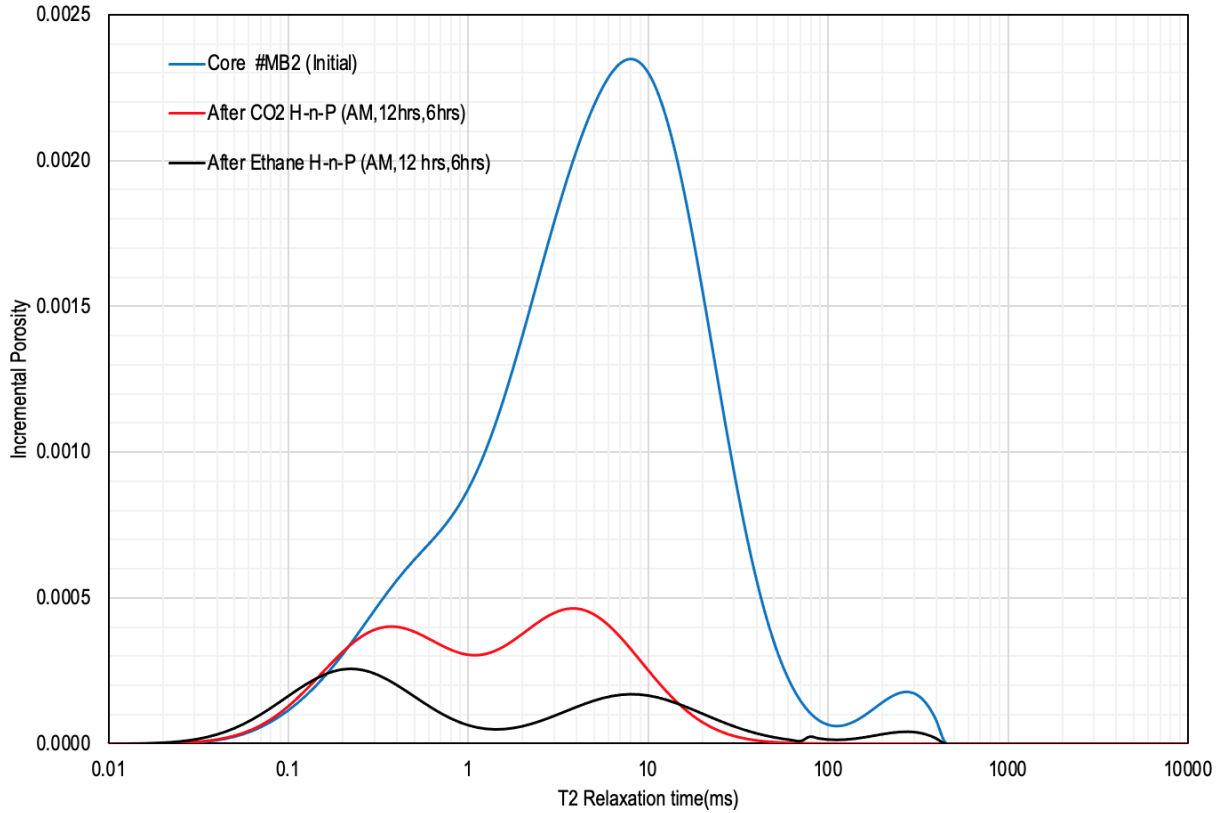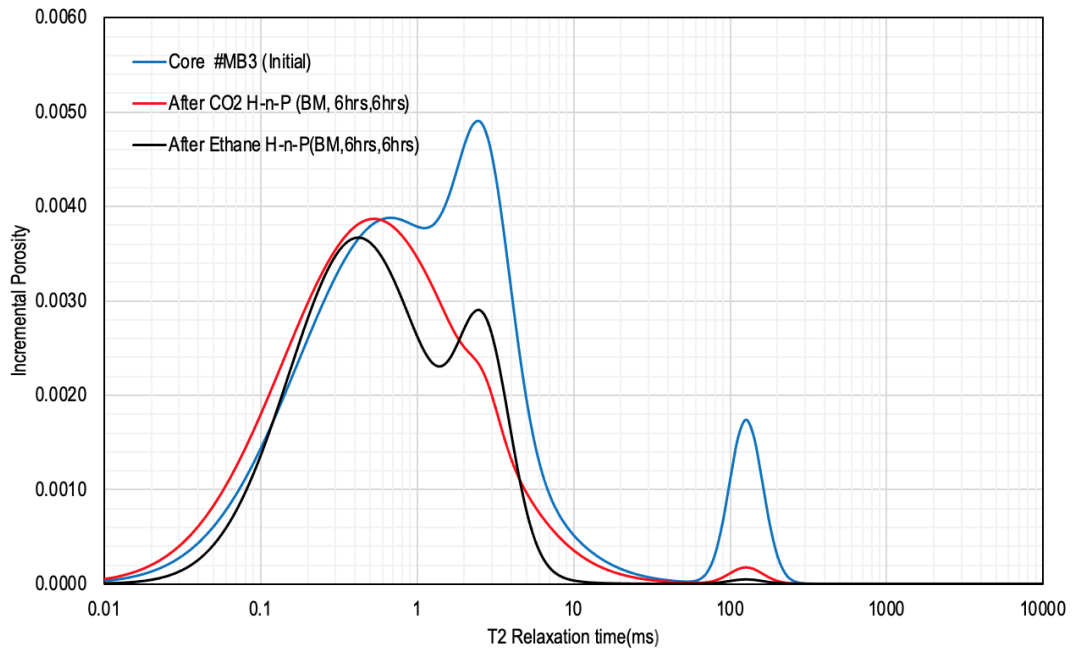

sample.

Figure 30:Comparison of T₂ spectrum distributions of sample #MB3 before and after H-n-P under BM condition, 6-hour soak period and 6-production period.
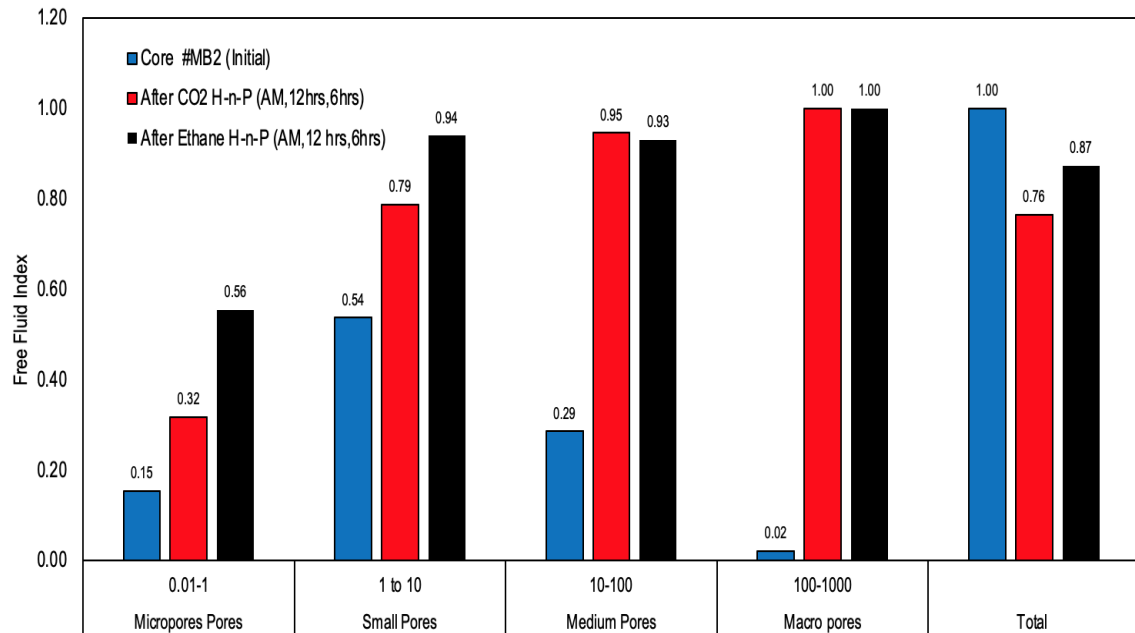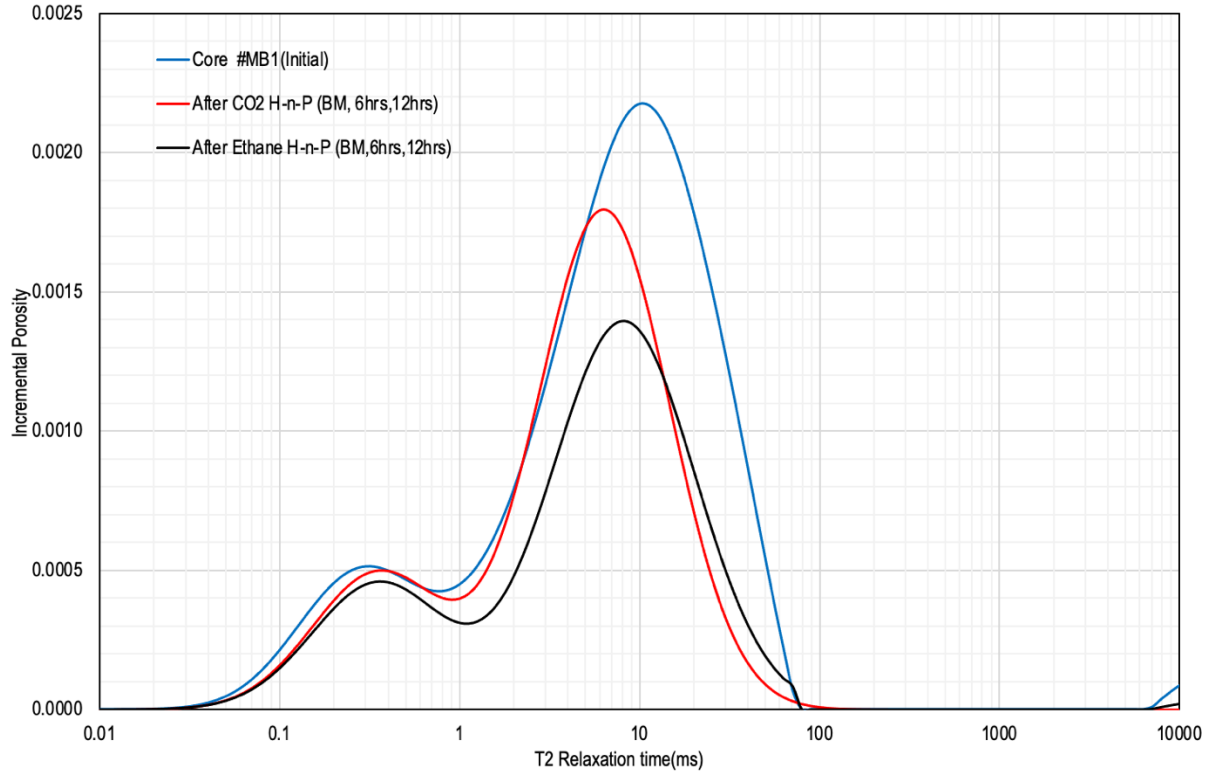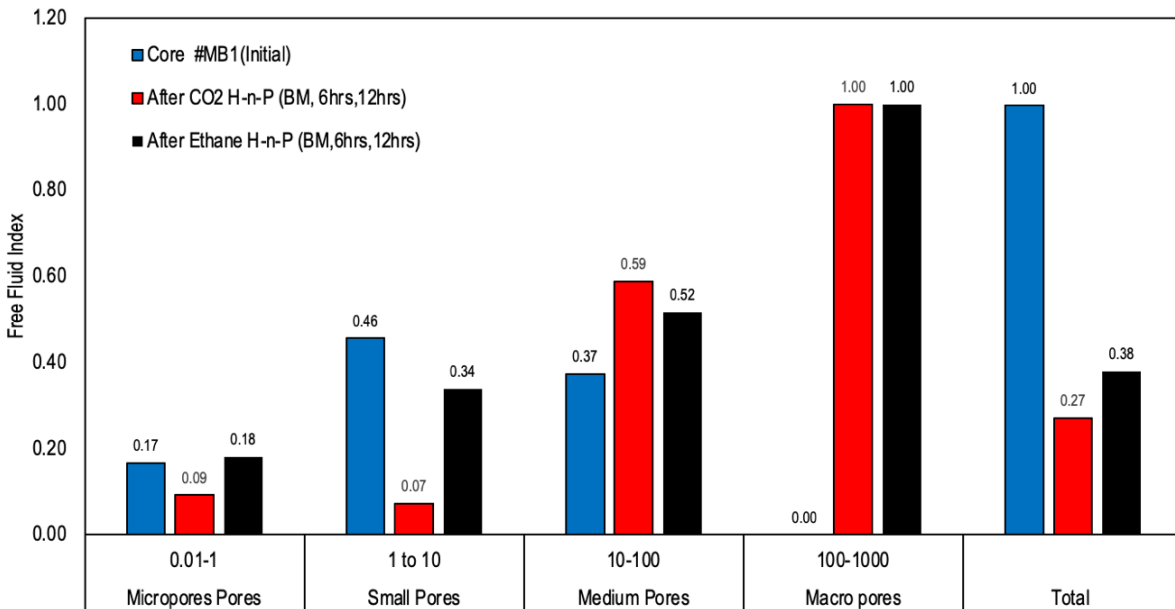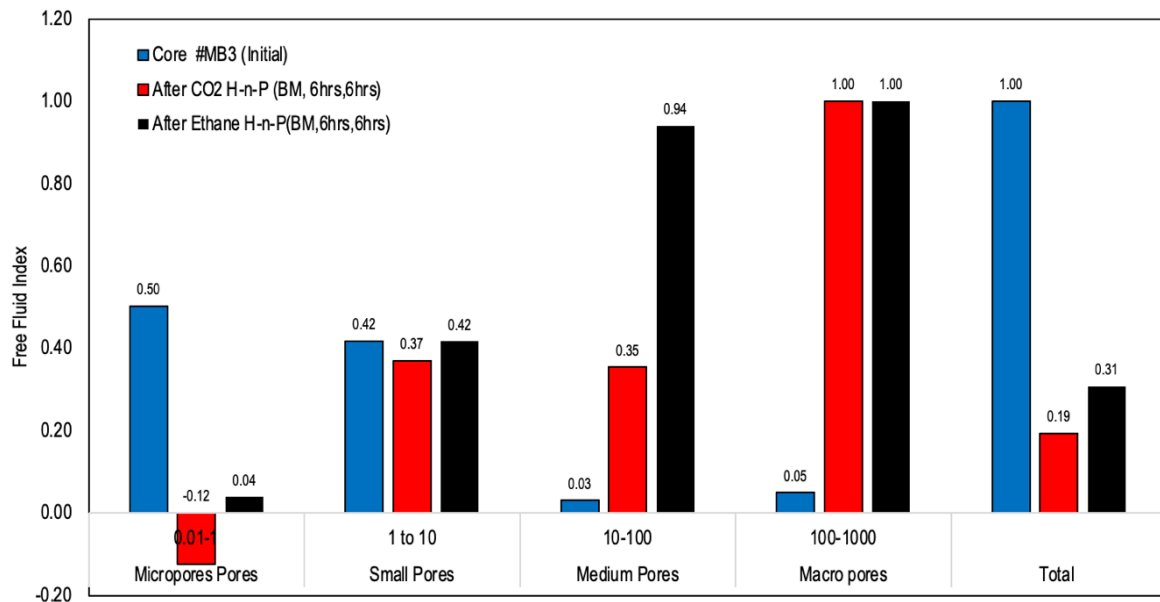

Figure 31: Comparison of free fluid indices in various pore sizes (and overall FFI), for core #MB3 under BM condition, 6-hour soak period and 6-hour production period.

Figure 32 depicts the compared PSDs after H-n-P under AM conditions. The figure shows that CO_2 and ethane displaced a substantial portion of the residing fluids under AM conditions, as expected. Under AM conditions, CO_2 swept $\approx 58\%$ from the micropores, $\approx 76\%$ from the small pores, $\approx 86\%$ from the medium pores and 100% from the macro pores (**Figure 33**). Ethane swept $\approx 75\%, 60\%, 99\%$ *and* 100% from the micro, small, medium and macro pores, respectively. Overall, CO_2 and ethane recovered 69% and 83% of the fluids in the pores, respectively.
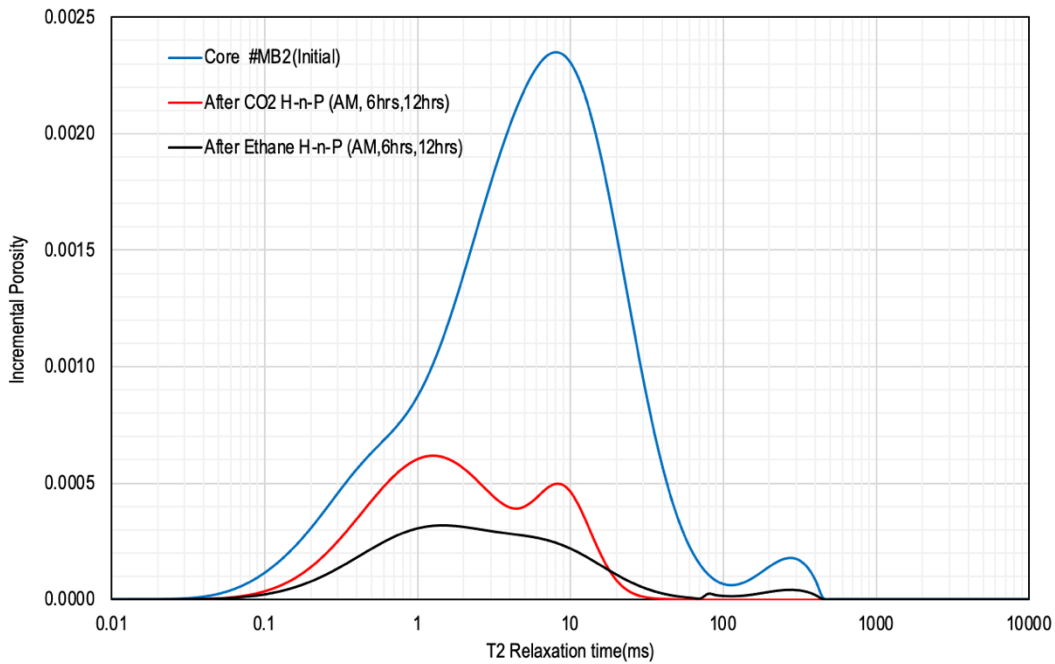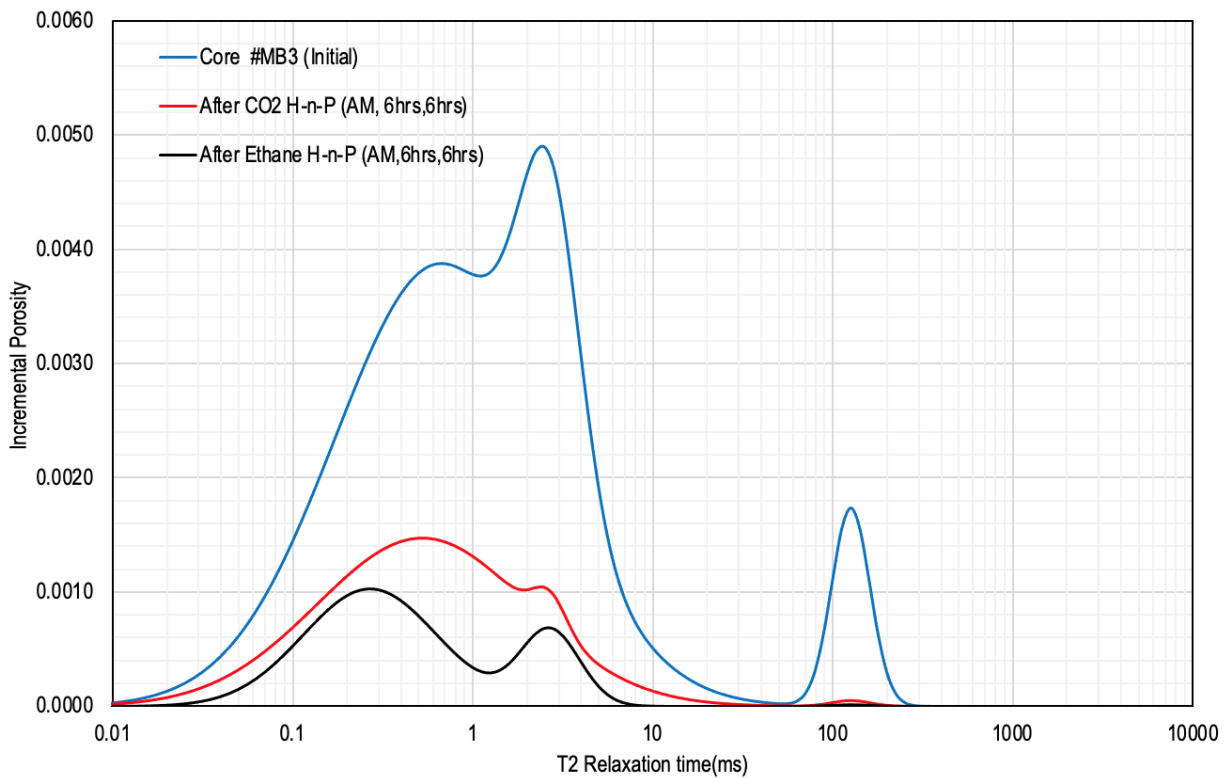

Figure 32: Comparison of T_2 spectrum distributions of sample #MB3 before and after H-n-P under AM condition, 6-hour soak period and 6-production period.
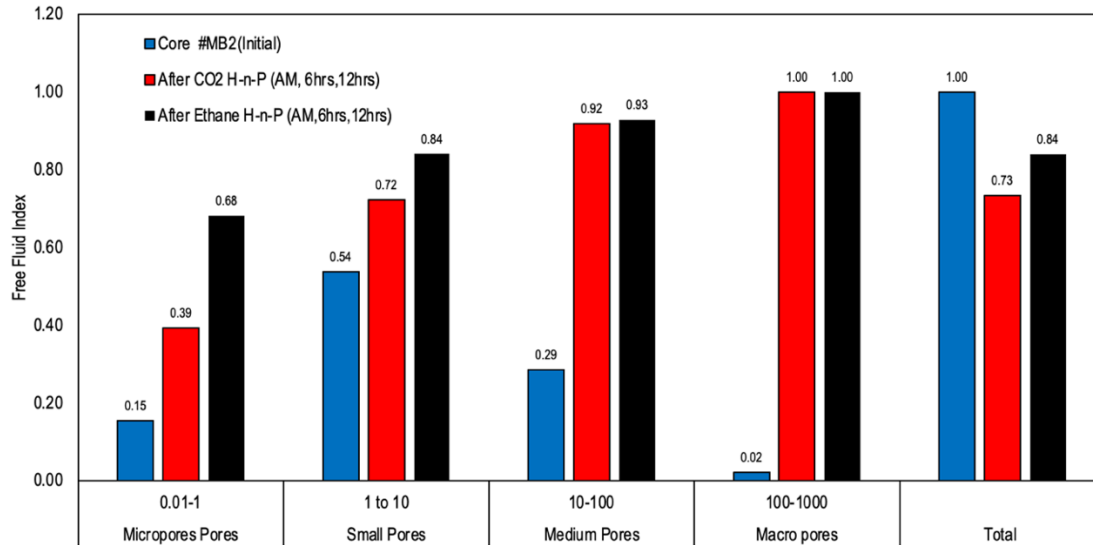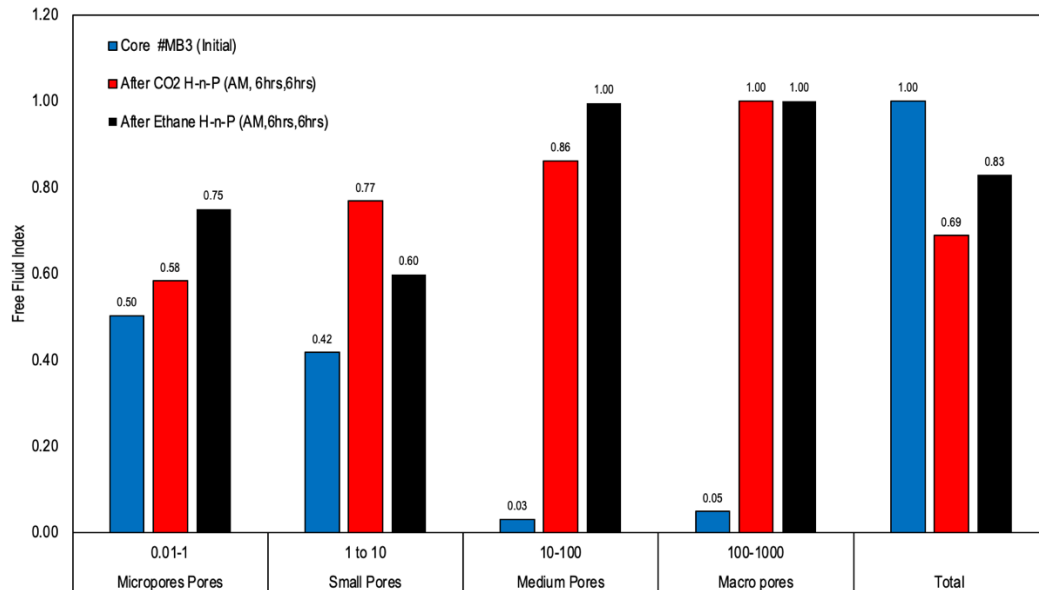
Figure 33: Comparison of free fluid indices in various pore sizes (and overall FFI) for core #MB3 under AM condition, 6-hour soak period and 6-hour production period.

A comparison of the overall FFIs with that of 4.8 in^2/in^3 core samples shows a remarkable difference between the FFIs under BM conditions but less of a difference under AM conditions. The variation in the pore structures of the core sample could be one explanation for this observation. Core MB3 has a more significant proportion of micropores compared to core MB1 and MB2, hence the lower FFI under BM conditions. Second, a change in SA/V simultaneously affects the two primary underlying recovery mechanisms: diffusion and advection. According to Darcy's Law, which governs the advection mechanism, in radial flow geometry, a decrease in the radius (increase SA/V) results in a more significant pressure gradient (DP/Dr), which increases flow to the surface of the core sample. On the other hand, Fick's law, which governs the diffusion mechanism, predicts that an increase in the surface area enhances the diffusive flux of gas molecules into the core. Thus, an increase(decrease) in SA/V will enhance (diminish) the recovery process. Under BM conditions, the already low-pressure gradient and diffusive flux are more impacted by a decrease in SA/V. At AM conditions, however, it is evident that a change in SA/V less influences the already high-pressure gradient and diffusive flux. In addition, because there is

miscibility, other mechanisms such as oil swelling, lighter component extraction and viscosity reduction further reduce the impact of SA/V, which may explain the lack of significant difference in recovery under AM conditions. Our results suggest that injecting gases at higher pressure may compensate for a reduced simulated reservoir volume (SRV) in the field. However, more studies at the field scale are recommended to ascertain this conclusion.

4.4 Conclusions

In this work, NMR relaxometry was used to study the pore-level sweep efficiency of solvent H-n-P in Middle Bakken core samples. The effectiveness of two solvent gases, CO_2 and ethane, and the influence of gas composition and miscibility conditions were investigated. In addition, the effect of soak period, production period and rock-surface-to-volume ratio and their variable interactions with gas compositions and miscibility conditions were ascertained. First, initial PSDs based on NMR T_2 distributions were measured in 100% saturated core samples. Next, the core samples were subjected to laboratory-scale H-n-P experiments with different solvent compositions and design parameters. Then, PSDs were measured after the H-n-P experiments. By comparing the initial PSD with the post-H-n-P PSD, deductions on the pore-level sweep efficacy and mechanisms are deduced. Some of the key findings are summarized as follows:

1) The pore-level sweep efficiency generally varied with gas composition, miscibility conditions, soak period, production period and rock-surface-to-volume ratio, and the interaction among these variables. Consequently, the degree of fluid recovery measured by the free fluid index varied widely in different pore size ranges.

2) Below miscibility conditions (with a 6-hour soak period, 6-hour production period and SA/V of 4.8 in^2/in^3), both gases target the small to macro pores but fail to penetrate the micropores.

Above miscibility conditions, although sweep in the small to macro pores by CO_2 was improved, sweep in the micropores was still limited. However, injection above miscibility condition for ethane ensured a significant improvement in FFI across all pore sizes. Overall, ethane outperformed CO_2 under both BM and AM conditions.

3) The effect of the soak period on the pore level sweep efficiency depended on the miscibility condition and gas composition. Under BM conditions, increasing the soak period did not significantly improve the FFI in the micropores over a shorter soak period. However, under AM conditions, prolonging the soak period resulted in significant improvement of FFI across all pore sizes for both gases. The highest recovery was achieved using ethane, with a prolonged soak period.

4) The effect of the production period was also influenced by both composition and miscibility conditions. Under BM conditions, the production period had minimal influence on FFI. Under AM conditions, a prolonged production period remarkably impacted FFI. The improvement was more pronounced with CO_2, where a prolonged production period resulted in a significant sweep in the micropores.

5) The effect of the rock surface-to-volume ratio was pronounced under BM conditions and less impactful under AM conditions. Under BM conditions, a reduced SA/V (increased core volume) resulted in a decline in FFI in the pores. However, this observation could also be caused by the different pore structures encountered in the core samples.

It is important to note that this work had certain limitations. Even though the core samples were selected from proximity to one another, heterogeneities exist, as demonstrated by the variations in porosity and permeability values in Table 1. These heterogeneities may influence the work's conclusions. In addition, the re-use of core samples and cyclic saturation and desaturation may alter

core properties due to hysteresis and physical damage to the samples, which may influence the conclusion of this study (Badrouchi et al., 2022). Finally, we used a dead oil sample with a different composition than live oil under reservoir conditions; therefore, we caution against extrapolating the presented results to the reservoir scale. Despite these limitations, we believe the results will aid the comprehension and design of enhanced oil recovery strategies in unconventional reservoirs.

Chapter 5

Optimization of CO_2 Huff-n-Puff EOR in the Bakken Formation using Numerical Simulation and Response Surface Methodology

5.1 Introduction

Although the existing body of research has shed light on the effectiveness of huff-n-puff and how to optimize critical operating parameters, a closer examination of these studies reveals that most of them employ the one-factor-at-a-time (OFAT) method in their study procedure (Gamadi et al., 2014; L. Li & Sheng, 2016). In this approach, the optimization experiments are conducted by changing one factor while holding the others constant. First, one factor is varied until its optimal setting is identified and fixed at that level. Then, another factor is changed until its best values are found. This process is repeated for all the independent variables (Wahid & Nadir, 2013). The approach is favored by most researchers as it requires minimum experimental runs and has proven to be sufficient in cases where the extra effort needed to conduct a complex multi-factor analysis is not warranted. Furthermore, some researchers have argued that OFAT can be more effective than other complex methods under certain conditions where the primary goal is to attain minor improvements in a system.

However, a major pitfall of this approach is that it is less precise than other complex multi-factor analysis methods and requires more experimental runs to achieve the precision offered by other methods, which can be costly. Also, the approach ignores the interactions among the factors and their effects on the optimum response value (Wahid & Nadir, 2013).

It appears OFAT is an oversimplified approach for optimizing complex processes such as gas huff-n-puff. Optionally, there are several robust methodologies for optimizing process variables, such as the genetic algorithm (Holland, 1992), particle swarm algorithm (Kennedy &

Eberhart, 1995)), random search (Baba, 1981), tabu search (Glover & Laguna, 1998), simulated annealing (Kirkpatrick et al., 1983) and many others. Although the above-mentioned advanced optimization techniques use complex mathematical computation and have proven to be more accurate, they may be computationally expensive and often require large datasets. This requirement can make them prohibitive for a process that requires time-consuming and computationally expensive experiments and simulations. For example, sampling from flow experiments in low permeability unconventional cores can take a considerable time. Likewise, numerical flow simulation can be computationally expensive when investigating enhanced oil recovery in unconventional reservoirs. This high cost is because they usually require fully coupled compositional flow simulations to describe the complex underlying physical phenomenon. As a result, obtaining sufficient samples for use in advanced optimization techniques can be challenging. So, it is not surprising that advanced optimization techniques have scarcely been applied to gas injection experiments and simulations in unconventional resources.

Compared to OFAT and sophisticated optimization techniques, response surface techniques (RSM) provide a decent compromise in sampling demand and accuracy. RSM is a collection of statistical methods for investigating the correlations between several explanatory variables and one or more response variables. Typically, the established relationship can be used to determine the factor settings that yield the best responses. The technique leverages the available design of experiments (DOE) methods to minimize the number of trials and recognize the influence of process parameters (Wahid & Nadir, 2013). All data points are used to estimate each factor's effect and interactions, a property of concealed replication (Wahid & Nadir, 2013). This characteristic of the technique makes it superior to the OFAT method, which essentially uses just two observations to evaluate the effect of each component and neglects the interactions among the

factors. Thus, the estimates of the impact of each factor are more precise in comparison to OFAT. The lack of use of a well-defined DOE in OFAT frequently means one does a hit-or-miss scattershot series of trials from which it may be possible to predict interactions, but these are rarely realized. RSM enhances the predictability of the response by lowering the variability of the estimates of the response in the factor space, making process optimization more efficient since the ideal solution is sought over the whole factor space. The technique has been successfully used to optimize process parameters for wastewater treatment (J.P. Wang et al., 2007), food drying (Eren & Kaymak-Ertekin, 2007)), petroleum refinery effluent treatment (Rastegar et al., 2011), biodiesel production (Fayyazi et al., 2015(Fayyazi et al., 2015) and various topics in petroleum engineering (Baioco et al., 2020; B. Li et al., 2019; Obeyesekere et al., 2021(Baioco et al., 2020; Obeyesekere et al., 2021).

Realizing the benefits of RSM/DOE, we aim to apply the technique to study the influencing operational parameters for huff-n-puff CO_2 EOR in the Bakken Formation and optimize recovery. The influence of five operational factors (and their interactions) on oil recovery and gas utilization factors is studied using RSM. The independent variables considered include injection rate, injection period, soak period, production period, and production BHP. First, a compositional, near-well model is constructed. The model is intended to be representative of a well in the Sanish field, which targets the Middle Bakken play in the North Dakota portion of the Williston Basin. Thus, the properties of the model are tuned to history match primary recovery for this well. Then, CO_2 huff-n-puff is simulated to study the performance and efficiency of enhancing the Bakken Formation's oil recovery. Next, sample points are obtained from several simulation runs based on central composite design (CCD). The CCD design enables the fitting of a second-order polynomial proxy model that describes the relationship between operating parameters and target responses.

Finally, once the proxy model is obtained, it is used to optimize the huff-n-puff process to maximize oil recovery and gas utilization. This procedure has been summarized in the workflow diagram presented in **Figure 34.** The influence of the independent variables on the recovery and gas utilization factors, the interactions between them, and the results from the optimization process are discussed in detail.
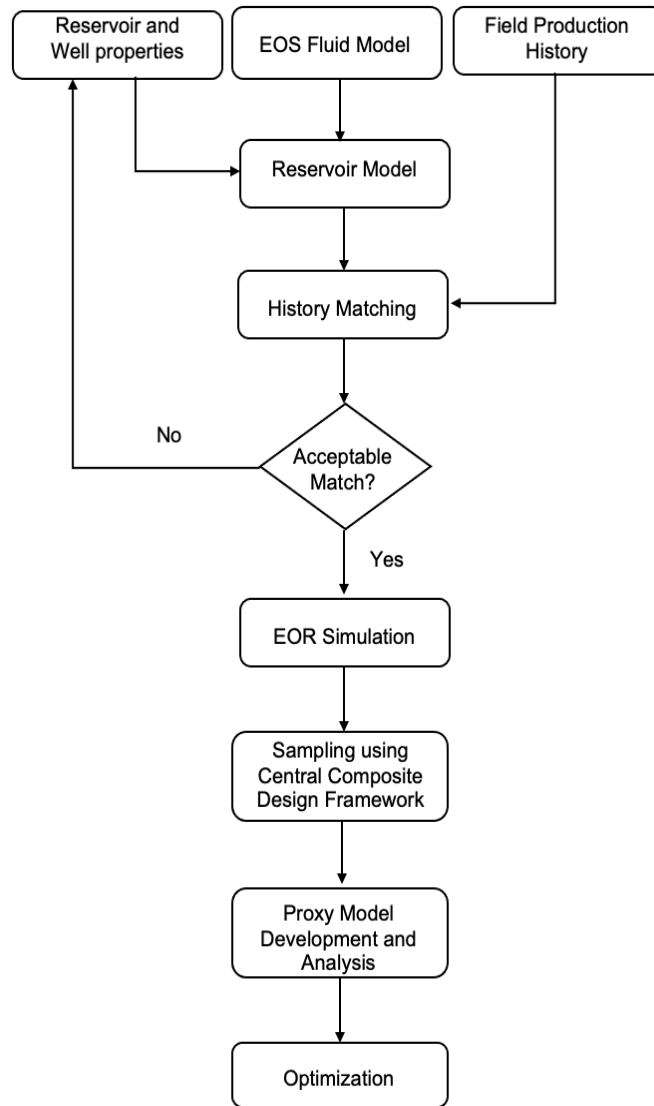
Figure 34: Workflow diagram summarizing the methodology employed in this study.

5.2 Methodology

5.2.1 Simulation process

A near-well simulation model was constructed using CMG-GEM (Computer Modelling Group, 2018), a commercial numerical compositional reservoir simulator. The underlying governing flow equation for the simulation has been presented by Thomas and Thanau (1983) and expressed in Equation 11. For M components partitioning among $\hat{M}$ mobile fluid phases, the flow equation can be expressed as

$$\nabla \cdot \left(\sum_{p=1}^{\hat{M}} C_{ip}\rho_p \frac{\vec{k}k_{rp}}{\mu_p} \nabla \Phi_p \right) \pm \sum_{p=1}^{\hat{M}} C_{ip}\bar{g}_p = \frac{\partial}{\partial t}\left[\phi \sum_{p=1}^{\hat{M}}(C_{ip}\rho_p S_p) \right], i = 1,2 \dots M.$$

Equation 11

where C_{ip} is the mass fraction of component i in phase p, ρ_p is the density of phase p, $\vec{k}$ is the permeability tensor, k_{rp} is the relative permeability of phase p, Φ_p is the potential of phase p, $\bar{g}_p$ is the mass rate per volume of phase p, ϕ is the porosity and S_p is the saturation of phase p. The above formulation can either be discretized in explicit or implicit schemes, each of which poses its own merits and demerits. Colins et al. (1992) proposed the adaptive-implicit method that benefits from both the explicit and implicit formulations while mitigating the demerits of both schemes. Here, most grid blocks are solved explicitly. However, the explicit formulation becomes unstable in grid blocks with high flow rates, such as near hydraulic fractures. Thus, the simulator adaptively switches to an implicit solution. This switching is based on a stability criterion specified as threshold changes in water saturation and hydrocarbon component global mole fractions.

The dual-porosity model was used since it has been observed that natural fractures play a significant role in the physics of fluid flow in the Middle Bakken formation (L. Wang & Yu, 2019).

In a dual-porosity model, the matrix and fractures are treated as separate elements, and the fluid flow equation is solved for each. The fractures are treated as orthogonal in three directions and serve as boundaries for matrix elements. The matrix blocks are disconnected from one another, and only the fractures provide channels for fluid flow. The governing equations for the dual-porosity model are an extension of the single porosity adaptive-implicit discretized formulation with included matrix-fracture transfer terms (Kazemi et al., 1976). In a compositional simulation, it is necessary to accurately determine phase compositions and their associated thermodynamic properties at each timestep. Thus, a robust stability test based on a Gibbs energy analysis is used to detect single-phase compositions in each block at each timestep. Where the hydrocarbon system is in the two-phase region at a given pressure, temperature, and composition, the phase compositions and splits are obtained by solving the thermodynamic-equilibrium equation where the component fugacities of the oil and gas phases are computed for the Peng-Robinson equation of state (Peng & Robinson, 2002). A single well is cycled between producer and injector modes to replicate a huff-n-puff operation. The mathematical treatment for production and injection in well blocks is adopted from Peaceman (1978). The resulting system of equations is solved to convergence using Newton's method, with volume consistency (Ngheim & Li, 1984).

5.3   Study Area, reservoir and well properties

The study area is the Sanish Field, located in Mountrail County on the North Dakota side of the Williston Basin. The field's porosity ranges between 4 and 10%, and its permeability averages 0.04 mD (Dong & Hoffman, 2013). Our near-well simulation model is built to simulate production from the Deadwood-43-28H well (Well file #16841), which is a horizontal well with an approximately 5000ft lateral section and targets the Middle Bakken formation. It is a hydraulically fractured well with eight (8) fracture clusters. The well started production in June

2008 and had produced around 0.456 MM bbl of oil and 20,000 Mcf of gas at the time of this study. However, production had decreased drastically, making it an excellent candidate for improved oil recovery investigations. Furthermore, the well is spaced far enough apart from other wells, allowing for uncomplicated history matching without concern of interference from neighboring wells. **Figure 35** shows the study area and location of this well.
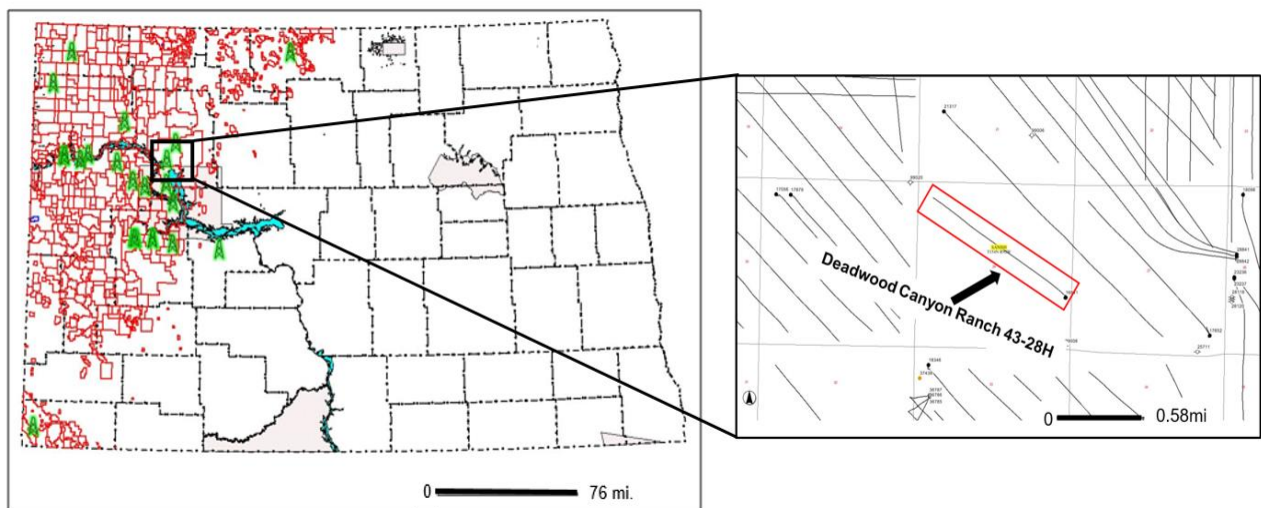
Figure 35: Map showing the study area. The red outline shown in the pop-out figure shows the boundary of the near-well model.

5.4 Fluid model

As mentioned, the phase densities in Equation 11 as a function of pressure, temperature, and composition are calculated using the Peng-Robinson EOS. The Peng-Robinson EOS parameters and reservoir fluid composition data for the Middle Bakken reservoir are adopted from Sanaie et al. (2018), based on experimental PVT data from the work of Adekunle and Hoffman (2014). Constant composition expansion (CCE), differential liberation experiment (DLE), and separator test were conducted on a recombined Bakken crude oil sample prepared from the

separator oil and gas. The single-stage separator tests indicated that the oil is light with 38 °API gravity at stock tank conditions. The constant composition expansion test at a reservoir temperature of 237 °F suggested that the bubble point pressure of the reservoir fluid is 2530 psi. The differential liberation test performed at the saturation pressure and 237 °F indicated an oil density of 0.6463 g/cm^3, oil viscosity of 0.392 cp, solution gas-oil ratio of 914.8 scf/stb and oil formation volume factor of 1.713 bbl/stb. Minimum miscibility pressure is one of the critical fluid-fluid parameters that determine the performance of gas-enhanced oil recovery. Extensive studies of MMP with various injection gases were conducted on dead and recombined fluid samples using a rising bubble apparatus (RBA). Results showed that the MMP of CO_2 with the recombined Bakken oil sample is 3293 psi at 237 °F (Adekunle & Hoffman, 2014).

The reservoir fluid is characterized into nine pseudo-components which are CO_2, N_2, C_1, C_2, C_3, C_4, C_5, C_6-C_7 and C_{8+}. The critical temperature, T_c, critical pressure, p_c, and acentric factors, ω, of the pseudo-components are determined based on the weight-based average of Tc, pc, and ω of the individual hydrocarbon components (Sanaei et al., 2018). The fluid model parameters are presented in **Table 10**. The gas viscosity was estimated from the Jossi, Stiel, and Thodos correlation (Jossi et al., 1962). The aqueous phase density and viscosity are calculated from the Rowe and Chou (1970) and the Kestin et al. (1978) correlations, respectively. To validate the fluid model, we calculated the MMP of CO_2 in oil using the methods available in CMG-WINPROP (Computer Modelling Group, 2018), namely the Cell-to-Cell (Zick, 1986), Key Tie Lines (Zhao et al., 2021)) and the Multiple-Mixing-Cell (Ahmadi & Johns, 2011) methods. The MMP values obtained were within 7% of the reported experimental value.

Table 10: Peng Robinson EOS fluid model parameters

Component	Mole Fraction	Pc (atm)	Tc (K)	Acentric Factor	Molecular Weight	Parachor
N_2	0.030	33.50	126.20	0.040	28.013	41.00
CO_2	0.004	72.80	304.20	0.225	44.010	78.00
C_1	0.273	45.80	190.60	0.008	16.043	77.00
C_2	0.108	48.20	305.40	0.098	30.070	108.00
C_3	0.077	41.90	369.80	0.152	44.097	150.30
C_4	0.051	37.26	422.44	0.190	58.124	188.57
C_5	0.037	33.34	466.44	0.243	72.151	229.28
C_6-C_7	0.098	27.83	528.30	0.330	94.916	296.85
C_{8+}	0.321	23.09	748.40	0.565	178.806	457.08

Table 10 Continued: Binary interaction coefficients

Component	N_2	CO_2	C_1	C_2	C_3	C_4	C_5	C_6-C_7	C_{8+}
N_2	0.00								
CO_2	0.00	0.00							
C_1	0.03	0.00	0.00						
C_2	0.01	0.00	0.00	0.00					
C_3	0.09	0.01	0.00	0.00	0.00				
C_4	0.10	0.02	0.00	0.00	0.00	0.00			
C_5	0.11	0.02	0.00	0.00	0.00	0.00	0.00		
C_6-C_7	0.11	0.03	0.00	0.00	0.00	0.00	0.00	0.00	
C_{8+}	0.13	0.03	0.13	0.02	0.01	0.01	0.01	0.00	0.00

5.5 Reservoir model

A three-dimensional cartesian grid system consisting of 31 grid blocks in the x-direction, 30 grid blocks in the y-direction, and five(5) grid blocks in the z-direction was built. The overall number of grid blocks is 11650, including grid blocks refined locally near hydraulic fractures. The model's dimensions are 1550 ft x 6000 ft x 168 ft, representing the reservoir's length, width, and depth. The top and bottom layers represent the Upper and Lower Bakken formations, respectively,

while the three middle layers represent the Middle Bakken formation. The model incorporates a single horizontal well with a lateral length of 5150 ft placed in the Middle Bakken layer. The horizontal well has eight hydraulic fracture stages. Each fracture stage has a single perforation, resulting in one perforation per stage and a total of eight effective hydraulic fractures. Hydraulic fractures are represented in the horizontal well by planar fractures with a half-length of 238 ft, a spacing of 600 ft, and a fracture conductivity of 30 mD-ft. As hinted, local grid refinement was used to model hydraulic fracture explicitly, which can accurately capture the fluid transport behavior from shale matrix to fracture. **Figure 36** shows the resulting reservoir model.

Water-oil and liquid-gas relative permeability curves for matrix and fractures are generated using Stone's second model as normalized by Aziz and Settari (1979), with quadratic smoothening applied. The main matrix and fracture properties and parameters for the relative permeability correlations are tuned via history matching with production history for the Deadwood Canyon Ranch-43-28H well in the Sanish field after initial average values are provided. The production data represents 12 years of primary production from this well. During history matching, the surface oil rate is used as a constraint, and effort is made to match the gas and water rates while adjusting model parameters. **Figure 37** a-c compares the simulated oil, water, and gas surface production rates with the historical well data. It is observed that the simulated and the historical data are reasonably matched. The oil rate is exactly matched because it was used as a constraint during the history match process. The water rate is matched within 1.5% and the gas rate within 12.0% **Table 11**. summarizes the history-matched reservoir and well parameters. After history matching, the CO_2 huff-n-puff is simulated following primary injection. Diffusion has been identified as a critical property to describe the physics of enhanced oil recovery by CO_2. CO_2 diffusion into oil was considered in our simulation with a defined constant CO_2 diffusivity

coefficient of 5.5×10^{-5} cm^2/s, which is within the range of values reported by Grogan et al. (1988).
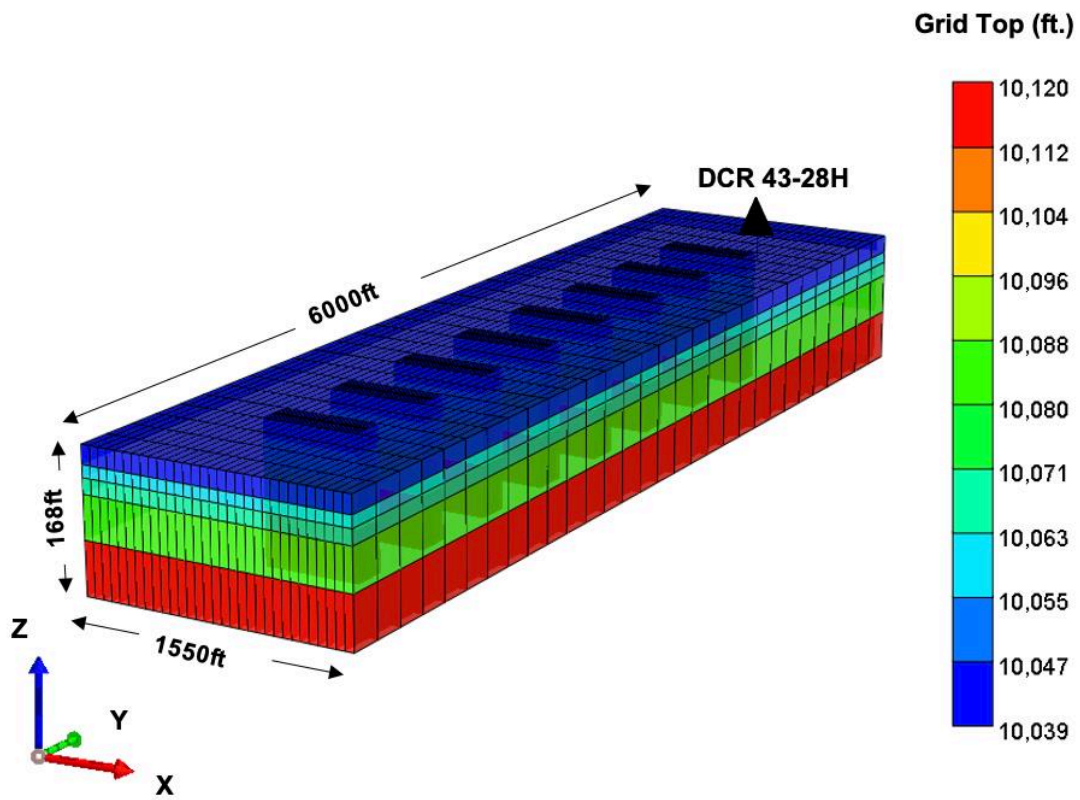
Figure 36: Bakken reservoir model used in this work

a)
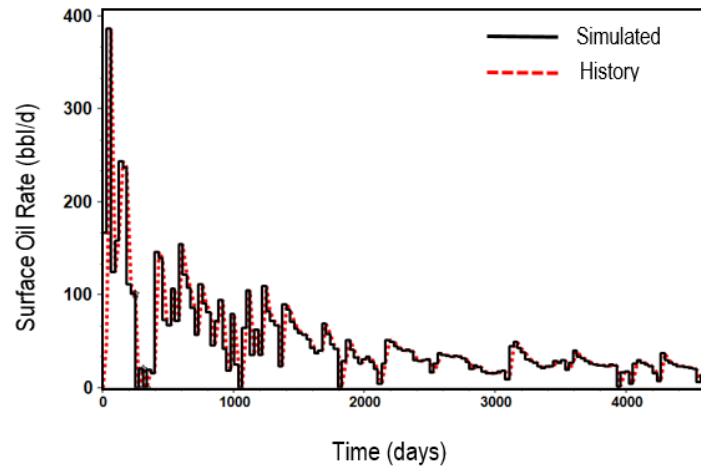
b)
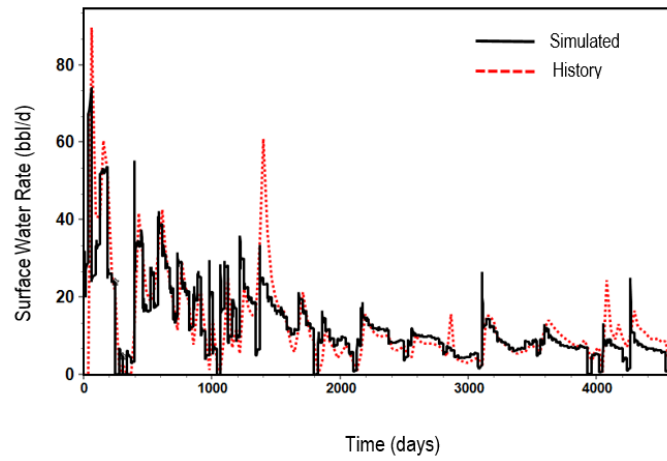
c)
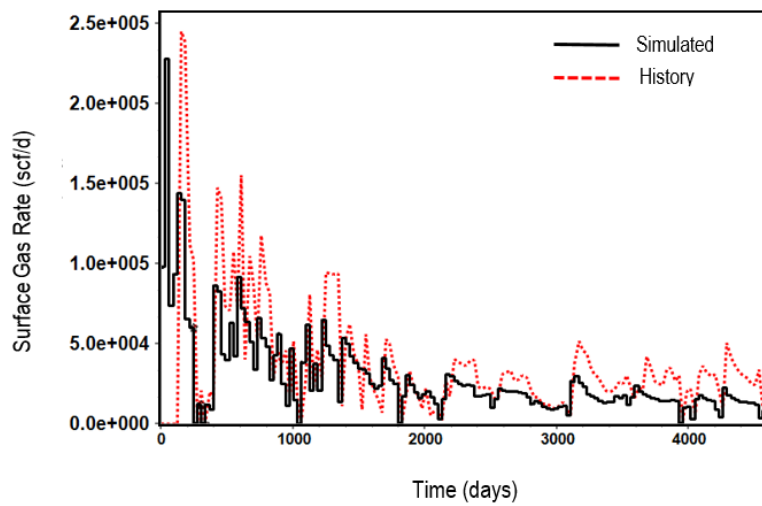
Figure 37: History matching results for a) oil rate b) water rate c) gas rate

Table 11: History-matched reservoir and well properties.

Parameter	Value	Unit
Model dimension	1550 x 6000 x 168	ft
Number of gridlocks	31 x 30 x 5	-
Initial reservoir pressure gradient	0.73	psi/ft
Reservoir temperature	240	°F
Reservoir thickness		
Upper Bakken (UB)	17	ft
Middle Bakken (MB)	64	ft
Lower Bakken (LB)	48	ft
Reservoir permeability (I=J)		
Matrix (MB)	0.003	mD
Fracture (MB)	0.3	mD
Matrix (UB, LB)	0.0001	mD
Fracture (UB, LB)	0.001	mD
Reservoir porosity		
Matrix (MB)	0.07	-
Fracture (MB)	0.007	-
Matrix (UB, LB)	0.05	-
Fracture (UB, LB)	0.005	-
Permeability Anisotropy (Kv/Kh)	0.1	-
Initial water saturation	0.4	-
Total compressibility	7.1 e-6	psi^{-1}
Well length	5150	ft
Number of stages	8	-
Clusters per stage	1	
Cluster spacing	600	ft
Fracture half-length	238	ft
Fracture conductivity	30	mD-ft

5.6 Sampling and proxy model development

At least five operational parameters have been identified as critical for enhanced oil recovery performance by CO_2 huff-n-puff in tight formations (Sheng, 2020). These parameters, including injection rate, injection period, soak period, production period, and production bottom-hole pressure (BHP), are considered for this study. The two responses of interest are the recovery factor and the gas utilization factor. The recovery factor is defined here as the proportion of total oil-in-place produced during primary and secondary production at the end of the simulation period. While the recovery factor is a measure of the performance of the EOR technique, the gas utilization factor is a measure of the efficiency of the injection process. The gas utilization factor has been defined in various ways in the literature, and there seems to be no industry consensus(Azzolina et al., 2015; Hughes, 2009). Here, we define it as the total amount of oil recovered, in bbl, per 1,000 scf of CO_2 injected, including recycled CO_2. This definition can be expressed as

$$UF_{CO_2} = \frac{N_{P,inc}}{V_{co_2,inj.} - V_{co_2,prod}}$$

Equation 12

where UF_{CO_2} is the gas utilization factor in bbl/Mscf, $N_{P,inc}$ is the incremental oil produced due to CO_2 injection in bbl, $V_{co_2,inj.}$ is the cumulative volume of CO_2 injected in Mscf and $V_{co_2,prod}$ is the cumulative volume of CO_2 produced in Mscf.

RSM was used to investigate the effects and interactions of the five operational variables on the two responses. In general, the process involves designing experimental points within a chosen design space using the Design of Experiments (DOE) approach, performing the experiments, analyzing the results using statistical techniques, checking for appropriate

assumptions, fitting the data with a polynomial function and optimizing the responses. Choosing the correct DOE method is critical to the success of the methodology. Several DOE methods have been used in literature, with Box-Benkhen design (BBD) and central composite designs (CCD) being the most common (Myers et al., 2009). In this work, CCD was used for designing the experimental data. The CCD is a well-known classical response surface design with up to five levels ($-\alpha$, -1, 0, +1, $+\alpha$). It requires fewer runs than BBD, especially when the number of factors is five or more. For a rotatable design, $\alpha = \sqrt{2}^k$; thus, with five factors, we use α =2.37. The CCD has three components: factorial points, axial points, and center points. These components allow a second-order polynomial to be fitted to the experimental data. The form of this second-order polynomial can be written as follows for five factors:

$$Y = \beta_O + \sum_{i=1}^{5} \beta_i x_i + \sum_{i=1}^{5} \beta_{ii} x_i^2 + \sum_{i=1}^{4} \sum_{j=1+1}^{5} \beta_{ij} x_i x_j + \epsilon$$

Equation 13

Where Y denotes the response, and $\beta_O, \beta_i, \beta_{ii}, \beta_{ij}$ denote the coefficient of intercept, main effect, quadratic effects, and interaction effects, respectively. ϵ represents the random error. The factorial points are used to estimate the first-order and two-factor interactions, while the axial points are used to estimate pure quadratic effects. The center points are usually a repeat of the same experimental points and are used to estimate the pure error in the experiments. For a computational simulation study like this, a replication of an experiment will generate the same results. That is, there is no pure error. The number of design points, N_D, can be calculated from

$$N_D = 2^k + 2k + n_C$$

where k is the number of factors, and n_C is the number of center points. Forty-three(43) experiments were run in total, noting that only one center point was used (no pure error). The experimental levels (coded and actual) are presented in **Table 12.** The design was carried out using Design-Expert® software (Stats-Ease Inc., 2021) and the experimental runs were automated using CMG-CMOST (Computer Modelling Group, 2018).

During the model fitting process, several diagnostic plots were used to check for assumptions of ordinary least squares. This step also included identifying and removing outliers with diagnostic plots such as normal probability plots and residual plots. Where necessary, data transformation is also applied to the data. Several models are tested in a preliminary phase to select the most appropriate model. Beginning with a simple linear model that contains only linear terms, the model becomes increasingly complex as two-factor interaction, quadratic, and cubic terms are added sequentially. The increase in model significance, lack of fit, and R-squared (R^2) values are then evaluated, and a suitable starting model is selected. Using analysis of variance (ANOVA), the chosen model is tuned by selecting only the significant terms. The backward elimination method is used to remove insignificant terms based on p-values. An alpha value of 0.05 was used for this elimination process. The final second-order polynomial is passed on for analysis and optimization of the responses.

Table 12: Factors and their levels used in the rotatable central composite design of experiments.

				Coded Levels				
Factor #	**Variable**	**Units**	**Symbol**	**-α**	**-1**	**0**	**+1**	**+α**
1	Injection Rate	Mscf/d	A	50.00	470.18	775.00	1079.82	1500.00
2	Injection Period	Days	B	5.00	90.48	152.50	214.52	300.00
3	Soak Period	Days	C	5.00	90.48	152.50	214.52	300.00
4	Production Period	Days	D	5.00	90.48	152.50	214.52	300.00
5	Production BHP	Psi	E	100.00	1519.90	2550.00	3580.09	5000.00

5.7 Optimization

After fitting the appropriate second-order polynomial to the experimental data for recovery and gas utilization factors, the two responses were optimized using the desirability function approach. The desirability function approach is a technique for multi-response optimization that is commonly utilized in the industry (Costa et al., 2011). It is based on the premise that a process with many responses is not optimal unless all the responses fall within some defined desire limits. The approach entails transforming the estimated second-order response models (y) into discrete desirability values (d). For multiple responses, each response is converted to an individual desirability value via the desirability function. The desirability function $di\ (\widehat{Y}i)$ assigns values between 0 and 1 to the possible values of $\widehat{Y}i$ for each response $\widehat{Y}i(x)$, with di $(\widehat{Y}i)\ =\ 0$

representing a completely undesired value of $\hat{Y}i$ and $di\ (\hat{Y}i) = 1$ representing an entirely desirable or ideal response value. A combination of operating conditions that provide the "most desirable" response values is found for each response. The individual desirability values are then aggregated to form a composite function (D) for the entire process.

Several desirability functions have been proposed in the literature (Costa et al., 2011). We adopt the desirability function proposed by Derringer and Such (1980). Here, different desirability functions $(di\ (\hat{Y}i))$ are used depending on whether the specific response, $\hat{Y}i$, is to be maximized, minimized, or assigned a target value. If a response is assigned a target value, then its desirability function is

$$d_i(\hat{Y}_i) = \begin{cases} 0 & if\ \hat{Y}_i(x) < L_i \\ \left(\dfrac{\hat{Y}_i(x) - L_i}{T_i - L_i}\right)^s & if\ L_i \le \hat{Y}_i(x) \le T_i \\ \left(\dfrac{\hat{Y}_i(x) - U_i}{T_i - U_i}\right)^t & if\ T_i \le \hat{Y}_i(x) \le U_i \\ 0 & if\ \hat{Y}_i(x) > U_i \end{cases}$$

Equation 15

Where Li, Ui and Ti are the lower, upper, and target values, respectively and $Li \le Ti \le Ui$. The exponents *s* and *t* determine how important it is to hit the target value. If a response is to be maximized instead, the individual desirability is defined as

$$d_i(\hat{Y}_i) = \begin{cases} 0 & if\ \hat{Y}_i(x) < L_i \\ \left(\dfrac{\hat{Y}_i(x) - L_i}{T_i - L_i}\right)^s & L_i \le \hat{Y}_i(x) \le T_i \\ 1 & if\ \hat{Y}_i(x) > T_i \end{cases}$$

Equation 16

Finally, if a response is to be minimized, then desirability is defined as

$$d_i(\hat{Y}_i) = \begin{cases} 1 & if\ \hat{Y}_i(x) < T_i \\ \left(\dfrac{\hat{Y}_i(x) - U_i}{T_i - U_i}\right)^s & T_i \le \hat{Y}_i(x) \le U_i \\ 0 & if\ \hat{Y}_i(x) > U_i \end{cases}$$

<div align="right">*Equation 17*</div>

The geometric mean is then used to aggregate the individual desirability values to yield the overall desirability D:

$$D = \left[d_1(\hat{Y}_1)d_2(\hat{Y}_2)d_3(\hat{Y}_3)....d_n(\hat{Y}_n)\right]^{1/n}$$

<div align="right">*Equation 18*</div>

where *n* is the number of responses.

Using numerical optimization approaches such as those described suggests operational points in the factor space that give the optimal responses. This approach may sometimes be impractical for field operations as other constraints (such as regulatory, economic, and environmental) may not permit setting operational parameters precisely as recommended. Providing optimal regions rather than optimal points gives engineers operational flexibility while optimizing productivity. Thus, in addition to using the desirability approach for optimizing recovery and gas utilization factors, we used the graphical overlay method to delineate operational areas that give the best of both responses simultaneously. The technique works by overlaying response contours on each other and identifying regions where factor settings simultaneously

satisfy the desired response values. The result is a graphical display of areas of feasible response values in the factor space.

5.8   Results and Discussion

5.8.1   Simulation results

We carried out a base case simulation without any CO_2 injection to establish a baseline for investigating the effectiveness of CO_2 for oil recovery. For all other cases with CO_2 injection, injection began after 4645 days of primary recovery. **Figure 38** illustrates a comparison of the case without CO_2 and an example case (run 42) with CO_2 injection. The figure shows that CO_2 significantly improves the oil recovery compared to the case without CO_2 injection. The projected recovery factor without CO_2 injection is 5.38%. All the runs with CO_2 injection outperformed the case without CO_2 injection, indicating that CO_2 injection can improve recovery even without optimization.

Figure 39 depicts the behavior of the injection bottom pressure during huff-n-puff cyclic injection. As indicated in the figure, a single cycle consists of an injection stage (denoted as I), a soaking stage (denoted as S) and a production stage (denoted as P). During the injection stage, the injection BHP increases sharply to a value depending on the injection rate. Surface compressor pressure ratings may limit the volume of CO_2 that can practically be injected. Therefore, we set an injection BHP limit to 10,000 psi. For the range of injection rates used in this work, the injection BHP did not exceed 7,000 psi, indicating that the specified volumes of CO_2 were successfully delivered into the formation. During the soaking phase, injection is halted, and the well is shut-in (no production). As seen in **Figure 39**, there is a slight pressure drop during this phase, which may indicate the mixing of CO_2 and oil. Finally, during the production stage, the well is opened to

production. The BHP decreases sharply to the set production BHP as fluid is produced to the surface.

Also shown in **Figure 37** is the amount of CO_2 injected and CO_2 produced. Notably, the cumulative CO_2 injected at the end of the simulation period is higher than the cumulative CO_2 produced. This phenomenon is because a portion of the injected CO_2 is retained in the formation. The study assumes that the produced CO_2 can be reinjected and accounted for in the gas utilization formulation. Thus, although CO_2 retention is desirable in several studies for environmental considerations, it negatively impacts the gas utilization factor if it is not commensurate with an increase in oil recovery.

5.9   Proxy model evaluation

Table 3 summarizes the results of the 43 simulation runs using CCD with five factors and two responses. As mentioned, the two responses are the recovery factor and the gas utilization factor, and henceforth will occasionally be denoted by Y_1 and Y_2, respectively. We model each response independently. An initial evaluation indicated the need to transform the two responses. *Figures* **40** a and b show the distributions of recovery and gas utilization factors obtained from the 43 runs (without outliers). Consequently, the recovery and gas utilization factors were transformed using a power transform (power=2.72) and a square root transform, respectively. The initial model selection phase suggested that the quadratic model best fits the experimental data as expected with CCD. The selected model is fine-tuned by performing an iterative fitting procedure based on the p-value of each model coefficient and the backward elimination of insignificant terms. For Y_1, the two-factor interaction terms AC, AD, BC, CE and BD, and the quadratic terms B^2 and C^2 were eliminated. For Y_2, the two-factor interaction terms AC, AC and CE and the quadratic terms C^2

and E^2 were insignificant and therefore removed. We retained all the main factors to maintain the hierarchy in the model.
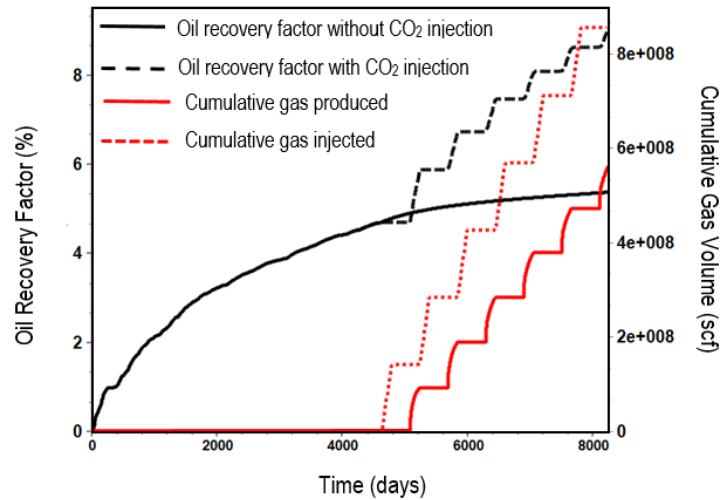
Figure 38: Comparison of cumulative oil recovery factor for primary recovery and a typical case with CO_2 injection. Also shown is the cumulative CO_2 injected compared to the cumulative CO_2 produced for the case with CO_2 injection.
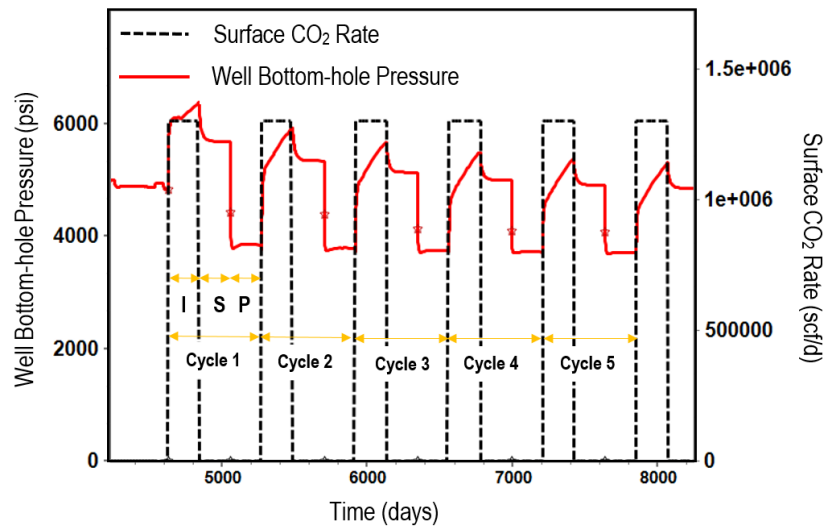
Figure 39: Typical injection well BHP behavior during huff-n-puff cycles with corresponding injection gas rates. The plot shows the cycle stages and the number of cycles for a typical cyclic schedule.
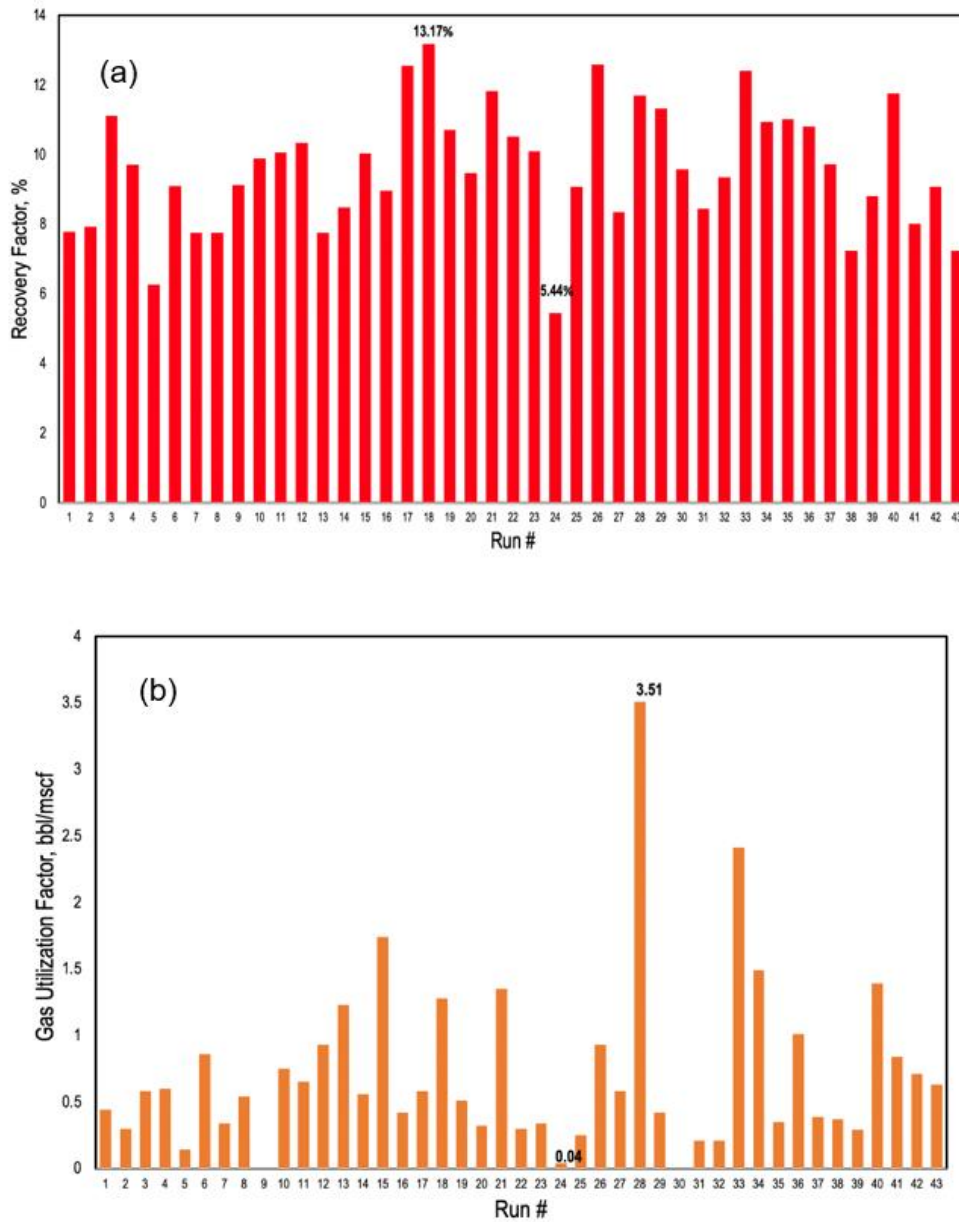
Figure 40: Distributions of the a) Recovery factor and b) Gas utilization factor obtained from simulation runs

Table 12 lists the results of ANOVA for the final quadratic models for the two responses.

Ficher's test (F-test) of overall significance is the formal hypothesis test used in this work. Based

on the chosen significance level of 0.05, it is observed that the p-values for the obtained overall F-

values are lower than the significance level. This finding indicates that our sample data provide sufficient evidence to conclude that the polynomial model fits the data better than a model without independent variables (the F-test's reference basis). Additionally, all the independent variables' F-values are significant (that is, have p-values< 0.05), indicating that all terms contribute to the model's overall predictive power. This result is true for both the Y_1 and Y_2. The coefficient of determination (R^2), the adjusted R^2 (adj. R^2) and the predicted R^2 (pred. R^2) are important in model evaluation. The difference in the values of these metrics demonstrates the quadratic polynomial model's fit and predictive capability in general. For instance, our analysis shows that for Y_1, the R^2, adj. R^2, and pred. R^2 values are 0.984, 0.9796, and 0.9657, respectively. This R^2 value indicates that the five factors correctly explain 98.84% of the variance in the recovery factor. The slight difference between R^2 and adj R^2 suggests that the fitted model contains enough terms, neither under nor over-specified. The pred. R^2 value obtained is also reasonably close to the adj. R^2 value, demonstrating that the model is not overfitted and can sufficiently predict the response values outside the design space (although this is not recommended). Similarly, we could make an argument for Y_2. Finally, the "adequate precision" quantifies the model's signal-to-noise ratio. Generally, an adequate precision greater than 4 is desirable and vice versa. The signal-to-noise is desirable for both responses, indicating that the models can navigate the design space.

In addition to the various goodness-of-fit measures used for the proposed model, it is critical to check the behavior of the residuals. These checks are accomplished using a variety of diagnostic plots, namely the normal probability of residuals, predicted versus actual values and residual versus predicted values. As the name implies, a normal probability plot indicates whether the residuals have a normal distribution, a critical assumption for ordinary least square (OLS) modeling. The externally studentized residuals, rather than the raw residuals, were used.

Studentizing the residuals maps all the different normal distributions to a single standard normal distribution and has been shown to be more effective for detecting outliers than raw residuals (Myers et al., 2009). **Figure 41 a** and **c** illustrate the normal plot with externally studentized residuals for Y_1 and Y_2. The plots demonstrate that most sample points are positioned within a tight range along the reference normal probability line, with only modest departures from this line for both responses. This characteristic demonstrates the data's normality and the residuals' independence, which supports the model's high validity for approximation.

Table 13: Five-factor CCD used for RSM. It shows the values for independent factors and corresponding recovery and gas utilization factors obtained from numerical simulation. The values with asterisks (*) were considered outliers.

Run #	Space type	Factor 1 (A) Injection Rate (Mscf/d)	Factor 2 (B) Injection Period (Days)	Factor 3 (C) Soak Period (Days)	Factor 4 (D) Production Period (Days)	Factor 5 (E) Production BHP (psi)	Response 1 (Y_1) Recovery Factor (%)	Response 2 (Y_2) Gas Utilization Factor (bbl/Mscf)
1	Factorial	470.18	214.52	214.52	214.52	3580.09	7.79	0.44
2	Factorial	1079.82	90.48	214.52	90.48	3580.09	7.94	0.30
3	Factorial	1079.82	90.48	90.48	90.48	1519.90	11.11	0.58
4	Center	775.00	152.50	152.50	152.50	2550.00	9.71	0.60
5	Axial	775.00	152.50	152.50	152.50	5000.00	6.27	0.14
6	Factorial	470.18	214.52	214.52	90.48	1519.90	9.09	0.86
7	Factorial	470.18	214.52	90.48	90.48	3580.09	7.75	0.34
8	Factorial	470.18	90.48	90.48	90.48	3580.09	7.75	0.54
9	Axial	50.00	152.50	152.50	152.50	2550.00	9.12	15.55*
10	Factorial	470.18	214.52	90.48	90.48	1519.90	9.88	0.75
11	Factorial	1079.82	90.48	214.52	90.48	1519.90	10.06	0.65
12	Axial	775.00	152.50	152.50	300.00	2550.00	10.34	0.93

13	Factorial	470.18	90.48	214.52	214.52	3580.09	7.76	1.23
14	Factorial	1079.82	90.48	214.52	214.52	3580.09	8.48	0.56
15	Factorial	470.18	90.48	214.52	90.48	1519.90	10.03	1.74
16	Factorial	1079.82	90.48	90.48	214.52	3580.09	8.97	0.42
17	Factorial	1079.82	214.52	90.48	214.52	1519.90	12.55	0.58
18	Axial	775.00	152.50	152.50	152.50	100.00	13.17	1.28
19	Axial	775.00	152.50	5.00	152.50	2550.00	10.70	0.51
20	Factorial	1079.82	214.52	214.52	90.48	1519.90	9.47	0.32
21	Factorial	1079.82	90.48	214.52	214.52	1519.90	11.82	1.35
22	Factorial	1079.82	214.52	90.48	90.48	1519.90	10.51	0.30
23	Factorial	1079.82	214.52	90.48	214.52	3580.09	10.10	0.34
24	Axial	775.00	152.50	152.50	5.00	2550.00	5.44	0.04
25	Factorial	1079.82	214.52	214.52	214.52	3580.09	9.07	0.25
26	Factorial	1079.82	90.48	90.48	214.52	1519.90	12.58	0.93
27	Factorial	470.18	214.52	90.48	214.52	3580.09	8.35	0.58
28	Factorial	470.18	90.48	214.52	214.52	1519.90	11.70	3.51
29	Factorial	1079.82	214.52	214.52	214.52	1519.90	11.32	0.42
30	Axial	775.00	5.00	152.50	152.50	2550.00	9.58	20.34*
31	Factorial	1079.82	214.52	214.52	90.48	3580.09	8.45	0.21
32	Factorial	1079.82	214.52	90.48	90.48	3580.09	9.36	0.21
33	Factorial	470.18	90.48	90.48	214.52	1519.90	12.40	2.41
34	Factorial	470.18	90.48	90.48	90.48	1519.90	10.94	1.49
35	Axial	1500.00	152.50	152.50	152.50	2550.00	11.01	0.35
36	Factorial	470.18	214.52	214.52	214.52	1519.90	10.81	1.01
37	Axial	775.00	300.00	152.50	152.50	2550.00	9.73	0.39
38	Factorial	470.18	214.52	214.52	90.48	3580.09	7.23	0.37
39	Factorial	1079.82	90.48	90.48	90.48	3580.09	8.81	0.29
40	Factorial	470.18	214.52	90.48	214.52	1519.90	11.75	1.39
41	Factorial	470.18	90.48	90.48	214.52	3580.09	8.02	0.84
42	Axial	775.00	152.50	300.00	152.50	2550.00	9.07	0.71
43	Factorial	470.18	90.48	214.52	90.48	3580.09	7.24	0.63

The plot of externally studentized residuals against the predicted values in **Figure 42 b** and **c** also exhibit a desirable behavior of the residuals. The plots reveal that all sample points are randomly scattered and located within a constant defined range across the plot, which indicates constant variance (Myers et al., 2009). Based on these diagnostics, we can confidently conclude that the model is adequate. There is no reason to suspect any violation of the independence or constant variance assumption in all runs.

The final quadratic models for the two responses are presented in Equations 19 and 20. **Figure 43 a-b** shows the predicted versus actual plot, indicating how well the proposed quadratic model predicts the actual data for responses Y_1 and Y_2. The plots show a good match between actual and predicted values across the entire range of our sample data, confirming the performance of the second-order quadratic model.

For recovery factor, Y_1:

$$Y_1^{2.72} = 988.450 - 0.429A - 2.438B - 0.878C + 5.840D - 0.297E + 0.000979AB + 0.000051AE$$
$$+ 0.000596BE - 0.000932DE + 0.000191A^2 - 0.006623D^2 + 0.000024E^2$$

Equation 19

For the gas utilization factor, Y_2:

$$\sqrt{Y_2} = 2.159 - 0.00197A - 0.00618B + 0.00209C + 0.00803D - 0.00380E + 2.101 \times 10^{-6}AB$$
$$- 1.148 \times 10^{-6}AD + 2.005 \times 10^{-7}AE - 0.000011BC - 9.499 \times 10^{-6}BD$$
$$+ 8.473 \times 10^{-7}BE - 4.520 \times 10^{-7}DE + 4.828 \times 10^{-7}A^2 + 0.000011B^2$$
$$- 8.564 \times 10^{-6}D^2$$

Equation 20

Table 14: Analysis of variance for the quadratic models.

Source	Recovery Factor (%)		Gas Utilization Factor (bbl/Mscf)	
	F-value	P-value	F-value	P-value
Model	224.99	< 0.0001	99.26	< 0.0001
A-Injection Rate	75.74	< 0.0001	357.79	< 0.0001
B-Injection Period	4.76	0.0345	257.97	< 0.0001
C-Soak Period	143.87	< 0.0001	7.93	0.0075
D-Production Period	388.83	< 0.0001	225.08	< 0.0001
E-Production BHP	1747.87	< 0.0001	450.75	< 0.0001
AB	12.29	0.0011	18.35	0.0001
AC	-	not significant	-	not significant
AD	-	not significant	5.47	0.0244
AE	9.11	0.002	46.08	< 0.0001
BC	-	not significant	22.06	< 0.0001
BD	-	not significant	15.52	0.0003
BE	51.89	0.0042	34.06	< 0.0001
CE	-	< 0.0001	-	not significant
DE	126.96	< 0.0001	9.69	0.0034
A^2	12.35	0.001	24.18	< 0.0001
B^2	-	not significant	19.78	< 0.0001
C^2	-	not significant	-	not significant
D^2	45.43	< 0.0001	24.35	< 0.0001
E^2	47.19	< 0.0001	-	not significant
R^2	0.984		0.9738	
Adjusted R^2	0.9796		0.964	
Predicted R^2	0.9657		0.9094	
Adequate Precision	66.94		51.33	
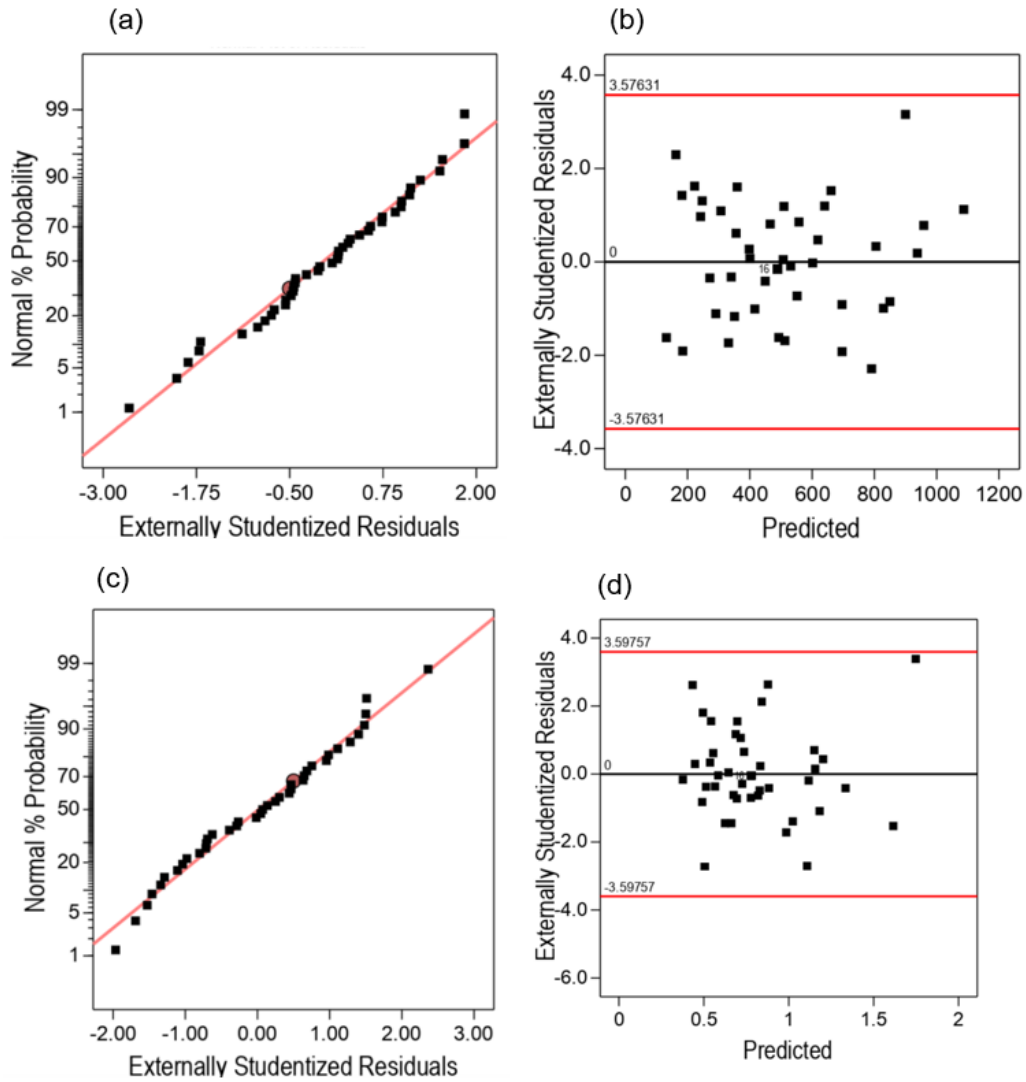
Figure 41: Diagnostic plots. a) normal plot for recovery factor b) residual vs. predicted plot for recovery factor c) normal plot for gas utilization factor d) residual vs. predicted plot for gas utilization factor.
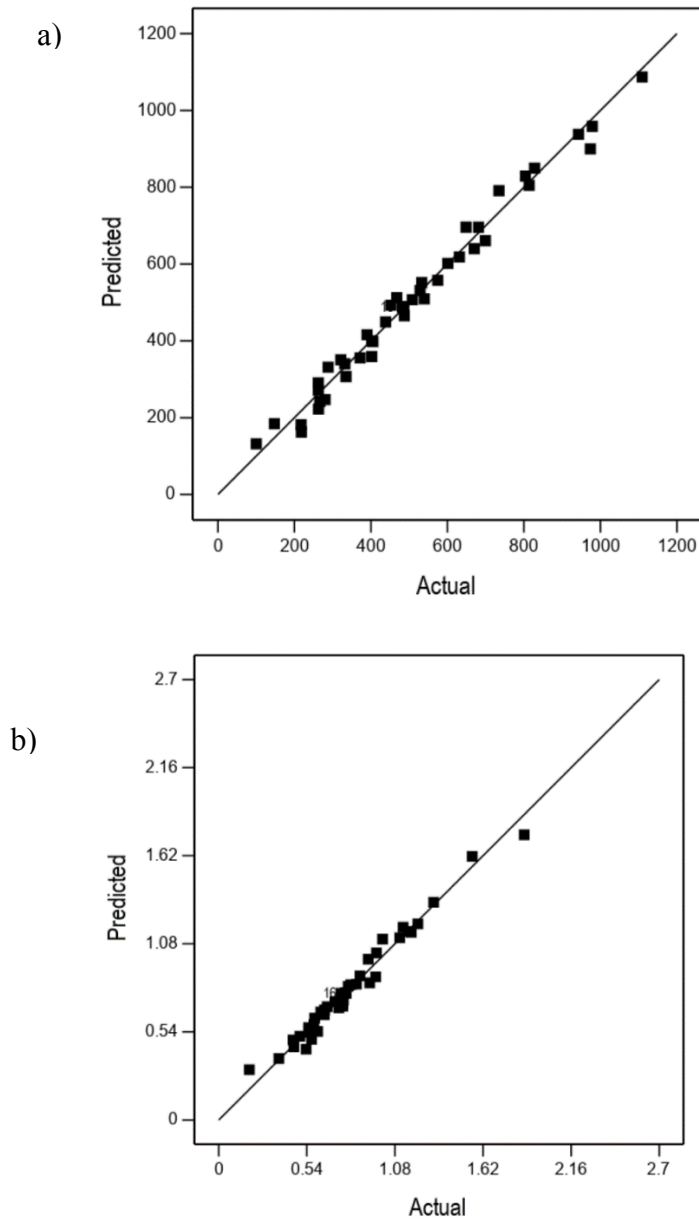
Figure 43: Actual vs. predicted plot for a) power transformed recovery factor and b) square root transformed gas utilization factor.

5.9.1 Main effects

The characteristics of the main effects (first-order terms) are best interpreted concisely using the perturbation plots. The perturbation plot helps to compare the influence of all the factors at a particular point in the design space. We set the reference point at the midpoint (coded 0) of all

the factors. On the perturbation plot, a high gradient reveals high response sensitivity to the related factor and vice versa. **Figure 43 a** shows the perturbation plot for the recovery factor. It can be observed that the recovery factor increases with an increase in injection rate (A). As more CO_2 is injected, the injection BHP rises along with the average pressures in the matrix and fractures. Increased pressure in the reservoir above the CO_2 MMP results in more significant gas dissolution in the oil, which causes swelling of the oil and resultant displacement of trapped oil. The benefit of increased pressure can also be realized even if the pressure does not reach the MMP. Below the MMP, CO_2 may be able to displace oil in the matrix into natural fractures immiscibly. If these natural fractures are connected to the well or hydraulic fractures, they may act as flow paths for oil to reach the surface.

However, compared to the other factors, we observed that the gradient of the slope corresponding to injection rate (A) is relatively small, indicating that the recovery factor is minimally sensitive to the injection rate. We follow from **Figure 43 b** that increasing the CO_2 rate to increase recovery may not be an efficient strategy to increase recovery. As the rate of injection is increased, the gas utilization factor decreases significantly. This finding indicates that although increasing the rate may improve oil production, the incremental benefits of the extra gas injected diminish as more gas is injected. In addition, the additional gas injected may permanently be retained in the formation and may not be produced for utilization.

Increasing the volume of gas injected into the reservoir can be achieved by either increasing the injection rate or the injection period. We observe that increasing the injection period does not have the same effect as increasing the injection rate. As **Figure 43a** illustrates, extending the injection period (B) has a marginally negative impact on recovery. For a fixed simulation period, prolonging the injection period may mean shortening the valuable production period. We found

that increasing the injection period does not result in an increase in the production oil rate to offset the production time lost. **Figure 43 b** also shows the negative influence of an increased injection period on the gas utilization factor. Essentially, this suggests that the increased amount of gas injected does not yield equal incremental oil recovery.

a)

b)
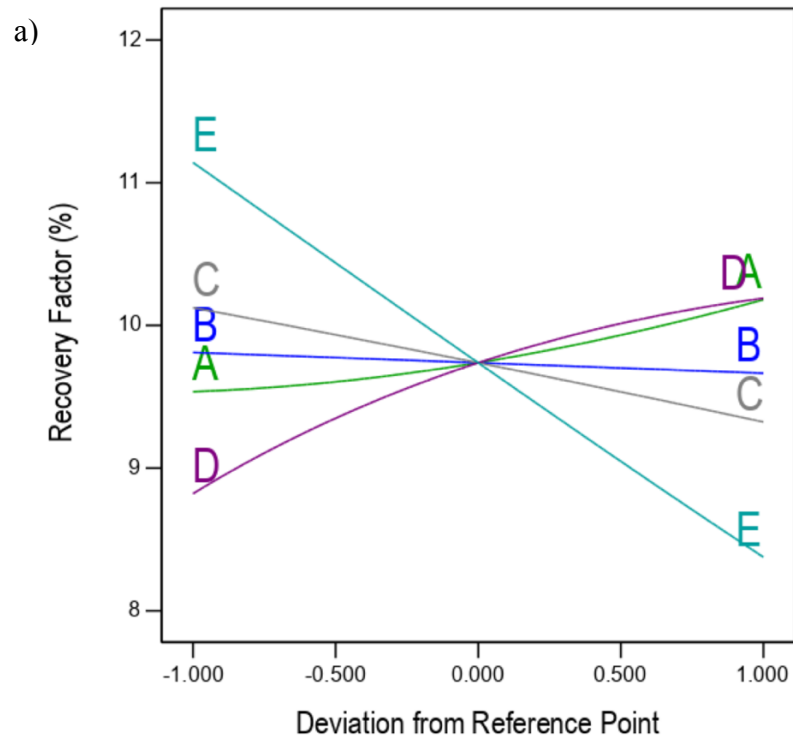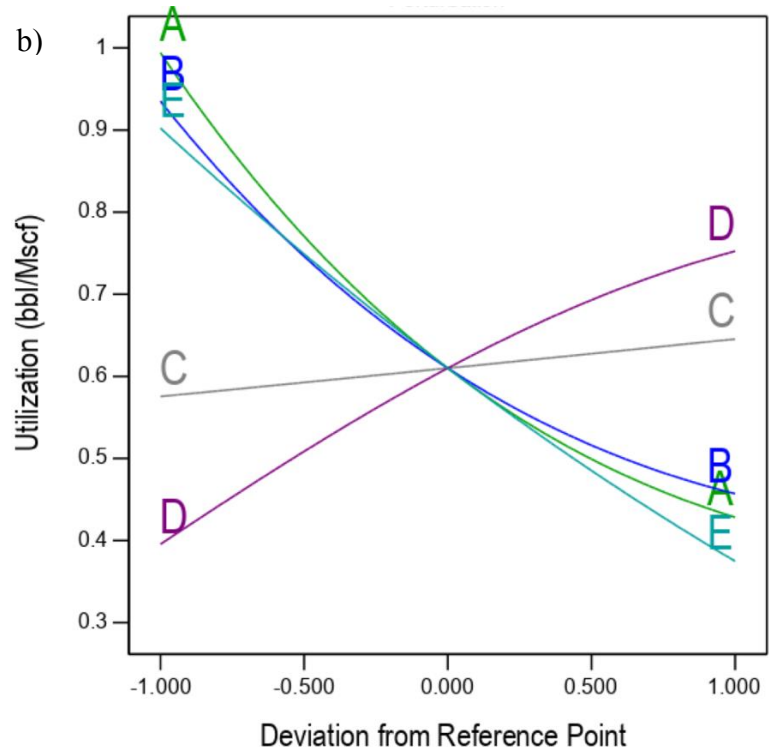
Figure 43: Perturbation plots for a) recovery factor and b) gas utilization factor. The letter representations are as follows: injection rate (A), injection period(B), soak period(C), production period(D), production BHP(E)

Figure 43a shows that extending the soak period (C) reduces the recovery factor. Like in the case of a prolonged injection period, as discussed above, increasing the soak period implies sacrificing some valuable production period, which negatively impacts the recovery factor. The importance of the soak period to the huff-n-puff scheme has been an issue of interest among researchers, and several differing opinions have been proposed. Our results agree with Chen et al. (2013), who observed that a shorter soak time resulted in a better recovery. Sanchez-Rivera et al. (2015) also observed that an extended soak time has no benefit to production and may even be detrimental to recovery. Other authors (Gamadi et al., 2014; W. Yu et al., 2014) have reported an

improvement in the oil recovery factor when soak time is increased. There appears to be a consensus among those investigations that CO_2 diffusion is the principal mechanism at work during soaking. Thus, a high diffusion rate will amplify the impact of the soak period on oil recovery. In this work, it is plausible the diffusion constant used here is not high enough to impact the oil recovery. Sensitivity studies on the effect of diffusion rate on recovery are beyond the scope of this work. Surprisingly, an increased soak period resulted in a slight increase in gas utilization (**Figure 43 b**). We observe that this is because of the significant factor interaction between the soak period and injection period and holds at the midpoint value of the injection period (and all other factors). This finding highlights the importance of analyzing the interaction effects.

As expected, the recovery factor increases with the length of the production time (D), as illustrated in **Figure 43 a**. The plot indicates an impending plateau at long production times following a significant initial increase. This trend is because as production increases along with the production of injected gas, the pressure in the reservoir reduces gradually, leading to a decrease in production. Likewise, the gas utilization factor increases with a prolonged production period (**Figure 43 b**). This improved gas utilization factor can be attributed to the increase in injected gas recovery with a proportionally increased oil production, positively impacting gas utilization.

Among all the factors, the production BHP (E) had the most impact on both recovery and gas utilization. **Figure 43 a** shows a significant inverse linear relationship between production BHP and recovery factor. That is, a low BHP positively impacts recovery and vice versa. A low production BHP results in a higher-pressure gradient, enhancing fluid flow from the matrix to the fractures and into the well. The high sensitivity of the recovery factor to BHP implies that gas drive may be a dominating mechanism in the recovery process. The high drawdown causes an increase in injected gas production that propels oil from the matrix to the fracture. This mechanism

also results in more CO_2 produced for utilization, thus increasing the gas utilization factor **(Figure 43 b).**

Figure 44 summarizes the relative influence of all factors in a tornado chart. The relative influence is measured by the coded coefficients (instead of the actual coefficients used in the proxy model). The plot includes two-factor interaction terms, which will be discussed in the next section.

5.9.2 Factor interactions

Understanding the interactions between the various factors is critical in assessing the performance of the process. When an interaction effect is present, the impact of one factor depends on the level of other factors. Unfortunately, this aspect is often ignored in several studies on CO_2 huff-n-puff, and only the main effects are usually considered. Analyzing only the main effects can result in inaccurate conclusions when interactions between factors are significant, as these conclusions are only valid at the fixed reference values. As seen in **Table 14,** some interaction effects are statistically significant for both responses, thus the need to interpret these interactions. Interaction plots are best used to describe these factor interactions by displaying the relationships between two factors while holding all other factors at their center points. Generally, nonparallel trends on interaction plots suggest an interaction between the variables, whereas parallel trends imply no interaction. The following section discusses some of the critical interactions among the factors considered.

Figure 45 a shows the interaction effects between injection rate (A) and injection period (B) on the recovery factor. It is observed that at a lower injection rate of 470 Mscf/d, a more extended injection period results in a lower recovery factor, as described in the main effects. In contrast, at a higher injection rate of 1071 Mscf/d, the recovery factor increases slightly as the

injection period increases. As already described, an increased injection time may imply a reduction in valuable production time for a fixed simulation duration. However, it is apparent that at a higher injection rate, the positive effect of injection rate on recovery offsets the negative influence of an increased injection period, thus an increase in recovery factor. This interaction effect is also significant for the gas utilization factor, though both factors have an inverse relationship with the gas utilization factor **Figure 45 a**. Thus, as previously noted on the perturbation plots, although a higher injection rate may improve recovery, it is detrimental to the gas utilization factor at any length of the injection period.

a)
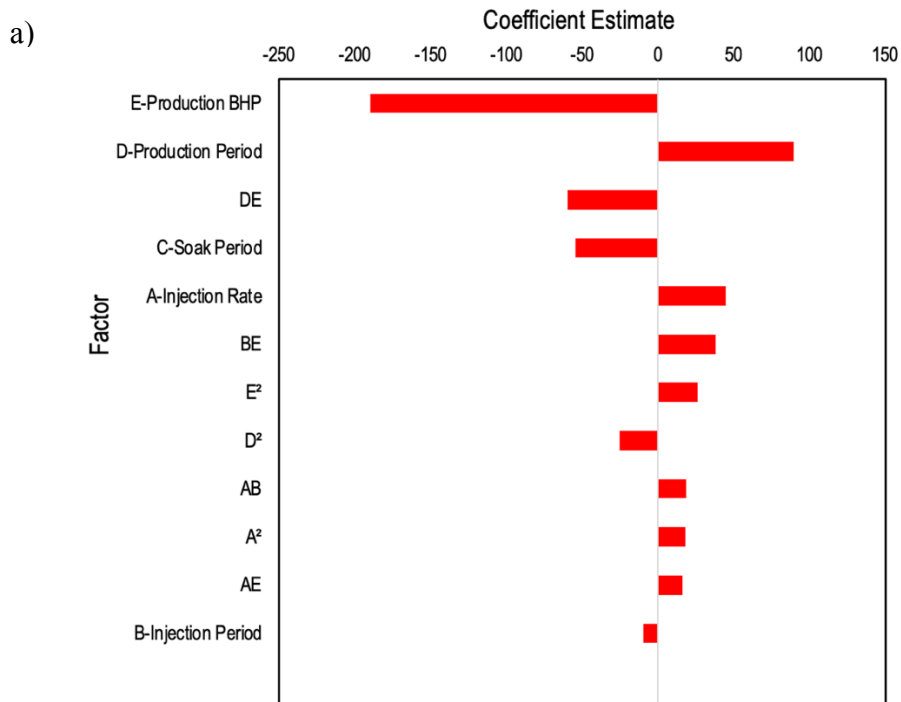
b)
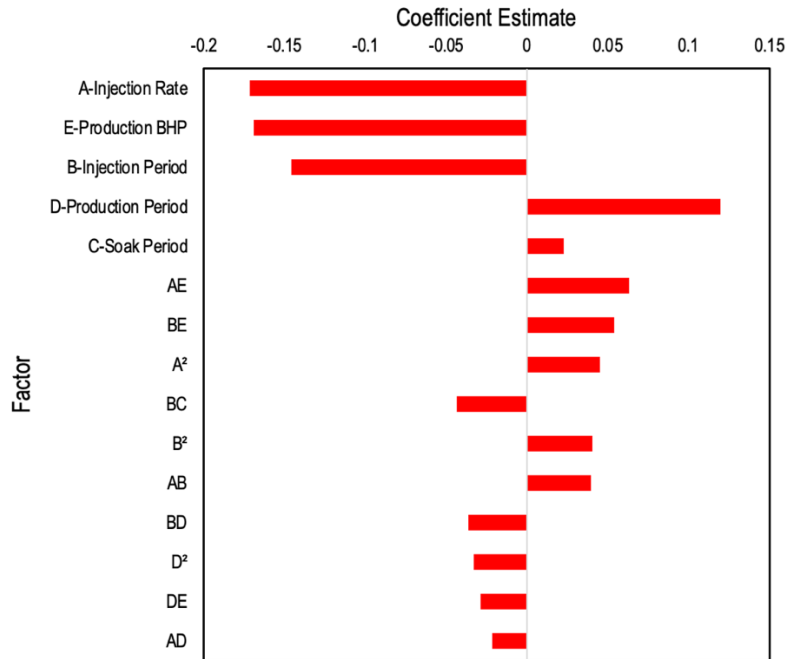
Figure 44: Tornado plots showing the relative influence of all factors on a) recover factor and b) gas utilization factor.

There is a significant interaction between injection rate (A) and production BHP(E), as shown in Figure 45. A higher injection rate positively impacts the recovery factor. The plot also shows that a lower production BHP results in a higher recovery at all conditions of injection rates. However, the recovery factor is less sensitive to injection rate at lower production BHP than higher values. Therefore, when BHP is maintained at low enough values, increased recovery may be achieved with lower injection rates; increasing the rate does not provide significant incremental benefit. The model also suggests in **Figure 46 b** a considerably improved gas utilization at lower BHP and low injection rates.

Figure 45 c illustrates a significant cooperative effect of injection period (B) and production BHP (E), which shows that a lower injection period positively impacts the recovery factor at lower BHP values. Notably, the influence of the injection period decreases as the BHP increases, and at a BHP of 2382 psi, there is no difference in recovery factor between the lowest

and highest values of the injection period. A plausible explanation for this observation is that at lower values of BHP, the recovery factor benefits more from an increased production period, such that increasing the injection period (and reducing the production period) negatively impacts the recovery. Conversely, at high values of BHP, the enhancement due to the production period increase is diminished such that the positive impact of the increased volume of injected gas becomes significant. This interaction is also seen to be statistically significant for the overall efficiency of the huff-n-puff injection (**Figure 45 c**). However, unlike the recovery factor, a lower injection period is better at all values of production BHP; there is no crossover of the plots. This trend implies that at higher BHP, although there may be an increased production with a higher injection period, injected gas production (for reinjection) is also stifled, negatively impacting the net gas utilization factor.

Figure 46 d depicts the interaction between the production period (D) and the production BHP (E). As mentioned, we observe that at low BHP values, the recovery factor is significantly higher for more extended production periods. At high BHP values, the benefit of an extended production period is less significant. As BHP is increased, the drawdown becomes too low to benefit from a prolonged production period. This mechanism is also directly related to gas utilization, as seen in **Figure 46 d.** The plots mirror that of the recovery factor. In addition to the recovery factor improvement at low BHP and longer production periods, injected gas production increases significantly at these conditions, which increases the gas utilization factor.

Interestingly, it is observed that all interaction terms that were significant for the recovery factor were also significant for gas utilization. However, the model for gas utilization has interaction terms that were not significant for the recovery factor. The terms AD, BC, and BD were exclusively significant to gas utilization**. Figure 46 e** illustrates the effect of injection rate (A) and

production period (D) on gas utilization. The interpretation of the main effects for both factors can be seen here; a lower injection rate implies less gas volume while a prolonged production period increases recovery, both of which positively impact gas utilization. However, the benefit of a low injection rate on gas utilization is magnified as the production period is prolonged.

As mentioned previously, **Figure 46 f** shows an apparent interaction between the injection period (B) and soak time (C). It appears there is some benefit of soak time on recovery factor and gas utilization, but this is only observed at a shorter injection period. Soaking allows CO_2 to diffuse into oil, enhancing mixing and subsequent swelling and viscosity reduction. However, at longer injection periods, the benefits of the soak time are negated by the shorter production period. In addition, longer injection periods mean more injected gas volume and more gas retained, negatively impacting gas utilization.

Finally, we observe a significant cooperative effect between the injection period (B) and production period (D) (**Figure 46 g**). A relatively high value of the gas utilization factor is obtained at the shortest injection period and a prolonged production period. Understandably, the sensitivity of gas utilization to injection is highest at a longer production period than a shorter period. Extending the production periods increases the oil recovery factor and CO_2 gas production, positively impacting gas utilization. Conversely, a longer injection period increases the volume of gas injected, negatively impacting the gas utilization factor. Therefore, maintaining the shortest injection period at any length of the production period is beneficial for gas utilization.
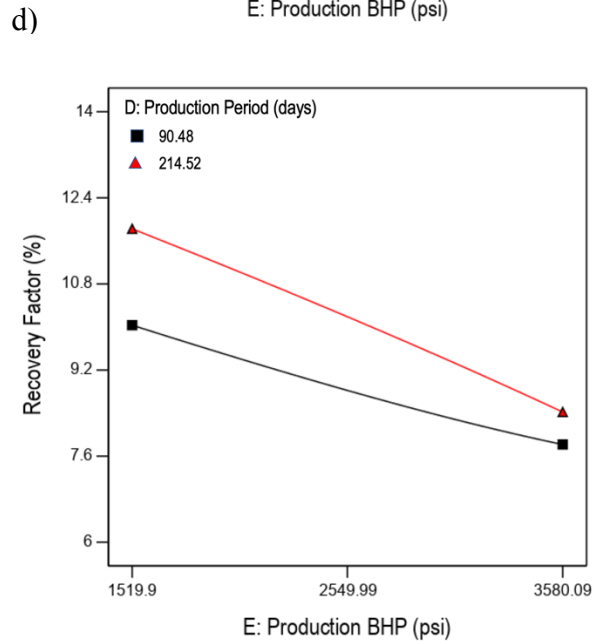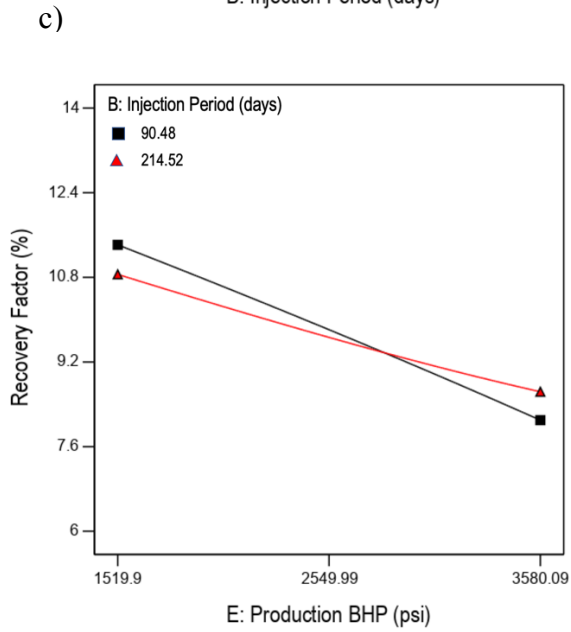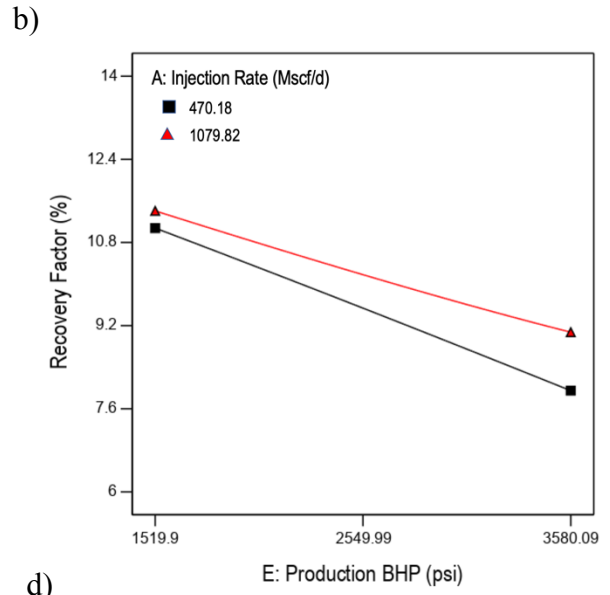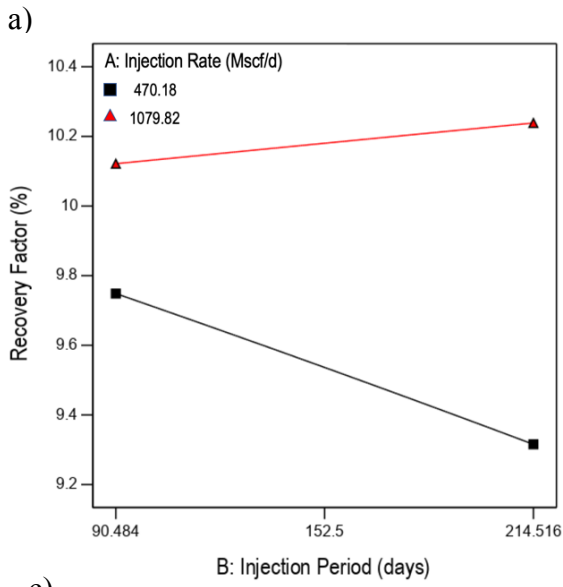
Figure 45: Interaction plots for the significant factor interactions for recovery factor.

e)

f)

g)
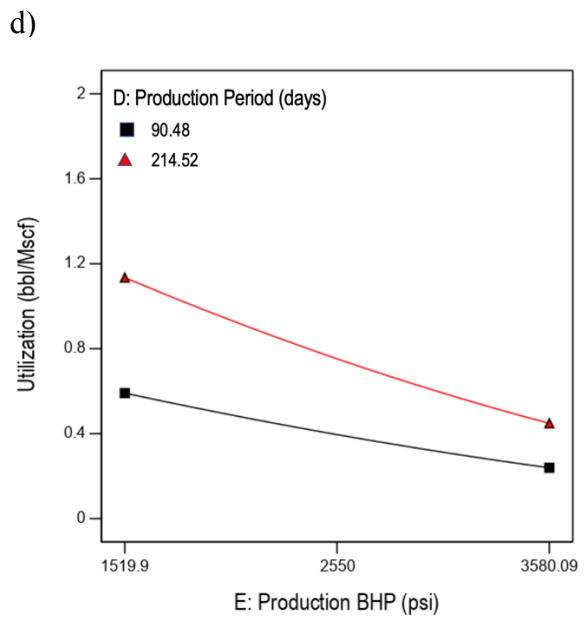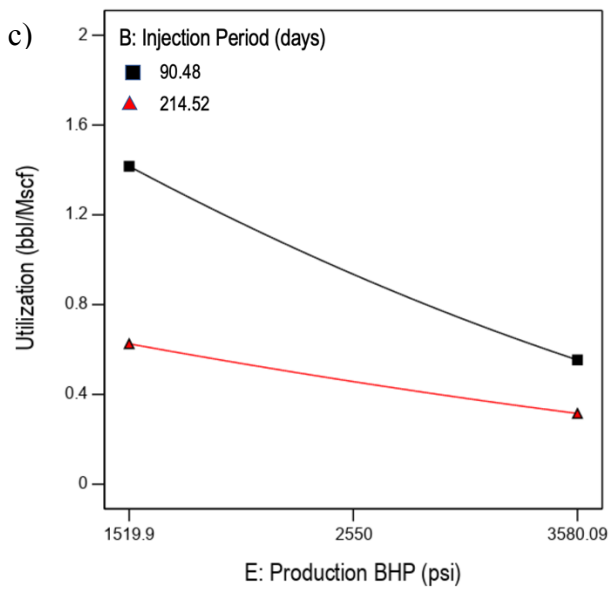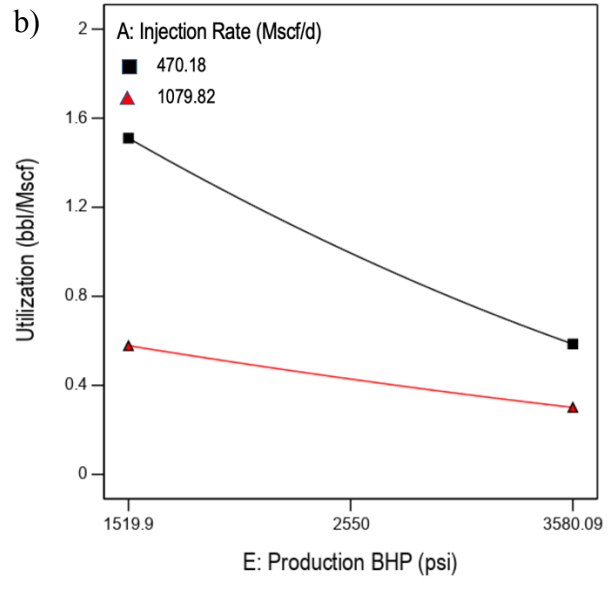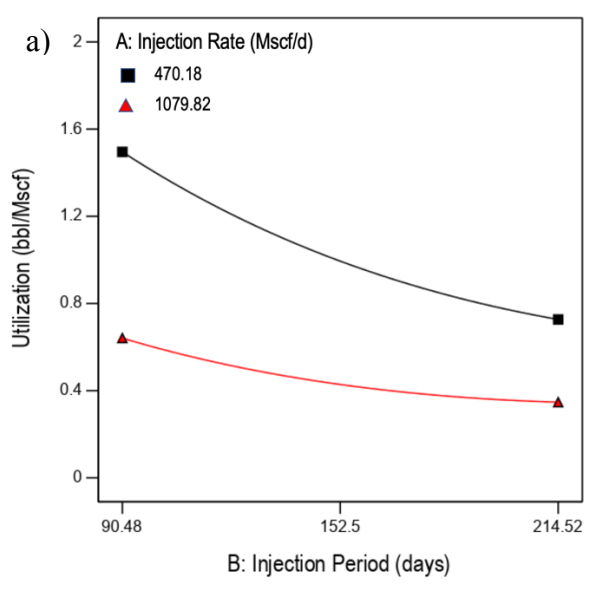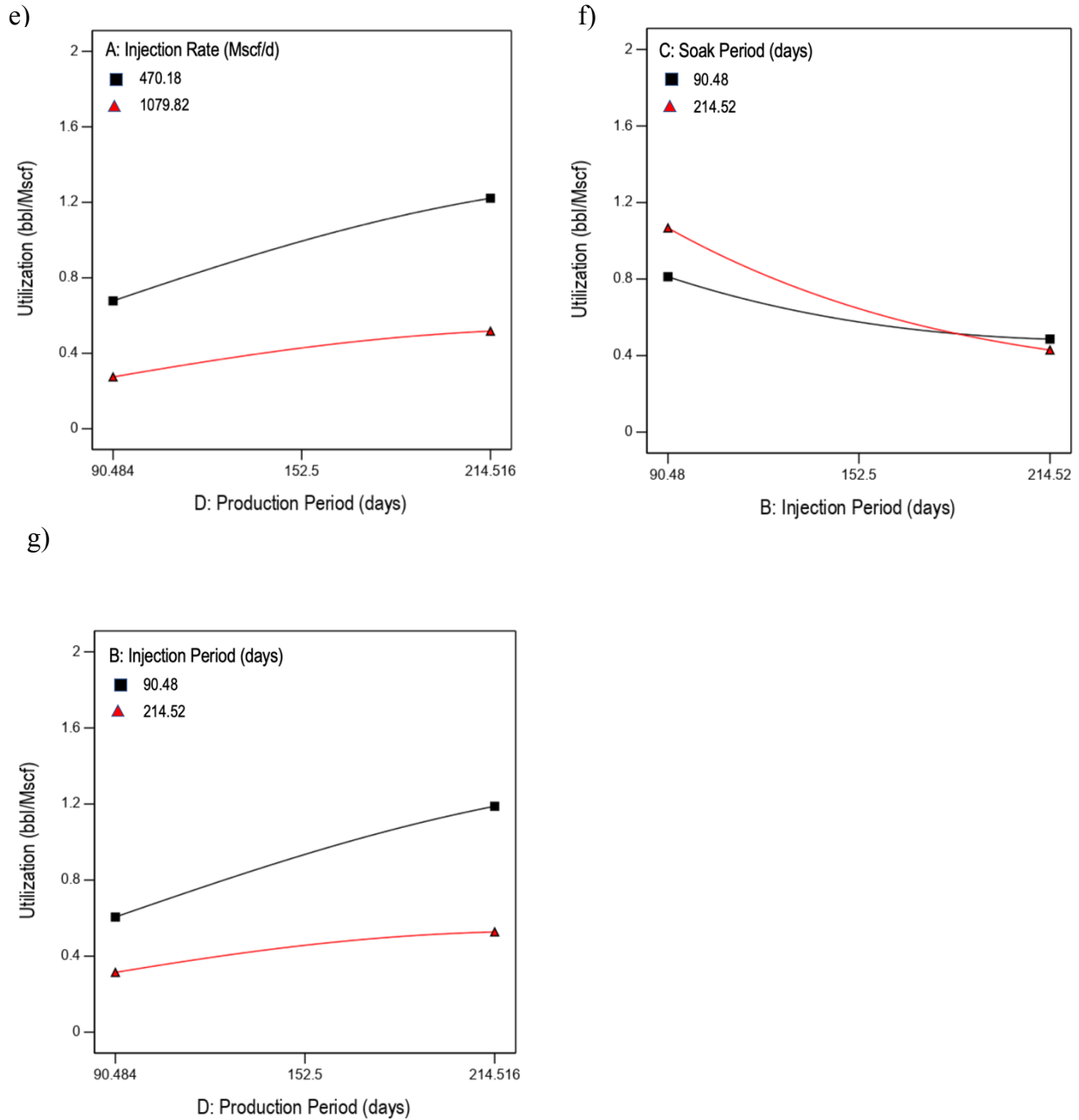
Figure 46: Interaction plots for the significant factor interactions for the gas utilization factor.

5.9.3 Optimization

We applied the desirability function to find the optimum conditions of injection rate, injection period, soak period, production period, and production BHP for maximized recovery and gas utilization. We set the constraints on the factors to range the entire factor space. For multi-

response optimization, it is critical to specify a level of importance to each of the responses. Thus, the recovery factor and gas utilization were both allocated equal importance.

As with most numerical optimization techniques, several local maxima are detected in the design space. A total of 100 solutions were obtained from the numerical optimization, each with a corresponding desirability value. The solution with the highest desirability of 0.838 is selected as the optimum. The optimum attained recovery factor was 12.368%, which represents a 7.23% incremental recovery factor. The gas utilization at the optimized setting is 2.62 bbl/Mscf, which is an acceptable efficiency. We observed that the optimum solutions are concentrated in an identifiable region in the design space. The optimum solutions are close to the lower limit of injection rate, injection period, soak period and production BHP, and the higher limit of production period in the design space. Specifically, we obtained the optimum recovery and utilization at an injection rate =470.181 Mscf/d, injection period=90.484 days, soak period=102.087 days, production period =214.516 days and production BHP=1521.425 psi. **Figure 47** depicts the response surface plots with recovery factor (a) and utilization factor (b) plotted against production BHP and production period, which are the most influencing factors.

In addition to the numerical solutions, the results of the graphical overlay to identify feasible operational areas for optimal operation are presented in **Figure 48 .** These overlays present a more practical recommendation for process optimization by offering some flexibility to the factor tuning. To define the feasible regions, it is necessary to specify optimal cutoff values for the two responses. Setting the cutoffs too close to the optimal may yield narrow operating regions that may be impractical to implement. Based on the obtained optimal values from numerical optimization, we define the optimal cutoffs for the recovery factor and gas utilization factor as 11% and 1.2

bbl/Mscf, respectively. Below these cutoffs, the corresponding operational settings are considered suboptimal. It is worth mentioning that these cutoffs are arbitrary.

Figure 48 a shows the overlay plot for injection rate vs. production BHP. The plot indicates that the optimal operation region is located at low production BHP and low injection rate. The first limiting factor to increasing production BHP will be the recovery factor and gas utilization at a further higher BHP. Increasing the injection rate to the high limit within the factor space can yield at least 11% recovery, but gas utilization will be the limiting factor. From **Figure 48 b**, the optimal region of the production period is located at higher values. The critical limiting factor to reducing the production period will be the recovery factor. The plot in **Figure 48 c** indicates that the optimal region spans the entire production period range at low production BHP.
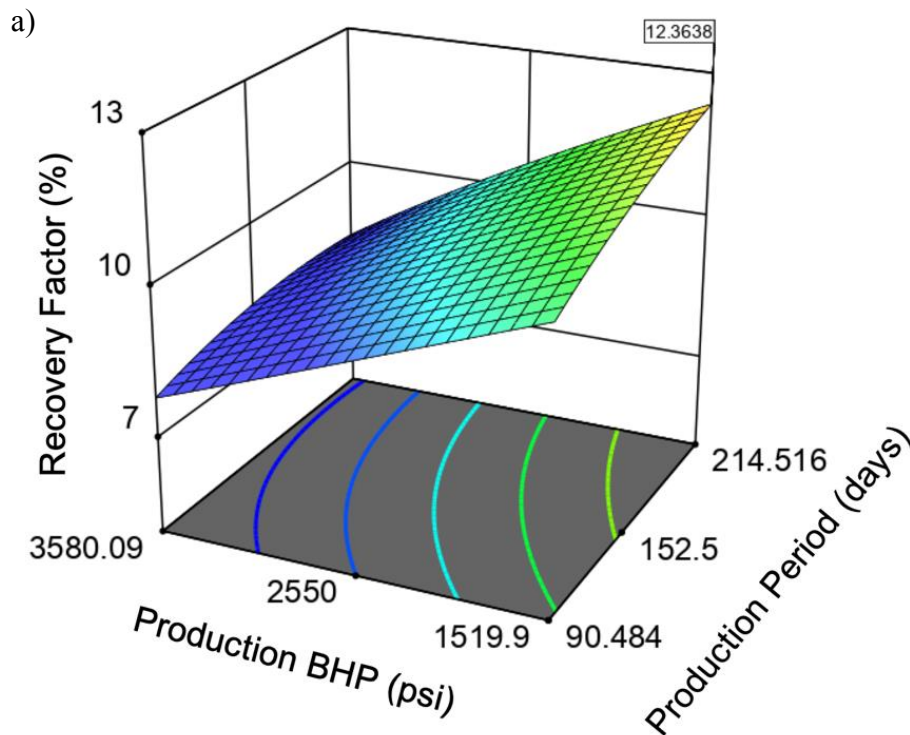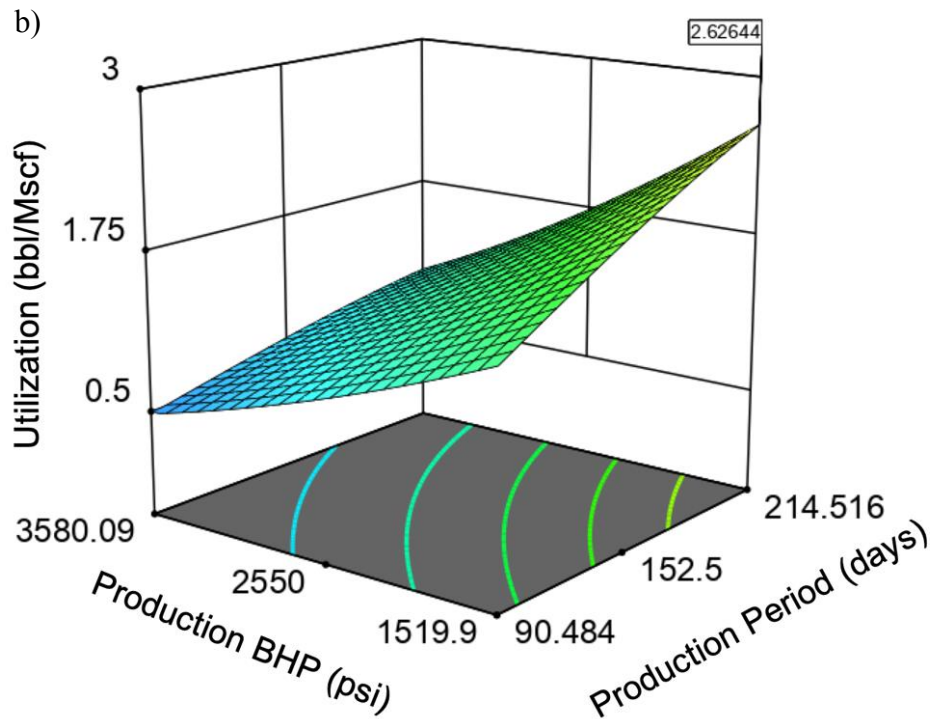
Figure 47: Response surface plots showing optimum operation settings for a) recovery factor and b) gas utilization.

At BHP higher than approximately 1800 psi, gas utilization becomes the primary limiting factor at the high injection period. **Figure 48 d** presents the overlay plot for the soak period against production BHP. The plot shows that the feasible soak period covers the entire range in the factor space with the chosen cutoffs. At low production BHP, less than approximately 1900 psi, optimal recovery factor and gas utilization can be achieved irrespective of the soak period. The soak period has minimal influence based on the chosen cutoffs.
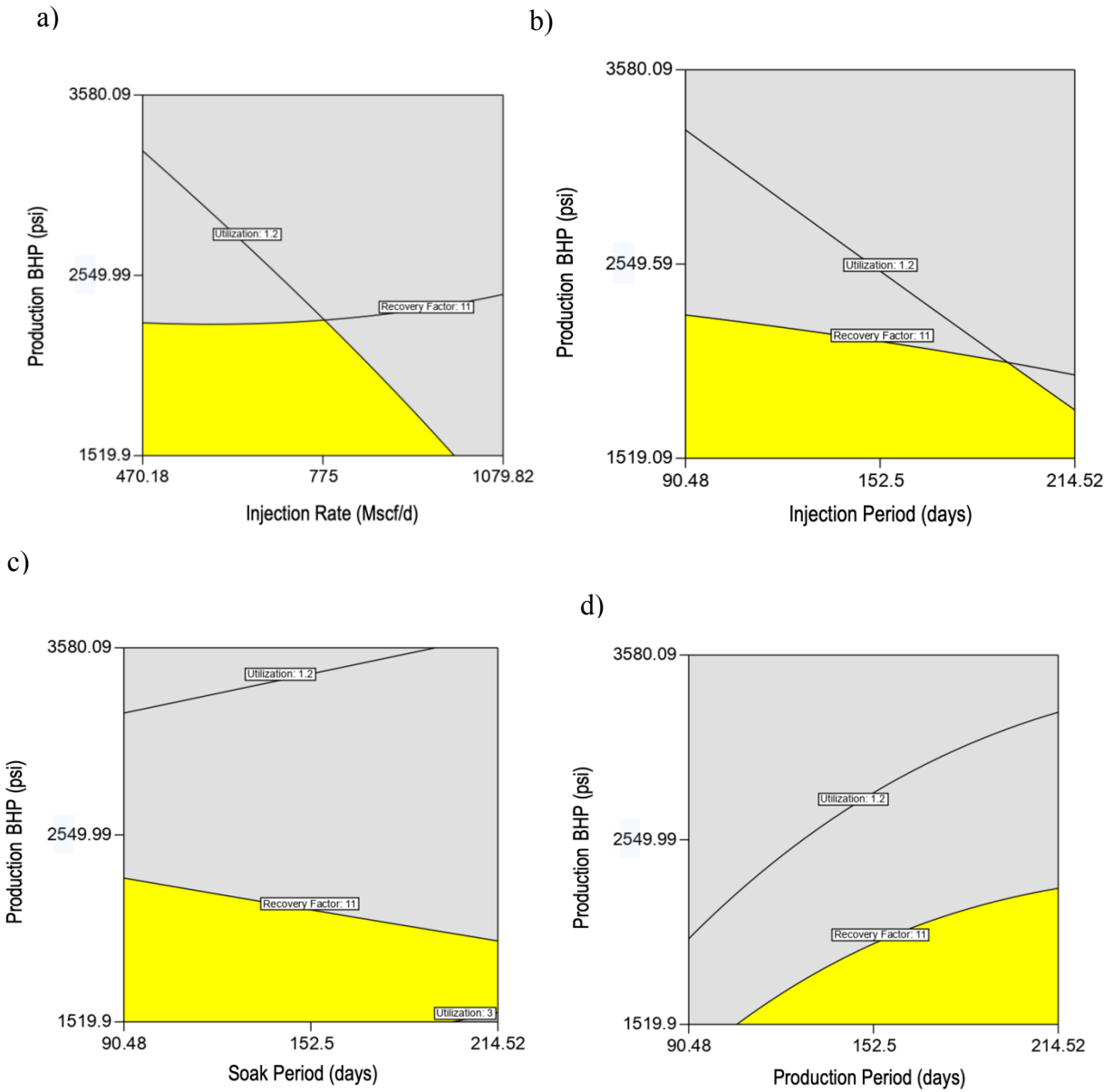
Figure 48: Contour plots overlays for multi-response optimization. All factors are plotted against production BHP, which is the most influencing factor. a) Injection rate b) Injection period c) soak period d) production period

5.10 Conclusion

In this study, we have simulated CO_2 huff-n-puff enhanced oil recovery in a single hydraulically fractured well in the Bakken formation using a compositional reservoir simulator. The near-well simulation model was calibrated with production data from a representative well in the Sanish Field, Williston basin. Response surface methodology based on CCD was applied to evaluate the influence of the injection rate, injection period, soak period, production period, and BHP on recovery and gas utilization factors. The use of CCD enabled the fitting of a second-order polynomial to recovery factor and gas utilization factors obtained from 43 simulation runs. The individual and interaction effects of the five operational parameters on the recovery factor and gas utilization factor were investigated based on rigorous statistical analysis. The results show that production BHP and production period have the most significant influence on recovery factor, whereas injection rate and injection period have much less influential roles on recovery. The injection rate and production BHP were the most influencing factors on the gas utilization factor; the injection period and the production period had a moderate influence on the gas utilization factor. In addition, we observed that the soak period has an overall negative effect on the recovery factor. However, at certain conditions of the injection period, an increased soak time may prove beneficial to the gas utilization factor.

The cooperative effect of injection rate-injection period, injection rate-production BHP, production period-production BHP, and production period-production BHP were significant for both recovery and gas utilization factors. The injection rate-production period, injection period-soak period, and injection period-production period interaction effects were significant for gas utilization but not recovery factors. Numerical optimization based on the desirability function approach shows that an optimum recovery factor of 12.32% and gas utilization of 2.653 Mscf/bbl

can be achieved at an injection rate =470.181 Mscf/d, injection period=90.484 days, soak period=102.087 days, production period =214.516 days and production BHP=1521.425 psi. Graphical overlays to identify optimum operation regions indicate that a recovery factor of at least 11% and a gas utilization factor of at least 1.2 bbl/Mscf can be achieved if operation parameters are kept within the identified feasible ranges.

It is worth mentioning that what is optimum will depend on a project's economics. This work did not consider economic parameters such as net present value, internal rate of return etc. Optimization based on these parameters may yield different results. In addition, our simulation did not consider other engineering design considerations such as surface facility design, wellbore configuration, artificial lift facilities etc. For example, not all fields will have the pump capacity to inject or produce at the optimal rates obtained in this work. These notwithstanding, we believe our methodology and results can guide engineers to better design CO_2-enhanced recovery projects in the Bakken formation.

Chapter 6

Thesis Conclusions, Limitations and Recommendations

6.1 Conclusion

This research aimed to elucidate the effectiveness of gaseous solvent cyclic injection (also known as huff-n-puff) as an enhanced oil recovery strategy in unconventional formations at different length scales and their underlying mechanisms. The study was divided into three major sections, as presented in Chapters 3 through 5. The Bakken formation in the Williston basin was used as the study area. In the premier part of this work, presented in Chapter 3, core-scale laboratory H-n-P experiments were conducted to assess the viability of CO_2 and C_2H_6 as H-n-P gaseous solvents for enhancing recovery in the Middle Bakken formation. The influence of injection pressure (miscibility condition), soak period, surface area to volume ratio and production period on oil recovery were elucidated. More importantly, the influence of the design mentioned above parameters is assessed by considering the miscibility conditions of the injection gases. By so doing, the dependency of the effects of the design parameters on miscibility conditions, the gas composition, and the role of gas composition-dependent mechanisms are better evaluated.

In the second part of this work, presented in Chapter 4, we investigate the pore scale sweep efficiency of two gaseous solvents, CO_2 and C_2H_6, in the Bakken formation. State-of-the-art nuclear magnetic resonance technology is employed for this purpose. To achieve our goal, the instrument is employed to measure the core samples' initial pore size distributions (PSD), after which CO_2 and ethane H-n-P experiments were carried out at different miscibility conditions and operating parameters. Then, the cores' fluid distribution (PSD) is measured by recording the NMR

T_2 distribution after the H-n-P experiments. We then compared the initial and post H-n-P PSDs to evaluate the recovery efficiency of the H-n-P experiment in specific pore sizes. By so doing, the effects of miscibility condition (injection pressure), soak period, production period and rock surface-to-volume ratio on pore-level sweep efficiency were assessed, including the underlying mechanisms of gaseous solvent cyclic injection at the pore scale.

In the final part, presented in Chapter 5, we aimed to study the influencing operational parameters for huff-n-puff CO_2 EOR in the Bakken formation and optimize recovery at the well scale. To achieve this goal, we leveraged a compositional numerical simulation with response surface methodology and ancillary techniques such as the design of experiment (DOE) and numerical optimization. We assessed the influence of five operational factors on oil recovery and gas utilization factors. The independent variables considered include injection rate, injection period, soak period, production period, and production BHP. Notably, using RSM enabled us to assess the elusive variable interaction among these parameters. A compositional, near-well model was constructed to represent a well in the Sanish field, which targets the Middle Bakken play in the North Dakota portion of the Williston Basin. The properties of the model are tuned via history matching with historical oil, water, and gas production from the selected well. Then, CO_2 huff-n-puff is simulated to study the performance and efficiency of enhancing the Bakken Formation's oil recovery. Then, sample points from several simulation runs based on the central composite design are obtained (CCD). A second-order polynomial proxy model that describes the relationship between operating parameters and target responses was then fitted using the CCD design. After obtaining the proxy model, it is used to optimize the huff-and-puff process to maximize oil recovery and gas utilization.

The most important findings of this study can be outlined as follows. At the core scale:

- The recovery factor typically increases with increasing pressure for both CO_2 and C_2H_6. Irrespective of the gas composition, the recovery factor at AM > NM > BM, albeit this increase, is not linear. The results indicate that an increase in pressure from BM to NM improved the recovery factor more than an increase in pressure from NM to AM.

- While C_2H_6 outperformed CO_2 under all miscibility conditions, the disparity in performance varied based on the miscibility condition. This disparity was smallest under BM settings and greatest under AM conditions.

- Across all experiments, the initial cycles yielded the greatest oil recovery, whereas recovery steadily dropped with each succeeding cycle. However, the behavior was not as noticeable under BM conditions as it was under NM and AM conditions.

- We observed a strong interaction between the soak period, miscibility condition and gas compositions. Under BM and NM conditions, the soak length showed little effect. However, under AM conditions, a long soak period dramatically boosted recovery.

- Similarly, there exist significant variable interactions between miscibility and production period. Regardless of gas composition, the puff period did not affect the recovery factor under BM and NM conditions, according to our findings. Under AM conditions, however, the influence of the production period was evident.

- Overall, core samples with a lower SA/V resulted in a lower oil recovery factor; however, SA/V's effects depend on miscibility conditions, with a noticeable impact under BM and NM conditions and a less pronounced effect under AM conditions.

- C_2H_6 outperforms CO_2 regardless of miscibility conditions. These results imply that gas-oil interactions (such as diffusion rates, oil swelling, component extraction, etc.) that are dependent on gas composition may play a crucial role in oil recovery by gas huff-n-puff.

At the pore scale:

- In general, the effectiveness of pore-level sweep varied with gas composition, miscibility conditions, soak period, production period, rock surface-to-volume ratio, and their interaction. Additionally, as measured by the free fluid index, the degree of fluid recovery varied considerably across a wide range of pore sizes.

- Under BM conditions, both gases could assess the small to large pores but were ineffective at penetrating micropores. Although CO_2 displacement of oil in the small to macro pores was enhanced above miscibility conditions, sweep in the micropores remained constrained. However, injection of ethane under AM condition resulted in a considerable increase in FFI across all pore sizes. Ethane performed better than carbon dioxide under both BM and AM circumstances.

- The influence of the soak period on the efficiency of pore level sweep is dependent on the miscibility condition and gas composition. Under BM conditions, increasing the soak time did not significantly improve the FFI in the micropores compared to a shorter soak time. However, increasing the soak time significantly improved FFI across all pore sizes for both gases under AM conditions. The highest recovery was achieved using ethane, with a prolonged soak period.

- Both composition and miscibility conditions influence the effect of the production period on pore-level displacement efficacy. The production period has little effect on the pore scale sweep under BM circumstances. However, FFI was significantly impacted by a prolonged production period under AM circumstances. The improvement was more evident with CO_2, where a more extended production period resulted in a significant micropore sweep.

- At the pore level, under BM conditions, the effect of the rock surface-to-volume ratio was more evident than under AM conditions. Reduced SA/V (increased core volume) under BM conditions led to a decrease in FFI in the pores. However, this observation may also be attributable to the various pore shapes observed in the core samples.

From the well-scale reservoir simulations, the important findings can be summarized as follows:

- The production BHP and production period had the most significant influence on the recovery factor, whereas injection rate and injection period have much less influential roles on recovery. In addition, we observed that the soak period as a single factor had a limited negative influence on the recovery factor. Production BHP as a single factor had a strong inverse effect on the recovery factor, while the production period directly affected the recovery factor.

- The injection rate and production BHP were the most influencing factors on the gas utilization factor, with inverse relationships with the gas utilization factor; the injection period and the production period had a moderate (inverse and direct, respectively) influence on the gas utilization factor.

- The cooperative effect of injection rate-injection period, injection rate-production BHP, production period-production BHP, and production period-production BHP were significant for both recovery and gas utilization factors.

- At a lower injection rate, a more prolonged injection period resulted in a lower recovery factor. However, at a higher injection rate, the recovery factor increased only slightly as the injection period increased.

- We also observed that although a higher injection rate positively impacts the recovery factor, the recovery factor is less sensitive to the injection rate at lower production BHP than at higher values.

- The significant cooperative effect of injection period and production BHP shows that a lower BHP positively impacts the recovery factor at a lower injection period. However, at a higher production BHP, a prolonged injection is preferable for enhanced recovery.

- We observe that at low production BHP values, the recovery factor is significantly higher for more extended production periods. Conversely, at high production BHP values, the benefit of an extended production period is less significant.

- The injection rate-production period, injection period-soak period, and injection period-production period interaction effects were significant for gas utilization but not recovery factors.

- Numerical optimization based on the desirability function approach shows that an optimum recovery factor of 12.32% and gas utilization of 2.653 Mscf/bbl can be achieved at an injection rate =470.181 Mscf/d, injection period=90.484 days, soak period=102.087 days, production period =214.516 days and production BHP=1521.425 psi.

- A graphical overlay to identify optimum operation regions indicates that a recovery factor of at least 11% and a gas utilization factor of at least 1.2 bbl/Mscf can be achieved if operation parameters are kept within defined feasible ranges.

6.2 Limitations and recommendations

We outline below some of the limitations and associated recommendations for future improvements and extensions of the work:

- Even though the core samples were collected in close proximity to one another, heterogeneities exist. These differences may have an impact on the conclusions of this study. Therefore, in future work, we recommend that several samples from different locations be used for experiments to incorporate the effect of heterogeneities. Several samples could be used for each run to enable a rigorous statistical analysis to ascertain the statistical significance of the results obtained.

- The re-use of core samples and the cyclic saturation and desaturation may alter core properties due to hysteresis and physical damage to the samples, which could affect the conclusion of this work. Therefore, where possible, samples should be used only once. We also recommend that future work track the changes in the rock properties after each experiment and account for such changes in the core samples.

- As mentioned, we used a dead oil sample for the experiments in this work. However, the dead oil samples likely have most lighter components vaporized, leaving the heavier hydrocarbon fractions. Thus, we recommend that live oil be used in future experiments, requiring specialized apparatus for handling. In addition, the oil and gas PVT properties and compositions can be tracked before and after cyclic injection to provide further insight into the mechanisms of gaseous solvent EOR.

- The NMR measurement employed in this work can be described as ex-situ measurements. In-line NMR equipment can provide dynamic in-situ measurements of pore fluid

occupancies for better accuracy. In addition, this measurement technique could be coupled with other advanced imaging techniques for further insight.

- The well-scale simulation studies outlined in Chapter 5 used average reservoir properties. Future work should incorporate a more robust reservoir model that integrates seismic data and well logs to account for reservoir heterogeneities. In addition, a more accurate model can be constructed by history matching with additional field production data (such as gas-oil ratio and water cut) and laboratory core-flood data with injection fluid such as CO_2 and ethane. Attention should also be paid to the gridding structure of the model, as it may impact simulation results.

- We also recommend expanding the study area to include several wells and account for natural fracture connectivity and well interference.

- In modeling hydraulic fractures, planar fractures were employed, which is an oversimplification of actual hydraulic fractures that are non-planar, branched and interconnected. Future work should incorporate realistic fracture network models from which the effect of fracture properties can be studied.

Nomenclature

Abbreviations	
AB	Above miscibility
ANOVA	Analysis of Variance
BBD	Box Benkhen Design
BHP	Bottom hole Pressure
BM	Below Miscibility
BTPS	Bakken Total Petroleum System
BVI	Bound Volume Index
C_2H_6	Ethane
C_3H_8	Propane
CCD	Central Composite Design
CCE	Constant Composition Expansion
CH_4	Methane
CO_2	Carbon dioxide
CP	Cumulative Porosity
CRF	Cumulative Oil Recovery Factor
CT	Computed Tomography
DLE	Differential Liberation Experiment
DOE	Design of Experiment
EOR	Enhanced Oil Recovery
ESEM	Environmental Scanning Electron Microscope
FFI	Free Fluid Index
GOR	Gas Oil Ratio
H-n-P	Huff and Puff
IFT	Interfacial Tension
IP	Incremental Porosity
LB	Lower Bakken
MB	Middle Bakken
MICP	Mercury Injection Capillary Pressure
MMP	Minimum Miscibility Pressure
N_2	Nitrogen
NM	Near Miscibility

NMR	Nuclear Magnetic Resonance
NPV	Net Present Value
OFAT	One-factor-at-a-time
OOIP	Original Oil-in-Place
PSD	Pore Size Distributions
PVT	Pressure-Volume-Temperature
RF	Recovery Factor
RSM	Response Surface Methodology
SA/V	Surface Area-to-Volume Ratio
SCAL	Special Core Analysis
TOC	Total Organic Content
UB	Upper Bakken

Symbols	
A	Area covered by the T_2 spectrum and x-axis after solvent H-n-P
A_i	Amplitude
A_o	Area covered by the original T_2 spectrum
C_{ip}	Mass fraction of component, i
$CP_{T2,L}$	Cumulative porosity at the lower bound T_2 value of the pore size range at 100% fluid saturation
$CP_{T2, L,100\%}$	Cumulative porosity at the lower bound T_2 value of pore size range at 100% saturation
$CP_{T2, L,irr}$	Cumulative porosity at the lower bound T_2 value of pore size range at irreducible saturation
$CP_{T2,max,100\%}$	Total porosity at 100% saturation
$CP_{T2,max,irr}$	Total porosity at irreducible saturation
$CP_{T2,u}$	Cumulative porosity at the upper bound T_2 value of the pore size range at 100% fluid saturation
$CP_{T2,u,100\%}$	Cumulative porosity at upper bound T_2 value of pore size range at 100% saturation
$CP_{T2,u,irr}$	Cumulative porosity at upper bound T_2 value of pore size range at irreducible saturation
$CP_{T2,u,max}$	Total porosity at 100% saturation
D	Diffusion-induced relaxation
$d_i(Y_i)$	Desirability function
D_{ov}	Overall desirability
FFI_{total}	Overall Fluid flow index
F_S	Pore shape factor
g_p	Mass rate per volume of phase p
$\vec{k}$	Permeability tensor
k	Number of factors

krp	Relative permeability of phase p
Li	Upper value
$M_{i(t)}$	Transverse magnetization decay signal
n_c	Number of center points
N_D	Number of design points
$N_{P,inc}$	Incremental oil produced due to CO_2 injection
r	Pore radius
S	Pore surface
S_i	Initial saturation
Sp	Saturation of phase p
T_{2_bulk}	Transverse relaxation time due to bulk relaxation of the pore fluid
T_{2_D}	Relaxation time due to diffusion in the magnetic field gradient
$T_{2\_surface}$	Transverse relaxation time due to surface relaxation
T_i	Decay time constant
T_i	Target Value
UF_{CO2}	CO_2 Gas utilization factor
U_i	Lower value
V	Pore fluid volume
$V_{CO2,inj}$	Cumulative volume of CO_2 injected
$V_{CO2,prod}$	Cumulative volume of CO2 produced
W_{sat}	Saturated Weight of Core Sample
W_{dry}	Dry Weight of Core Sample
W_i	Weight of Core after gas Injection
Y	Response
β_i	Main effect
β_{ii}	Quadratic effects
β_{ij}	Interaction effects
β_o	Coefficient of intercept
ϵ	Random error
ρ_2	T_2 surface relaxivity
ρ_p	Density of phase, p
ϕ	Porosity
ϕ_p	Potential of phase, p

References

Adekunle, O., & Hoffman, B. T. (2014). Minimum Miscibility Pressure Studies in the Bakken. *All Days*, SPE-169077-MS. https://doi.org/10.2118/169077-MS

Adel, I. A., Tovar, F. D., Zhang, F., & Schechter, D. S. (2018, September 24). *The Impact of MMP on Recovery Factor During CO2 – EOR in Unconventional Liquid Reservoirs*. SPE Annual Technical Conference and Exhibition. https://doi.org/10.2118/191752-MS

Ahmadi, K., & Johns, R. T. (2011). Multiple-Mixing-Cell Method for MMP Calculations | SPE Journal | OnePetro. *SPE Journal*. https://onepetro.org/SJ/article/16/04/733/204225/Multiple-Mixing-Cell-Method-for-MMP-Calculations

Akindipe, D., Saraji, S., & Piri, M. (2022). Carbonated Water Injection in Oil-Wet Carbonate Rock Samples: A Pore-Scale Experimental Investigation of the Effect of Brine Composition. *Energy & Fuels*, *36*(9), 4847–4870. https://doi.org/10.1021/acs.energyfuels.2c00326

Akita, E., Moghanloo, R. G., Davudov, D., & Tinni, A. (2018). *A Systematic Approach for Upscaling of the EOR Results from Lab-Scale to Well-Scale in Liquid-Rich Shale Plays*. D031S007R006. https://doi.org/10.2118/190188-MS

Alfarge, D., Wei, M., & Bai, B. (2017). *Comparative Study for CO2-EOR and Natural Gases Injection-Techniques for Improving Oil Recovery in Unconventional Oil Reservoirs*. CMTC-485175-MS. https://doi.org/10.7122/485175-MS

Alfarge, D., Wei, M., & Bai, B. (2018). Numerical simulation study on miscible EOR techniques

    for improving oil recovery in shale oil reservoirs. *Journal of Petroleum Exploration and*

    Production Technology, *8*(3), 901–916. https://doi.org/10.1007/s13202-017-0382-7

Alharthy, N., Teklu, T., Kazemi, H., Graves, R., Hawthorne, S., Braunberger, J., & Kurtoglu, B.

    (2015, September 28). *Enhanced Oil Recovery in Liquid-Rich Shale Reservoirs:*

    Laboratory to Field. SPE Annual Technical Conference and Exhibition.

    https://doi.org/10.2118/175034-MS

Al-Mahrooqi, S. H., Grattoni, C. A., Moss, A. K., & Jing, X. D. (2003). An investigation of the

    effect of wettability on NMR characteristics of sandstone rock and fluid systems.

    Reservoir Wettability, *39*(3), 389–398. https://doi.org/10.1016/S0920-4105(03)00077-9

Artun, E., Ertekin, T., Watson, R., & Miller, B. (2011). Performance Evaluation of Cyclic

    Pressure Pulsing in a Depleted, Naturally Fractured Reservoir with Stripper-Well

    Production. *Petroleum Science and Technology*, *29*(9), 953–965.

    https://doi.org/10.1080/10916460903514956

Ashraf, A., Hadia, N. J., Torsæter, O., & Tweheyo, M. T. (2010, January 20). *Laboratory*

    Investigation of Low Salinity Waterflooding as Secondary Recovery Process: Effect of

    Wettability. SPE Oil and Gas India Conference and Exhibition.

    https://doi.org/10.2118/129012-MS

Aziz, K., & Settari, A. (1979). *Petroleum Reservoir Engineering*. Applied Science Publishers.

Azzolina, N. A., Nakles, D. V., Gorecki, C. D., Peck, W. D., Ayash, S. C., Melzer, L. S., &

    Chatterjee, S. (2015). CO2 storage associated with CO2 enhanced oil recovery: A

    statistical analysis of historical operations. *International Journal of Greenhouse Gas*

    Control, *37*, 384–397. https://doi.org/10.1016/j.ijggc.2015.03.037

Baba, N. (1981). Convergence of a random optimization method for constrained optimization problems. *Journal of Optimization Theory and Applications*, *33*(4), 451–461. https://doi.org/10.1007/BF00935752

Badrouchi, N., Pu, H., Smith, S., Yu, Y., & Badrouchi, F. (2022). Experimental investigation of CO2 injection side effects on reservoir properties in ultra tight formations. *Journal of Petroleum Science and Engineering*, *215*, 110605. https://doi.org/10.1016/j.petrol.2022.110605

Baioco, J. S., Jacob, B. P., & Mazadiego, L. F. (2020, October 11). *Design of Experiment (DOE) Approach to Sensitivity Analysis of Hydraulic Fracturing*. The 30th International Ocean and Polar Engineering Conference. https://onepetro.org/ISOPEIOPEC/proceedings/ISOPE20/All-ISOPE20/ISOPE-I-20-1122/446244

Behnsen, J., & Faulkner, D. R. (2011). Water and argon permeability of phyllosilicate powders under medium to high pressure. *Journal of Geophysical Research: Solid Earth*, *116*(B12). https://doi.org/10.1029/2011JB008600

Burrows, L. C., Haeri, F., Cvetic, P., Sanguinito, S., Shi, F., Tapriyal, D., Goodman, A., & Enick, R. M. (2020). A Literature Review of CO$_2$, Natural Gas, and Water-Based Fluids for Enhanced Oil Recovery in Unconventional Reservoirs. *Energy & Fuels*, *34*(5), 5331–5380. https://doi.org/10.1021/acs.energyfuels.9b03658

Cannon, D. E., & Minh, C. C. (1998, September). Quantitaive NMR Intepretation. *Society of Petroleum Engineers Journal*. Annual Technical Conference and Exhibition, New Orleans.

Chaisoontornyotin, W., Mohamed, A., Bai, S., Afari, S. A., Mirchi, V., Recio, A., III, Pearl, M., & Piri, M. (2019). *The Impact of Fracture Surface Area to Rock Volume Ratio on Spontaneous Imbibition in Tight Rocks*. D033S058R006. https://doi.org/10.15530/urtec-2019-627

Chakraborty, N., Karpyn, Z. T., Liu, S., & Yoon, H. (2017). Permeability evolution of shale during spontaneous imbibition. *Journal of Natural Gas Science and Engineering*, *38*, 590–596. https://doi.org/10.1016/j.jngse.2016.12.031

Chen, C., Balhoff, M., & Mohanty, K. K. (2013, April 10). *Effect of Reservoir Heterogeneity on Improved Shale Oil Recovery by CO2 Huff-n-Puff*. SPE Unconventional Resources Conference-USA. https://doi.org/10.2118/164553-MS

Coates, G. R., Xiao, L., & Prammer, M. G. (1999). *NMR Logging Principles and Applications*. Elsevier Science. https://books.google.com/books?id=vptTAAAAMAAJ

Collins, D. A., Nghiem, L. X., Li, Y.-K., & Grabonstotter, J. E. (1992). An Efficient Approach to Adaptive- Implicit Compositional Simulation With an Equation of State. *SPE Reservoir Engineering*, *7*(02), 259–264. https://doi.org/10.2118/15133-PA

Computer Modelling Group. (2018). *CMG-GEM* (Version 2018). Computer Modelling Group Ltd. https://www.cmgl.ca

Congressional Research Service. (2015). *An Overview of Unconventional Oil and Natural Gas: Resources and Federal Actions*. Congressional Research Service. https://crsreports.congress.gov/product/pdf/R/R43148

Costa, N. R., Lourenço, J., & Pereira, Z. L. (2011). Desirability function approach: A review and performance evaluation in adverse conditions. *Chemometrics and Intelligent Laboratory Systems*, *107*(2), 234–244. https://doi.org/10.1016/j.chemolab.2011.04.004

Cudjoe, S., Vinassa, M., Henrique Bessa Gomes, J., & Barati, R. Gh. (2016). A comprehensive

   approach to sweet-spot mapping for hydraulic fracturing and CO2 huff-n-puff injection in

   Chattanooga shale formation. *Journal of Natural Gas Science and Engineering*, *33*,

   1201–1218. https://doi.org/10.1016/j.jngse.2016.03.042

Derringer, G., & Suich, R. (1980). Simultaneous Optimization of Several Response Variables.

   Journal of Quality Technology, *12*(4), 214–219.

   https://doi.org/10.1080/00224065.1980.11980968

Don W. Green & G. Paul Wilhite. (2018). *Enhanced Oil Recovery*. SPE.

   http://ebookcentral.proquest.com/lib/und/detail.action?docID=5381116

Dong, C., & Hoffman, B. T. (2013). Modeling Gas Injection into Shale Oil Reservoirs in the

   Sanish Field, North Dakota. *Unconventional Resources Technology Conference, Denver,*

   Colorado, 12-14 August 2013, 1824–1833. https://doi.org/10.1190/urtec2013-185

Du, F., & Nojabaei, B. (2019). A Review of Gas Injection in Shale Reservoirs: Enhanced

   Oil/Gas Recovery Approaches and Greenhouse Gas Control. *Energies*, *12*(12), Article

   12. https://doi.org/10.3390/en12122355

Duan, Q., & Yang, X. (2014). Experimental studies on gas and water permeability of fault rocks

   from the rupture of the 2008 Wenchuan earthquake, China. *Science China Earth*

   Sciences, *57*(11), 2825–2834. https://doi.org/10.1007/s11430-014-4948-7

Ekechukwu, G. K., Khishvand, M., Kuang, W., Piri, M., & Masalmeh, S. (2021). The Effect of

   Wettability on Waterflood Oil Recovery in Carbonate Rock Samples: A Systematic

   Multi-scale Experimental Investigation. *Transport in Porous Media*, *138*(2), 369–400.

   https://doi.org/10.1007/s11242-021-01612-3

Ellafi, A., & Jabbari, H. (2019, June). Coupling Geomechanics with Diffusion/Adsorption
Mechanisms to enhance Bakken CO2-EOR Modeling. *53 Rd US Rock
Mechanics/Geomechanics Symposium*.
https://onepetro.org/ARMAUSRMS/proceedings/ARMA19/All-ARMA19/ARMA-2019-
1795/124999

Energy and Environmental Research Center. (n.d.). *Oil Production, Bakken—Beyond the Boom*.
Retrieved January 29, 2022, from https://undeerc.org/bakken/oilproduction.aspx

Enick, R. M., Olsen, D., Ammer, J., & Schuller, W. (2012). Mobility and Conformance Control
for CO2 EOR via Thickeners, Foams, and Gels—A Literature Review of 40 Years of
Research and Pilot Tests. SPE Improved Oil Recovery Symposium.
https://doi.org/10.2118/154122-MS

Eren, İ., & Kaymak-Ertekin, F. (2007). Optimization of osmotic dehydration of potato using
response surface methodology. *Journal of Food Engineering*, *79*(1), 344–352.
https://doi.org/10.1016/j.jfoodeng.2006.01.069

Faulkner, D. R., & Rutter, E. H. (2000). Comparisons of water and argon permeability in natural
clay-bearing fault gouge under high pressure at 20°C. *Journal of Geophysical Research:
Solid Earth*, *105*(B7), 16415–16426. https://doi.org/10.1029/2000JB900134

Fayyazi, E., Ghobadian, B., Najafi, G., Hosseinzadeh, B., Mamat, R., & Hosseinzadeh, J. (2015).
An ultrasound-assisted system for the optimization of biodiesel production from chicken
fat oil using a genetic algorithm and response surface methodology. *Ultrasonics
Sonochemistry*, *26*, 312–320. https://doi.org/10.1016/j.ultsonch.2015.03.007

Fragoso, A., Selvan, K., & Aguilera, R. (2018). *An Investigation on the Feasibility of Combined
Refracturing of Horizontal Wells and Huff and Puff Gas Injection for Improving Oil*

Recovery from Shale Petroleum Reservoirs. D051S025R003.

https://doi.org/10.2118/190284-MS

Gala, D., & Sharma, M. (2018). Compositional and Geomechanical Effects in Huff-n-Puff Gas

Injection IOR in Tight Oil Reservoirs. *Day 3 Wed, September 26, 2018*, D031S039R003.

https://doi.org/10.2118/191488-MS

Gamadi, T. D., Elldakli, F., & Sheng, J. J. (2014). *Compositional Simulation Evaluation of EOR*

Potential in Shale Oil Reservoirs by Cyclic Natural Gas Injection. URTEC-1922690-MS.

https://doi.org/10.15530/URTEC-2014-1922690

Gamadi, T. D., Sheng, J. J., & Soliman, M. Y. (2013). *An Experimental Study of Cyclic Gas*

Injection to Improve Shale Oil Recovery. D031S041R009.

https://doi.org/10.2118/166334-MS

Gamadi, T. D., Sheng, J. J., Soliman, M. Y., Menouar, H., Watson, M. C., & Emadibaladehi, H.

(2014, April 12). *An Experimental Study of Cyclic CO2 Injection to Improve Shale Oil*

Recovery. SPE Improved Oil Recovery Symposium. https://doi.org/10.2118/169142-MS

Gaswirth, S. B., Marra, K. R., Cook, T. A., Charpentier, R. R., Gautier, D. L., Higley, D. K.,

Klett, T. R., Lewan, M. D., Lillis, P. G., Schenk, C. J., Tennyson, M. E., & Whidden, K.

J. (2013). *Assessment of undiscovered oil resources in the Bakken and Three Forks*

Formations, Williston Basin Province, Montana, North Dakota, and South Dakota, 2013

(Report No. 2013–3013; Fact Sheet, p. 4). USGS Publications Warehouse.

https://doi.org/10.3133/fs20133013

Glover, F., & Laguna, M. (1998). Tabu Search. In *Handbook of Combinatorial Optimization*.

Springer. https://doi.org/10.1007/978-1-4613-0303-9_33

Grogan, A. T., Pinczewski, V. W., Ruskauff, G. J., & Orr, F. M. (1988). Diffusion of CO2 at

    Reservoir Conditions: Models and Measurements. *SPE Reservoir Engineering*, *3*(01),

    93–102. https://doi.org/10.2118/14897-PA

Habibi, A., Yassin, M. R., Dehghanpour, H., & Bryan, D. (2017). Experimental investigation of

    CO2-oil interactions in tight rocks: A Montney case study. *Fuel*, *203*, 853–867.

    https://doi.org/10.1016/j.fuel.2017.04.077

Hawthorne, S. B., Gorecki, C. D., Sorensen, J. A., Steadman, E. N., Harju, J. A., & Melzer, S.

    (2013, November 5). *Hydrocarbon Mobilization Mechanisms from Upper, Middle, and*

    Lower Bakken Reservoir Rocks Exposed to CO2. SPE Unconventional Resources

    Conference Canada. https://doi.org/10.2118/167200-MS

Hawthorne, S. B., Jin, L., Kurz, B. A., Miller, D. J., Grabanski, C. B., Sorensen, J. A., Pekot, L.

    J., Bosshart, N. W., Smith, S. A., Burton-Kelly, M. E., Heebink, L. V., Gorecki, C. D.,

    Steadman, E. N., & Harju, J. A. (2017, February 15). *Integrating Petrographic and*

    Petrophysical Analyses with CO2 Permeation and Oil Extraction and Recovery in the

    Bakken Tight Oil Formation. SPE Unconventional Resources Conference.

    https://doi.org/10.2118/185081-MS

Hawthorne, S. B., Miller, D. J., Grabanski, C. B., Azzolina, N., Kurz, B. A., Ardakani, O. H.,

    Smith, S. A., Sanei, H., & Sorensen, J. A. (2019). Hydrocarbon Recovery from Williston

    Basin Shale and Mudrock Cores with Supercritical CO2: Part 1. Method Validation and

    Recoveries from Cores Collected across the Basin. *Energy & Fuels*, *33*(8), 6857–6866.

    https://doi.org/10.1021/acs.energyfuels.9b01177

Hawthorne, S. B., Miller, D. J., Grabanski, C. B., & Jin, L. (2020). Experimental Determinations

    of Minimum Miscibility Pressures Using Hydrocarbon Gases and CO2 for Crude Oils

from the Bakken and Cut Bank Oil Reservoirs. *Energy & Fuels*, *34*(5), 6148–6157. https://doi.org/10.1021/acs.energyfuels.0c00570

Hawthorne, S. B., Miller, D. J., Grabanski, C. B., Sorensen, J. A., Pekot, L. J., Kurz, B. A., Gorecki, C. D., Steadman, E. N., Harju, J. A., & Melzer, S. (2017). *Measured Crude Oil MMPs with Pure and Mixed CO2, Methane, and Ethane, and Their Relevance to Enhanced Oil Recovery from Middle Bakken and Bakken Shales*. D021S009R007. https://doi.org/10.2118/185072-MS

Hejazi, S. H., Assef, Y., Tavallali, M., & Popli, A. (2017). Cyclic CO2-EOR in the Bakken Formation: Variable cycle sizes and coupled reservoir response effects. *Fuel*, *210*, 758–767. https://doi.org/10.1016/j.fuel.2017.08.084

Hoffman, B. T. (2018). *Huff-N-Puff Gas Injection Pilot Projects in the Eagle Ford*. D012S001R001. https://doi.org/10.2118/189816-MS

Hoffman, B. T., & Evan, J. (2016, May). Improved Oil Recovery IOR Pilot Projects in the Bakken Formation. *Low Permeability Reservoirs Symposium*. SPE Rocky Mountain Petroleum Technology Conference, Denver, Colorado, USA. https://doi.org/10.2118/180270-MS

Hoffman, B. T., & Rutledge, J. M. (2019). *Mechanisms for Huff-n-Puff Cyclic Gas Injection into Unconventional Reservoirs*. D021S009R002. https://doi.org/10.2118/195223-MS

Holland, J. H. (1992). Genetic Algorithms. *Scientific American*, *267*(1), 66–73. https://www.jstor.org/stable/24939139

Hughes, R. (2009). *Evaluation and Enhancement of Carbon Dioxide Flooding Through Sweep Improvement* (No. 983791; p. 983791). https://doi.org/10.2172/983791

Igwe, U., Khishvand, M., & Piri, M. (2022). Retrograde condensation in natural porous media: An in situ experimental investigation. *Physics of Fluids*, *34*(1), 013102. https://doi.org/10.1063/5.0073801

Iraji, B., Shadizadeh, S. R., & Riazi, M. (2015). Experimental investigation of CO2 huff and puff in a matrix-fracture system. *Fuel*, *158*, 105–112. https://doi.org/10.1016/j.fuel.2015.04.069

Jácomo, M. H., Trindade, R. I. F., French, M., Lucas-Oliveira, É., Montrazi, E. T., & Bonagamba, T. J. (2019). Nuclear magnetic resonance characterization of porosity-preserving microcrystalline quartz coatings in Fontainebleau sandstones. *AAPG Bulletin*, *103*(9), 2117–2137. https://doi.org/10.1306/01301918104

Jia, B., Tsau, J.-S., & Barati, R. (2018). Role of molecular diffusion in heterogeneous, naturally fractured shale reservoirs during CO2 huff-n-puff. *Journal of Petroleum Science and Engineering*, *164*, 31–42. https://doi.org/10.1016/j.petrol.2018.01.032

Jiang, H., Lei, Y., Xiong, X., Yan, L., Pi, W., Li, X., & Yu, C. (2008). A CO2 immiscible displacement experimental study aiming at Fuyang extra-low permeability layer at the Daqing Changheng peripheral. *Geoscience*, *22*(4), 659–663.

Jin, L., Hawthorne, S., Sorensen, J., Kurz, B., Pekot, L., Smith, S., Bosshart, N., Azenkeng, A., Gorecki, C., & Harju, J. (2016, August 1). *A Systematic Investigation of Gas-Based Improved Oil Recovery Technologies for the Bakken Tight Oil Formation*. SPE/AAPG/SEG Unconventional Resources Technology Conference. https://doi.org/10.15530/URTEC-2016-2433692

Jin, L., Hawthorne, S., Sorensen, J., Pekot, L., Bosshart, N., Gorecki, C., Steadman, E., & Harju, J. (2017, April 18). *Utilization of Produced Gas for Improved Oil Recovery and Reduced*

Emissions from the Bakken Formation. SPE Health, Safety, Security, Environment, & Social Responsibility Conference - North America. https://doi.org/10.2118/184414-MS

Jin, L., Hawthorne, S., Sorensen, J., Pekot, L., Kurz, B., Smith, S., Heebink, L., Herdegen, V., Bosshart, N., Torres, J., Dalkhaa, C., Peterson, K., Gorecki, C., Steadman, E., & Harju, J. (2017). Advancing CO2 enhanced oil recovery and storage in unconventional oil play— Experimental studies on Bakken shales. *Applied Energy*, *208*, 171–183. https://doi.org/10.1016/j.apenergy.2017.10.054

Jin, L., Sorensen, J. A., Hawthorne, S. B., Smith, S. A., Pekot, L. J., Bosshart, N. W., Burton-Kelly, M. E., Miller, D. J., Grabanski, C. B., Gorecki, C. D., Steadman, E. N., & Harju, J. A. (2016). Improving Oil Recovery by Use of Carbon Dioxide in the Bakken Unconventional System: A Laboratory Investigation. *SPE Reservoir Evaluation & Engineering*, *20*(03), 602–612. https://doi.org/10.2118/178948-PA

Jossi, J. A., Stiel, L. I., & Thodos, G. (1962). The viscosity of pure substances in the dense gaseous and liquid phases. *AIChE Journal*, *8*(1), 59–63. https://doi.org/10.1002/aic.690080116

Katiyar, A., Patil, P., Rohilla, N., Rozowski, P., Evans, J., Bozeman, T., & Nguyen, Q. (2019). Industry-First Hydrocarbon-Foam EOR Pilot in an Unconventional Reservoir: Design, Implementation, and Performance Analysis. SPE/AAPG/SEG Unconventional Resources Technology Conference. https://doi.org/10.15530/urtec-2019-103

Kazemi, H., Merrill, L. S., Jr., Porterfield, K. L., & Zeman, P. R. (1976). Numerical Simulation of Water-Oil Flow in Naturally Fractured Reservoirs. *Society of Petroleum Engineers Journal*, *16*(06), 317–326. https://doi.org/10.2118/5719-PA

Kennedy, J., & Eberhart, R. (1995). Particle swarm optimization. *Proceedings of ICNN'95 -
International Conference on Neural Networks*, *4*, 1942–1948 vol.4.
https://doi.org/10.1109/ICNN.1995.488968

Kestin, J., Sokolov, M., & Wakeham, W. A. (1978). Viscosity of liquid water in the range −8 °C
to 150 °C. *Journal of Physical and Chemical Reference Data*, *7*(3), 941–948.
https://doi.org/10.1063/1.555581

Kirkpatrick, S., Gelatt, C. D., & Vecchi, M. P. (1983). Optimization by Simulated Annealing.
Science, *220*(4598), 671–680. https://doi.org/10.1126/science.220.4598.671

Kong, B., Wang, S., & Chen, S. (2016). *Simulation and Optimization of CO2 Huff-and-Puff
Processes in Tight Oil Reservoirs*. SPE-179668-MS. https://doi.org/10.2118/179668-MS

LeFever, J., Martinuik, C., Dancsok, E., & Mahnic, P. (1991, October). *Petroleum Potential of
the Middle Member, Bakken Formation, Williston Basin.* Sixth International Williston
Basin Symposium.

Li, H., Zheng, S., & Yang, D. (2013). Enhanced Swelling Effect and Viscosity Reduction of
Solvent(s)/CO2/Heavy-Oil Systems. *SPE Journal*, *18*(04), 695–707.
https://doi.org/10.2118/150168-PA

Li, L., & Sheng, J. J. (2016). Experimental study of core size effect on CH4 huff-n-puff
enhanced oil recovery in liquid-rich shale reservoirs. *Journal of Natural Gas Science and
Engineering*, *34*, 1392–1402. https://doi.org/10.1016/j.jngse.2016.08.028

Li, L., & Sheng, J. J. (2017). Numerical analysis of cyclic CH4 injection in liquid-rich shale
reservoirs based on the experiments using different-diameter shale cores and crude oil.
Journal of Natural Gas Science and Engineering, *39*, 1–14.
https://doi.org/10.1016/j.jngse.2017.01.017

Li, L., Sheng, J. J., & Sheng, J. (2016, May 5). *Optimization of Huff-n-Puff Gas Injection to Enhance Oil Recovery in Shale Reservoirs*. SPE Low Perm Symposium. https://doi.org/10.2118/180219-MS

Li, L., Sheng, J. J., Su, Y., & Zhan, S. (2018). Further Investigation of Effects of Injection Pressure and Imbibition Water on CO_2 Huff-n-Puff Performance in Liquid-Rich Shale Reservoirs. *Energy & Fuels*, *32*(5), 5789–5798. https://doi.org/10.1021/acs.energyfuels.8b00536

Li, L., Sheng, J. J., & Xu, J. (2017, February 15). *Gas Selection for Huff-n-Puff EOR in Shale Oil Reservoirs Based upon Experimental and Numerical Study*. SPE Unconventional Resources Conference. https://doi.org/10.2118/185066-MS

Li, L., Su, Y., Hao, Y., Zhan, S., Lv, Y., Zhao, Q., & Wang, H. (2019a). A comparative study of CO2 and N2 huff-n-puff EOR performance in shale oil production. *Journal of Petroleum Science and Engineering*, *181*, 106174. https://doi.org/10.1016/j.petrol.2019.06.038

Li, L., Su, Y., Hao, Y., Zhan, S., Lv, Y., Zhao, Q., & Wang, H. (2019b). A comparative study of CO2 and N2 huff-n-puff EOR performance in shale oil production. *Journal of Petroleum Science and Engineering*, *181*, 106174. https://doi.org/10.1016/j.petrol.2019.06.038

Li, L., Zhang, Y., & Sheng, J. J. (2017). Effect of the Injection Pressure on Enhancing Oil Recovery in Shale Cores during the CO2 Huff-n-Puff Process When It Is above and below the Minimum Miscibility Pressure. *Energy & Fuels*, *31*(4), 3856–3867. https://doi.org/10.1021/acs.energyfuels.7b00031

Li, S., & Luo, P. (2017). Experimental and simulation determination of minimum miscibility pressure for a Bakken tight oil and different injection gases. *Petroleum*, *3*(1), 79–86. https://doi.org/10.1016/j.petlm.2016.11.011

Loucks, R. G., Reed, R. M., Ruppel, S. C., & Hammes, U. (2012). Spectrum of pore types and
networks in mudrocks and a descriptive classification for matrix-related mudrock pores.
AAPG Bulletin, *96*(6), 1071–1098. https://doi.org/10.1306/08171111061

Liu, G., Sorensen, J. A., Braunberger, J. R., Klenner, R., Ge, J., Gorecki, C. D., Steadman, E. N.,
& Harju, J. A. (2014, April 1). *CO2-Based Enhanced Oil Recovery from Unconventional
Reservoirs: A Case Study of the Bakken Formation*. SPE Unconventional Resources
Conference. https://doi.org/10.2118/168979-MS

Ma, J., Wang, X., Gao, R., Zeng, F., Huang, C., Tontiwachwuthikul, P., & Liang, Z. (2015).
Enhanced light oil recovery from tight formations through CO2 huff 'n' puff processes.
Fuel, *154*, 35–44. https://doi.org/10.1016/j.fuel.2015.03.029

Mansour, E. M., Al-Sabagh, A. M., Desouky, S. M., Zawawy, F. M., & Ramzi, M. (2019). A
laboratory investigation of carbon dioxide-enhanced oil recovery by focusing on CO2-oil
physical properties. *Egyptian Journal of Petroleum*, *28*(1), 21–26.
https://doi.org/10.1016/j.ejpe.2018.10.004

Meng, X., Meng, Z., Ma, J., & Wang, T. (2019). Performance Evaluation of CO2 Huff-n-Puff
Gas Injection in Shale Gas Condensate Reservoirs. *Energies*, *12*(1).
https://doi.org/10.3390/en12010042

Mohamed, A. I. A., Khishvand, M., & Piri, M. (2020). A pore-scale experimental investigation
of process-dependent capillary desaturation. *Advances in Water Resources*, *144*, 103702.
https://doi.org/10.1016/j.advwatres.2020.103702

Morrow, N., & Buckley, J. (2011). Improved Oil Recovery by Low-Salinity Waterflooding.
Journal of Petroleum Technology, *63*(05), 106–112. https://doi.org/10.2118/129421-JPT

Morsy, S., Sheng, J. J., & Soliman, M. Y. (2013, November 11). *Waterflooding in the Eagle Ford Shale Formation: Experimental and Simulation Study*. SPE Unconventional Resources Conference and Exhibition-Asia Pacific. https://doi.org/10.2118/167056-MS

Müller-Huber, E., Börner, F., Börner, J. H., & Kulke, D. (2018). Combined interpretation of NMR, MICP, and SIP measurements on mud-dominated and grain-dominated carbonate rocks. *Journal of Applied Geophysics*, *159*, 228–240. https://doi.org/10.1016/j.jappgeo.2018.08.011

Myers, R., Montgomery, D., & Anderson-Cook, C. (2009). *Response Surface Methodology: Process and Product Optimization Using Designed Experiments* (3rd ed.). John Wiley & Sons, Inc.

Ngheim, L., & Li, Y.-K. (1984). Computation of multiphase equilibrium phenomena with an equation of state—ScienceDirect. *Fluid Phase Equilibria*, *77–95*. https://www.sciencedirect.com/science/article/pii/0378381284800138

Nguyen, C., Kothamasu, R., He, K., & Xu, L. (2015, April 27). *Low-Salinity Brine Enhances Oil Production in Liquids-Rich Shale Formations*. SPE Western Regional Meeting. https://doi.org/10.2118/174041-MS

North Dakota Department of Mineral Resources. (n.d.). *North Dakota Drilling and Production Statistics*. North Dakota General Statistics. Retrieved July 12, 2023, from https://www.dmr.nd.gov/oilgas/stats/statisticsvw.asp

Obeyesekere, N., Wylde, J., Wickramarachchi, T., & Kemp, L. (2021, April). *Formulation of Corrosion Inhibitors Using Design of Experiment (DOE) Methods and Discovering Highly Performing Inhibitors by High Throughput Experimentation (HTE) Methods Using Critical Micelle Concentration*. CORROSION 2021.

https://onepetro.org/NACECORR/proceedings/CORR21/3-CORR21/D031S015R007/464057

Peaceman, D. W. (1978). Interpretation of Well-Block Pressures in Numerical Reservoir

Simulation(includes associated paper 6988). *Society of Petroleum Engineers Journal*,

18(03), 183–194. https://doi.org/10.2118/6893-PA

Peng, D.-Y., & Robinson, D. B. (2002, May 1). *A New Two-Constant Equation of State* (world).

ACS Publications; American Chemical Society. https://doi.org/10.1021/i160057a011

Phan, T. N., Cronk, B. R., Almasoodi, M. M., & Reza, Z. A. (2018). *Lithologic and*

Geomechanical Control on CO2 Huff-n-Puff Enhanced Oil Recovery Processes Using

Integrated Modeling Framework in Wolfcamp. D013S017R003.

https://doi.org/10.15530/URTEC-2018-2901346

Rastegar, S. O., Mousavi, S. M., Shojaosadati, S. A., & Sheibani, S. (2011). Optimization of

petroleum refinery effluent treatment in a UASB reactor using response surface

methodology. *Journal of Hazardous Materials*, *197*, 26–32.

https://doi.org/10.1016/j.jhazmat.2011.09.052

Reverse Engineering the North Dakota Bakken Data – Peak Oil Barrel. (2014, February 21).

https://peakoilbarrel.com/reverse-engineering-north-dakota-bakken-data/

Rowe, A. M., & Chou, J. C. S. (1970). Pressure-volume-temperature-concentration relation of

aqueous sodium chloride solutions. *Journal of Chemical & Engineering Data*, *15*(1), 61–

66. https://doi.org/10.1021/je60044a016

Salman, M., Kostarelos, K., Sharma, P., & Lee, J. H. (2020). Application of Miscible Ethane

Foam for Gas EOR Conformance in Low-Permeability Heterogeneous Harsh

Environments. SPE Journal, 25(04), 1871–1883. https://doi.org/10.2118/201189-PA

Sanaei, A., Abouie, A., Tagavifar, M., & Sepehrnoori, K. (2018, July 23). *Comprehensive Study of Gas Cycling in the Bakken Shale*. SPE/AAPG/SEG Unconventional Resources Technology Conference. https://doi.org/10.15530/URTEC-2018-2902940

Sanchez-Rivera, D., Mohanty, K., & Balhoff, M. (2015). Reservoir simulation and optimization of Huff-and-Puff operations in the Bakken Shale. *Fuel*, *147*, 82–94. https://doi.org/10.1016/j.fuel.2014.12.062

Schmidt, M., & Sekar, B. K. (2014). *Innovative Unconventional2 EOR-A Light EOR an Unconventional Tertiary Recovery Approach to an Unconventional Bakken Reservoir in Southeast Saskatchewan*. D033S004R004.

Schmoker, J. W., & Hester, T. C. (1983). Organic Carbon in Bakken Formation, United States Portion of Williston Basin1. *AAPG Bulletin*, *67*(12), 2165–2174. https://doi.org/10.1306/AD460931-16F7-11D7-8645000102C1865D

Sennaoui, B., Pu, H., Rylander, E., Afari, S., & Malki, M. L. (2022). *An Experimental Study of CO2 Huff-N-Puff Enhanced Oil Recovery in Three Forks Formation, Williston Basin*. ARMA-2022-0334. https://doi.org/10.56952/ARMA-2022-0334

Shelley, R. F. (2013). *A North American Review of Commercial Shale Plays; Have We Learned Anything Besides Serendipity?* 13. https://doi.org/10.2118/166229-MS

Sheng, J. J. (2017a). Critical review of field EOR projects in shale and tight reservoirs. *Journal of Petroleum Science and Engineering*, *159*, 654–665. https://doi.org/10.1016/j.petrol.2017.09.022

Sheng, J. J. (2017b). Optimization of huff-n-puff gas injection in shale oil reservoirs. *Petroleum*, *3*(4), 431–437. https://doi.org/10.1016/j.petlm.2017.03.004

Sheng, J. J. (2020). Huff-n-puff gas injection in oil reservoirs. In *Enhanced Oil Recovery in Shale and Tight Reservoirs*. Gulf Professional Publishing.

Sheng, J. J., & Chen, K. (2014). Evaluation of the EOR potential of gas and water injection in shale oil reservoirs. *Journal of Unconventional Oil and Gas Resources*, *5*, 1–9. https://doi.org/10.1016/j.juogr.2013.12.001

Sheng, J. J., Mody, F., Griffith, P. J., & Barnes, W. N. (2016). Potential to increase condensate oil production by huff-n-puff gas injection in a shale condensate reservoir. *Journal of Natural Gas Science and Engineering*, *28*, 46–51. https://doi.org/10.1016/j.jngse.2015.11.031

Shilov, E., Cheremisin, A., Maksakov, K., & Kharlanov, S. (2019). Huff-n-Puff Experimental Studies of CO2 with Heavy Oil. *Energies*, *12*(22). https://doi.org/10.3390/en12224308

Sohrabi, M., Danesh, A., Tehrani, D. H., & Jamiolahmady, M. (2008). Microscopic Mechanisms of Oil Recovery By Near-Miscible Gas Injection. *Transport in Porous Media*, *72*(3), 351–367. https://doi.org/10.1007/s11242-007-9154-z

Song, C., & Yang, D. (2017). Experimental and numerical evaluation of CO2 huff-n-puff processes in Bakken formation. *Fuel*, *190*, 145–162. https://doi.org/10.1016/j.fuel.2016.11.041

Sonnenberg, S. A. (2018). Sequence Stratigraphy of the Bakken and Three Forks Formations, Williston Basin, USA. In B. Hart, N. C. Rosen, D. West, A. D'Agostino, C. Messina, M. Hoffman, & R. Wild (Eds.), *Sequence Stratigraphy: The Future Defined* (Vol. 36, p. 0). SEPM Society for Sedimentary Geology. https://doi.org/10.5724/gcs.17.121

Sorensen, J. A., Pekot, L. J., Torres, J. A., Jin, L., Hawthorne, S. B., Smith, S. A., Jacobson, L. L., & Doll, T. E. (2018). *Field Test of CO2 Injection in a Vertical Middle Bakken Well to*

Evaluate the Potential for Enhanced Oil Recovery and CO2 Storage. D033S056R002.

https://doi.org/10.15530/URTEC-2018-2902813

Sorensen, J., & Hamlin, J. (2016). *Enhanced Oil Recovery: Historical Bakken Test Data Provide Critical Insights On EOR In Tight Oil Plays*. https://www.aogr.com/magazine/cover-story/historical-bakken-test-data-provide-critical-insights-on-eor-in-tight-oil-p

Stats-Ease Inc. (2021). *Design-Expert® software* (13.0.8.0). Stat-Ease, Inc. www.statease.com

Sun, R., Yu, W., Xu, F., Pu, H., & Miao, J. (2019). Compositional simulation of CO2 Huff-n-Puff process in Middle Bakken tight oil reservoirs with hydraulic fractures. *Fuel*, *236*, 1446–1457. https://doi.org/10.1016/j.fuel.2018.09.113

Teklu, T. W., Li, X., Zhou, Z., Alharthy, N., Wang, L., & Abass, H. (2018). Low-salinity water and surfactants for hydraulic fracturing and EOR of shales. *Journal of Petroleum Science and Engineering*, *162*, 367–377. https://doi.org/10.1016/j.petrol.2017.12.057

Tetteh, J., Brady, P., & Ghahfarokhi, R. B. (2020). Review of low salinity waterflooding in carbonate rocks: Mechanisms, investigation techniques, and future directions | Elsevier Enhanced Reader. *Advances in Colloid and Interface Science*, *284*. https://doi.org/10.1016/j.cis.2020.102253

Thomas, G. W., & Thurnau, D. H. (1983). Reservoir Simulation Using an Adaptive Implicit Method. *Society of Petroleum Engineers Journal*, *23*(05), 759–768. https://doi.org/10.2118/10120-PA

Tomomewo, O. S., Jabbari, H., Badrouchi, N., Onwumelu, C., & Mann, M. (2019). *Characterization of the Bakken Formation Using NMR and SEM Techniques*. ARMA-2019-1875.

Torres, J. A., Jin, L., Bosshart, N. W., Pekot, L. J., Sorensen, J. A., Peterson, K., Anderson, P. W., & Hawthorne, S. B. (2018). *Multiscale Modeling to Evaluate the Mechanisms Controlling CO2- Based Enhanced Oil Recovery and CO2 Storage in the Bakken Formation*. D023S039R003. https://doi.org/10.15530/URTEC-2018-2902837

Tovar, F. D., Barrufet, M. A., & Schechter, D. S. (2018). *Gas Injection for EOR in Organic Rich Shale. Part I: Operational Philosophy*. D031S007R005. https://doi.org/10.2118/190323-MS

Tovar, F. D., Eide, Ø., Graue, A., & Schechter, D. S. (2014). *Experimental Investigation of Enhanced Recovery in Unconventional Liquid Reservoirs using CO2: A Look Ahead to the Future of Unconventional EOR*. D031S007R005. https://doi.org/10.2118/169022-MS

United States Energy Information Administration. (2013). *Technically Recoverable Shale Oil and Shale Gas Resources*. https://www.eia.gov/analysis/studies/worldshalegas/pdf/overview.pdf

United States Geological Survey. (2021). *Assessment of Undiscovered Continuous Oil Resources in the Bakken and Three Forks Formations of the Williston Basin Province, North Dakota and Montana, 2021* [Fact Sheet]. https://pubs.usgs.gov/fs/2021/3058/fs20213058.pdf

US Energy Information Administration. (2011). *Review of Emerging Resources: U.S. Shale Gas and Shale Oil Plays*. U.S. Department of Energy. https://www.eia.gov/analysis/studies/usshalegas/pdf/usshaleplays.pdf

Vedachalam, N., Srinivasalu, S., Rajendran, G., Ramadass, G. A., & Atmanand, M. A. (2015). Review of unconventional hydrocarbon resources in major energy consuming countries and efforts in realizing natural gas hydrates as a future source of energy. *Journal of*

Natural Gas Science and Engineering, *26*, 163–175.

https://doi.org/10.1016/j.jngse.2015.06.008

Von Flatern, R. (2017). *Tackling the tight oil recovery challenge*.

https://www.upstreamonline.com/ upstreamtechnology/tackling-the-tight-oil-recovery-

challenge/1-1- 1275866.

Wahid, Z., & Nadir, N. (2013). Improvement of One Factor at a Time Through Design of

Experiments. *World Applied Sciences Journal*, *21*.

https://citeseerx.ist.psu.edu/viewdoc/download?doi=10.1.1.390.6353&rep=rep1&type=pd

f

Wan, T., & Liu, H.-X. (2018). Exploitation of fractured shale oil resources by cyclic CO2

injection. *Petroleum Science*, *15*(3), 552–563. https://doi.org/10.1007/s12182-018-0226-1

Wan, T., Meng, X., Sheng, J. J., & Watson, M. (2014). *Compositional Modeling of EOR Process*

in Stimulated Shale Oil Reservoirs by Cyclic Gas Injection. SPE-169069-MS.

https://doi.org/10.2118/169069-MS

Wang, J.-P., Chen, Y.-Z., Ge, X.-W., & Yu, H.-Q. (2007). Optimization of coagulation–

flocculation process for a paper-recycling wastewater treatment using response surface

methodology. *Colloids and Surfaces A: Physicochemical and Engineering Aspects*,

302(1), 204–210. https://doi.org/10.1016/j.colsurfa.2007.02.023

Wang, L., Tian, Y., Yu, X., Wang, C., Yao, B., Wang, S., Winterfeld, P. H., Wang, X., Yang, Z.,

Wang, Y., Cui, J., & Wu, Y.-S. (2017). Advances in improved/enhanced oil recovery

technologies for tight and shale reservoirs. *Fuel*, *210*, 425–445.

https://doi.org/10.1016/j.fuel.2017.08.095

Wang, L., & Yu, W. (2019). Mechanistic simulation study of gas Puff and Huff process for

    Bakken tight oil fractured reservoir. *Fuel*, *239*, 1179–1193.

    https://doi.org/10.1016/j.fuel.2018.11.119

Wang, L. L., Zhang, G. Q., Hallais, S., Tanguy, A., & Yang, D. S. (2017). Swelling of Shales: A

 Multiscale Experimental Investigation.Energy & Fuels,31(10),10442–

10451.https://doi.org/10.1021/acs.energyfuels.7b0122

Wang, X., Luo, P., Er, V., & Huang, S. (2010). Assessment of CO2 flooding potential for

    Bakken formation, Saskatchewan. *Canadian Unconventional Resources and*

    International Petroleum Conference.

Wang, Y. (2015). CO2 flooding test in Fayang reservoir in Daqing Yushulin oilfield. *Petroleum*

    Geology and Oilfield Development in Daqing, *34*(1), 136–139.

Webster, R. L. (1984). Petroleum Source Rocks and Stratigraphy of Bakken Formation in North

    Dakota: ABSTRACT. *AAPG Bulletin*, *68*(7), 953–953.

    https://doi.org/10.1306/AD46166F-16F7-11D7-8645000102C1865D

Wei, B., Gao, K., Song, T., Zhang, X., Pu, W., Xu, X., & Wood, C. (2020). Nuclear-Magnetic-

    Resonance Monitoring of Mass Exchange in a Low-Permeability Matrix/Fracture Model

    During CO2 Cyclic Injection: A Mechanistic Study. *SPE Journal*, *25*(01), 440–450.

    https://doi.org/10.2118/199345-PA

Wood, T., & Milne, B. (2011). *Waterflood potential could unlock billions of barrels: Crescent*

    Point Energy. https://docplayer.net/38428130-Waterflood-potential-could-unlock-

    billions-of-barrels.html

Xiao, L., Li, J., Mao, Z., Lu, J., Yu, H., Guo, H., & Li, G. (2018). A method to determine nuclear

    magnetic resonance (NMR) T2cutoff based on normal distribution simulation in tight

    sandstone reservoirs. *Fuel*, *225*, 472–482. https://doi.org/10.1016/j.fuel.2018.03.178

Yang, C., & Gu, Y. (2006). Diffusion coefficients and oil swelling factors of carbon dioxide,

    methane, ethane, propane, and their mixtures in heavy oil. *Fluid Phase Equilibria*,

    243(1), 64–73. https://doi.org/10.1016/j.fluid.2006.02.020

Yu, W., Lashgari, H. R., Wu, K., & Sepehrnoori, K. (2015). CO2 injection for enhanced oil

    recovery in Bakken tight oil reservoirs. *Fuel*, *159*, 354–363.

    https://doi.org/10.1016/j.fuel.2015.06.092

Yu, W., Lashgari, H., & Sepehrnoori, K. (2014). Simulation Study of CO2 Huff-n-Puff Process

    in Bakken Tight Oil Reservoirs. *All Days*, SPE-169575-MS.

    https://doi.org/10.2118/169575-MS

Yu, W., Zhang, Y., Varavei, A., Sepehrnoori, K., Zhang, T., Wu, K., & Miao, J. (2019).

    Compositional Simulation of CO2 Huff 'n' Puff in Eagle Ford Tight Oil Reservoirs With

    CO2 Molecular Diffusion, Nanopore Confinement, and Complex Natural Fractures. *SPE*

    Reservoir Evaluation & Engineering, *22*(02), 492–508. https://doi.org/10.2118/190325-

    PA

Yu, Y., Meng, X., & Sheng, J. J. (2016). Experimental and numerical evaluation of the potential

    of improving oil recovery from shale plugs by nitrogen gas flooding. *Journal of*

    Unconventional Oil and Gas Resources, *15*, 56–65.

    https://doi.org/10.1016/j.juogr.2016.05.003

Yu, Y., & Sheng, J. J. (2015, July 20). *An Experimental Investigation of the Effect of Pressure*

    Depletion Rate on Oil Recovery from Shale Cores by Cyclic N2 Injection.

SPE/AAPG/SEG Unconventional Resources Technology Conference.

https://doi.org/10.15530/URTEC-2015-2144010

Zhao, J., Wang, P., Yang, H., Tang, F., Ju, Y., & Jia, Y. (2021). Experimental Investigation of

the CO2 Huff and Puff Effect in Low-Permeability Sandstones with NMR. *ACS Omega*,

6(24), 15601–15607. https://doi.org/10.1021/acsomega.0c04250

Zhou, Z., Abass, H., Li, X., & Teklu, T. (2016). Experimental investigation of the effect of

imbibition on shale permeability during hydraulic fracturing. *Journal of Natural Gas*

Science and Engineering, *29*, 413–430. https://doi.org/10.1016/j.jngse.2016.01.023

Zick, A. A. (1986, October 5). *A Combined Condensing/Vaporizing Mechanism in the*

Displacement of Oil by Enriched Gases. SPE Annual Technical Conference and

Exhibition. https://doi.org/10.2118/15493-MS